Case Studies of Cool Season 500 hPa Cutoff Cyclone Precipitation Distribution

Abstract of a thesis presented to the Faculty

of the University at Albany, State University of New York

in partial fulfillment of the requirements

for the degree of

Master of Science

College of Arts & Sciences

Department of Earth and Atmospheric Sciences

Anthony R. Fracasso
2004

I. Introduction

1.1 Overview

The generation, evolution, and prediction of upper-air cutoff cyclones (also referred to as closed lows) and their influence on sensible weather have been an ongoing challenge to forecasters. An integral component of this challenge is quantitative precipitation forecasting (QPF). Forecasting improvements on the overall synoptic scale (e.g., pressure fields) have improved greatly with the advent of regional models such as the Nested Grid Model (NGM) (e.g., Junker and Hoke 1990). However, skill in QPF has lagged behind since the scale of precipitation is quite variable and much smaller than the typical synoptic scale (e.g., Anthes 1983; Roebber and Bosart 1998). This lag in forecast skill is certainly true with regard to cutoff cyclones, which are associated with 30% of the annual precipitation in the northeast United States (US) (Atallah and Aiyyer 2002). With such a considerable fraction attributed to cutoffs, the need for improved forecasts of precipitation in association with these systems is clearly self-evident.

The typical forward speed of a cutoff is often less than that of systems embedded in the steering flow aloft (e.g., Palmén 1949; Bell and Bosart 1989). This can lead to blocking patterns that complicate forecasts (e.g., Rex 1950a,b; Colucci 1985, 1987). The general thermodynamic structure of a cutoff is a coupled cold (warm) pool of air in the lower (upper) troposphere beneath (above) the circulation center. Often characterized by little vertical tilt and negative height anomalies in the troposphere (e.g., Dole 1986), cutoffs also tend to have relatively weak advection of both temperature and vorticity.

These very qualities of cutoffs often lend to their reduced predictability (Hawes and Colucci 1986). Coupled with a geographic area characterized by complex terrain (such as the Northeast), numerical forecast models often fail to adequately predict precipitation associated with cutoffs spatially, temporally, and quantitatively.

A first step in improving QPF is to construct a climatological distribution of cyclone frequency across the area of interest. Smith (2003) created a global distribution of cutoff frequency and also focused on the US and eastern North America. Adopting that study and focusing on the northeast United States, the precipitation associated with cutoff lows is stratified by month over the cool season, defined to be October through May. Najuch (2004) has conducted the warm season (June–September) counterpart of this research. In addition, the resultant precipitation distribution from four favored tracks affecting the Northeast is shown. One in-depth case study and, in addition, several supplementary case studies will provide a close look into the forecasting challenge of these systems.

1.2 Literature Review

1.2.1 Formation and Evolution of Cutoff Cyclones

Cutoff cyclones may develop in a number of ways, but their development is most easily explained by simple atmospheric thermodynamics. A separation of cold (warm) air equatorward (poleward) from the mean flow is the result of a deformation in the mean middle- and upper-tropospheric flows (e.g., Crocker, et al. 1947; Palmén 1949; Eliassen

and Kleinschmidt 1957). Since the strongest subsidence in the upper trough (say, at the 500-hPa level) is often stronger in the central part of the trough compared to the southern part, the cold air eventually vanishes from the midlevels, resulting in an isolated cold pool. This "cutoff" area of cold air is seen in Fig. 1.1. Such pools of cold air will undergo sinking as they travel equatorward.

Alternatively, the formation of a cutoff can also be explained using the conservation of potential vorticity (PV) in a barotropic atmosphere, as expressed in Rossby (1940):

$$\frac{\zeta + f}{\Delta p} = \text{const.} \qquad (1)$$

In (1), ζ is the relative vorticity, f is the Coriolis parameter, and Δp is the depth of the column in pressure coordinates. The relationships between the three variables clearly give credence to a cutoff's formation. As discussed in Palmén and Newton (1969, section 10.4), if a column of air is displaced equatorward from its source region and ζ is held at zero, then f is simply proportional to Δp; i.e., the column will decrease in depth as it travels equatorward. However, in the real atmosphere ζ is often variable. Thus, the decrease in f due to its equatorward motion must be balanced by an increase in ζ if the column is to maintain or increase its depth. The resultant increase in relative vorticity can be directly related to the strength of the cyclonic circulation of the air column; i.e., deeper (shallower) pools of cold air will generate stronger (weaker) circulations. Stronger circulations are able to deform the mean flow, which will occasionally result in an isolated area of cold air. Together with an embedded cyclonic circulation, a cutoff cyclone can form.

Berggren et al. (1949) have theorized that such processes, taking place repetitively, can be embedded in a larger-scale blocking episode as shown in Figs. 1.2a–f (taken from Fig. 26 of Berggren et al. 1949). This progression occurs when a strong zonal flow is located well upstream from the blocking region, allowing approaching troughs to slow down and increase in amplitude (Berggren et al. 1949). Cutoffs of cold (warm) air form to the south (north) as the flow is exceptionally deformed. Rex (1950) further explained both qualitatively and quantitatively this resultant blocking pattern. Depending on the strength and evolution of a cold trough, structures other than a cutoff cyclone can occur. Figures 1.3a–e show five such possibilities. Figure 1.3d is noticeably similar to the result of the discussion above (and Fig. 1.2), with a cold pool isolated south of the mean flow. Hsieh (1949) investigated one such event over North America. The process by which a cutoff forms as a result of an interaction between a preexisting trough or wave with an upstream wind maximum was further examined by Keyser and Shapiro (1986, sec. 2d), Bell and Bosart (1993), and Bell and Keyser (1993). It was found that as the wind maximum migrates to the base of the trough, vorticity is concentrated near the trough axis.

Relating the above theories back to a PV framework, a more complete picture can be obtained. Palmén and Newton (1969, sec. 10.1) examined an event first studied by Palmén and Nagler (1949), where a cutoff was linked to the higher latitude cold source by an “umbilical cord” in the form of a shear line (Fig. 1.4). This umbilical cord can be equated to an area of higher PV by way of a more general form of PV than in (1), as in Hoskins et al. (1985). Following this reasoning, the cold source of polar air is then equivalent to a reservoir of PV. Figure 5 of Hoskins et al. (1985) shows the evolution of

this umbilical cord and the subsequent creation of a cutoff in this PV framework. In a later study, Thorncroft et al. (1993) found that cutoffs can develop from two different life cycles. Figure 1.5 shows (a) an LC1 or anticyclonic wrapping and (b) an LC2 or cyclonic wrapping of PV. An LC1 wrapping results in a cutoff cyclone on the equatorward side of the mean jet, as in Bell and Bosart (1993). An LC2 wrapping results in a cutoff on the poleward side of the mean jet, as in Rogers and Bosart (1986). This latter type of evolution is found to occur with "bombs" (explosively deepening oceanic surface cyclones), as noted in Sanders and Gyakum (1980) and Konrad and Colucci (1988).

1.2.2 Characteristic Structure of Cutoff Cyclones

At the onset of the study of upper-level cyclones, it was theorized that the lower levels of the atmosphere operated relatively independently from, and not in conjunction with, the upper levels (Palmén 1949, Palmén and Nagler 1949, Hsieh 1949). These studies found that for the cases examined, little or no coincident cyclogenesis occurred at the surface. With the growth of the observational network worldwide since that time, this scenario has been disproved in many cases. Regardless, a cutoff cyclone impacts the sensible weather conditions at the surface, as was shown in a case study over Europe on 8–20 November 1959 first performed by Peltonen (1963). This case was further examined by Palmén and Newton (1969, sec. 10.2). The ideal cutoff cyclone has a symmetrical distribution of both temperature and geopotential height, with values decreasing toward the center. Palmén and Newton (1969) found this symmetric structure to occur in this case study, along with a remarkable temporal endurance.

Figures 1.6a–d show the structure of this case study cutoff at the surface, 850 hPa, 500 hPa, and 300 hPa, respectively, as analyzed by Palmén and Newton (1969). Clearly evident from Fig. 1.6c and similarly in Fig. 1.6d are the aforementioned symmetric temperature and geopotential height fields collocated near the center of the cyclone. Figure 1.7 shows the cross section through the cutoff along the line *a*–*a*. Notable are the depressed (elevated) isotherms and elevated (depressed) isentropes in the lower (upper) atmosphere near the cyclone center, comparable to idealized thermal structures in cutoffs of past studies. Coincident with the cyclone center is the depressed tropopause, referred to as the "tropopause funnel" by Palmén and Newton (1969, sec. 10.2). This thermal structure was retained for at least the next 36 h as the system moved westward.

More recently, Thorpe (1986) applied a PV framework to the vertical structure of an idealized cutoff cyclone. Figure 1.8 shows this idealized structure, with perfect symmetry about the cyclone center. Here, PV is used to describe the system based on the associated potential temperature field, which is obtained by applying the invertibility principle in conjunction with potential temperature conditions at the boundaries (surface and tropopause). Eliassen and Kleinschmidt (1957) first employed this procedure to describe balanced disturbances by their distinct PV structures. These studies were later followed by Davies et al. (1991) and Bell and Keyser (1993) who found that cutoffs are associated with areas of isolated and anomalously high PV, respectively.

1.2.3 Cutoff Cyclone Climatologies

1.2.3a Cutoff Cyclone Distribution and Genesis/Lysis

There have been only a handful of studies that deal with the genesis/lysis of cutoff cyclones. The first studies in the literature only examined parts of the Southern Hemisphere. Kerr (1953) and van Loon (1956) found that cutoffs preferably form in the Australia-New Zealand region, aided by a blocking regime. Palmén and Newton (1969, p. 278) stated only briefly that there are certain preferred areas of genesis located in the westerlies—namely, the western US and southwestern Europe. Tyson (1986) and Taljaard and Steyn (1991) studied cutoffs that formed over the western part of southern Africa and their associated precipitation over South Africa. Parker et al. (1989) examined cutoff cyclones over the western half of the Northern Hemisphere during a 36-year (1950–1985) period. It was not until Bell and Bosart (1989) that the entire Northern Hemisphere was examined. Using a 15-year (1963–1977) dataset, an objective distribution of 500 hPa closed circulation centers was produced. Similar to Palmén and Newton (1969), they found that the occurrence of cutoffs is maximized north of and within the main belt of westerlies. These regions included the North Pacific Ocean, eastern Canada and the northeast US toward Greenland, and the northeastern Atlantic Ocean. In addition, cutoffs were notably observed south of the westerlies such as the east-central Atlantic Ocean eastwards to central Asia. Other favored locations included the southwest US and the Mediterranean basin. Areas of lysis were found to be near or just downstream of areas of genesis, indicative of the slow-moving nature of many cutoffs. However, lysis areas in the North Atlantic were found a bit farther downstream from genesis areas, indicating more progressive systems.

Smith (2003) followed Bell and Bosart's (1989) procedure, but expanded the dataset to 54 years (1948–2001), used a higher resolution dataset (2.5 x 2.5 degree grid versus 2 x 5 degree grid), and included both the Northern and Southern Hemisphere. However, areas of activity in the Northern Hemisphere, as well as genesis/lysis areas, were found to be remarkably similar to Bell and Bosart (1989) and Parker et al. (1989), with some finer-scale details emerging due to the higher-resolution dataset. For the Southern Hemisphere, Smith (2003) found that cutoffs are most frequent in a ring surrounding Antarctica between 50°S and 65°S, with maxima between 120°E and 10°W and near 80°W and 60°E. Other favored areas include eastern Australia toward New Zealand, southeast of South America, southwest of southern Africa, and in the Mozambique Channel.

Other recent studies include Tennant and Van Heerden (1994), who found that topography played a crucial role in the development of cutoffs over southern Africa. Doyle and Shapiro (1999) discovered the importance of an orographically induced jet south of Greenland that aided in the cutoff formation. Bell and Bosart (1994) looked at cases of cutoffs in the southwest US, the eastern US, and in the lee of the Alps.

1.2.3b Cyclone Tracking

Until recent years, all cyclone tracking studies (e.g., Bowie and Weightman 1914; Klein 1957; Reitan 1974) were subjective due to constraints in data availability/reliability and computing power. Recently, many objective studies have arisen that track surface cyclones (e.g., Alpert et al. 1990; König et al. 1993; Ueno 1993; Hodges 1994; Sinclair

1997; Blender and Schubert 2000). Geng and Sugi (2001) studied winter surface cyclones during the 41-year period (1958–1998). Smith (2003) used a similar methodology and applied it to 500 hPa cyclones. An objective kinematic tracking scheme was used to track every cyclone over the 54-year period; see Smith (2003, sec. 2.2.2) for a complete description. Mean cool-season tracks were subjectively drawn (Fig. 1.9) using the objectively produced tracks, since their movement was confined to the grid points (2.5° apart by latitude and longitude). These tracks include the (1) Hudson Bay track: systems originating near Hudson Bay in Canada and moving south-southeastward toward northern New England; (2) Clipper track: southeastward moving systems originating in south-central Canada; (3) Southwest track: northeastward moving systems originating in the southwest US; (4) Mid-Atlantic track: northeastward moving systems along the Northeast coast; and (5) US/Canadian Maritime track: cutoffs that are a result of intense cyclogenesis over the western Atlantic Ocean.

1.2.4 Precipitation Within Cutoff Cyclones

Studies related specifically to precipitation in association with cutoff lows have been few and far between. Hsieh (1949) was one of the first to address the issue of precipitation in a cutoff case study over the northern US in March 1948 (Fig. 1.10). In this case, the precipitation is located primarily to the east and southeast of the cutoff, corresponding to an area of upper-level divergence, in agreement with Palmén and Newton (1969, sec. 10.2). A comprehensive climatology of cutoff low precipitation was nearly impossible prior to the 1960s due to a lack of readily available upper-air charts,

which also had a larger temporal and spatial resolution than other meteorological maps, such as surface charts (Jorgensen 1963). The first related climatology was of 700 hPa lows over the intermountain west of the US over a 39-month period (December–February 1951–1964) (Jorgensen et al. 1967). The area of maximum precipitation for intense 700 hPa lows was found to be located just southeast of the center. For lows of lesser intensity, the area of maximum precipitation shifted to the south and west of the center. However, nothing is stated with regard to speed or track of the low versus the distribution of precipitation.

Klein et al. (1968), using the same period of study as Jorgensen et al. (1967), investigated lows at the 850-, 700-, 500-, and 300-hPa levels and their relationship to areas of precipitation. Figure 1.11 shows that the area of maximum precipitation associated with 500 hPa lows occurs about 3.5° to the east and about 3° to the south of the low center. This result was derived from 172 500-hPa lows observed over the 39-month period. It was also found that about 50% of 500 hPa lows produce precipitation.

Taljaard (1985) studied cutoff lows at all mandatory levels (e.g., sea-level, 850-, 700-, 500-, 300-, and 200-hPa) over South Africa over a 10-year period. The area of heaviest precipitation was found to occur generally between northeast and southeast of the 300 hPa low. Taljaard also noted that orography plays a role in determining areas of widespread light-to-moderate precipitation and, less frequently, heavier precipitation.

Konrad and Colucci (1988) stated that the general synoptic climatology of 500 hPa cyclogenesis is an important topic for future research. Since then, only a climatology of frequency and favored tracks of cutoffs has been produced. The evident void in the

literature of an East Coast precipitation climatology of 500 hPa lows lends to the purpose of this research.

1.3 Study Goals

Cutoff cyclones have been a challenge to predict. Their focus in the literature is minimal, yet their effect on sensible weather can be significant. In light of these factors, this thesis has the following goals: (1) to present the climatological precipitation distribution variability across the Northeast in association with cutoff cyclones, (2) to stratify the variation of precipitation relative to four favored tracks near the Northeast, and (3) to present one multifaceted case study, along with several supporting cases, that illustrate the challenge in predicting the evolution of cutoff cyclones. It is the intention of the author that this research will provide assistance to forecasters in predicting the precipitation distribution when a cutoff cyclone approaches the northeast US. At a minimum, an increase in situational awareness should be attained.

The first part of this study develops a climatology of cool-season (October–May) average daily precipitation over the Northeast when a cutoff is located near the Northeast. Cutoffs of all tracks are averaged over the 51-year period (1948–1998). In addition, the impact cutoffs have with respect to the climatological average distribution of monthly precipitation across the Northeast is displayed.

The second part of this study incorporates four preferred tracks found by Smith (2003) and confirmed by the author. Monthly maps of both average daily precipitation

over the Northeast, as well as daily precipitation relative to each cyclone's track, are presented.

The last part of this study presents several cases of recent cutoffs. These cases show the difficulty in predicting the evolution of cutoff cyclones, as well as the effect they have on the sensible weather at locations near and at some distance from the cyclone center.

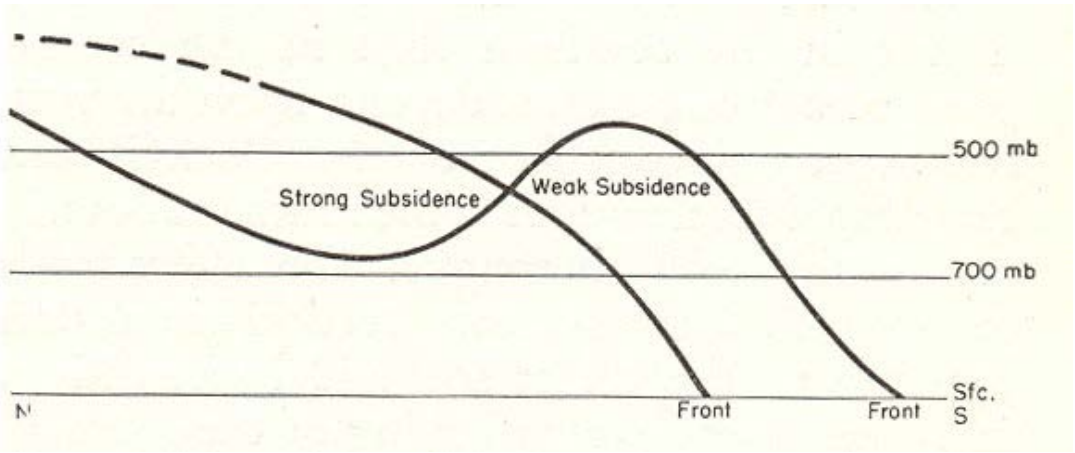

Fig. 1.1. Schematic meridional cross section through an upper-level trough. Solid lines indicate the profile of the polar air before and after the formation of a cutoff low. Source: Palmén (1949), Fig. 2.

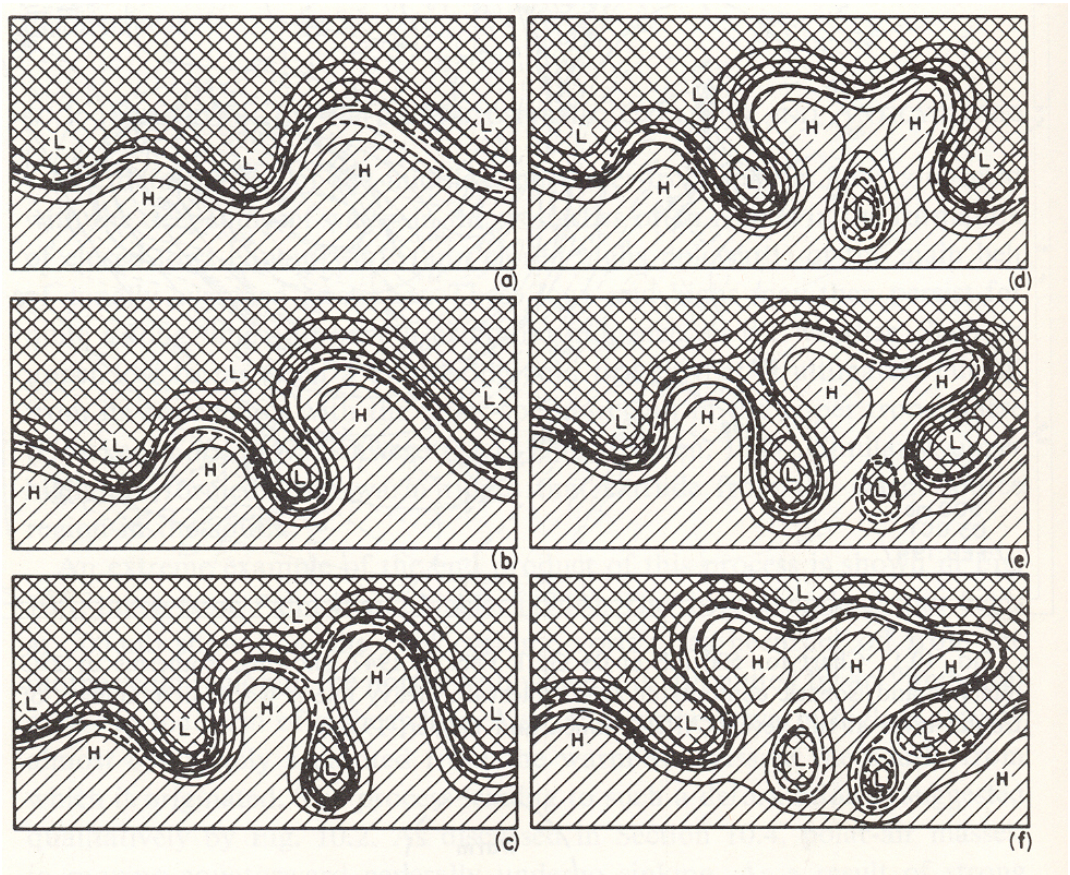

Figs. 1.2a–f. Idealized sketches of the development of unstable waves at 500 hPa in association with the establishment of a blocking anticyclone at high latitudes and a cutoff cyclone at low latitudes. Warm air (hatched) is separated from cold air (cross-hatched) by frontal boundaries (dashed lines). Solid lines represent streamlines. Source: Palmén and Newton (1969), Figs. 10.3a–f.

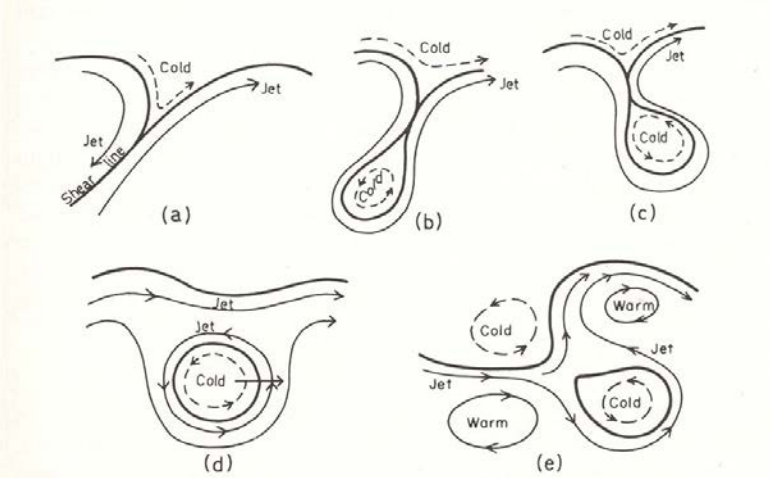

Figs. 1.3a–e. Five characteristic types of disturbances resulting from the extreme growth of upper-level waves. Solid heavy lines represent fronts. Streamlines in warm (cold) air are represented by solid (dashed) arrows. Source: Palmén and Newton (1969), Figs. 10.4a–e.

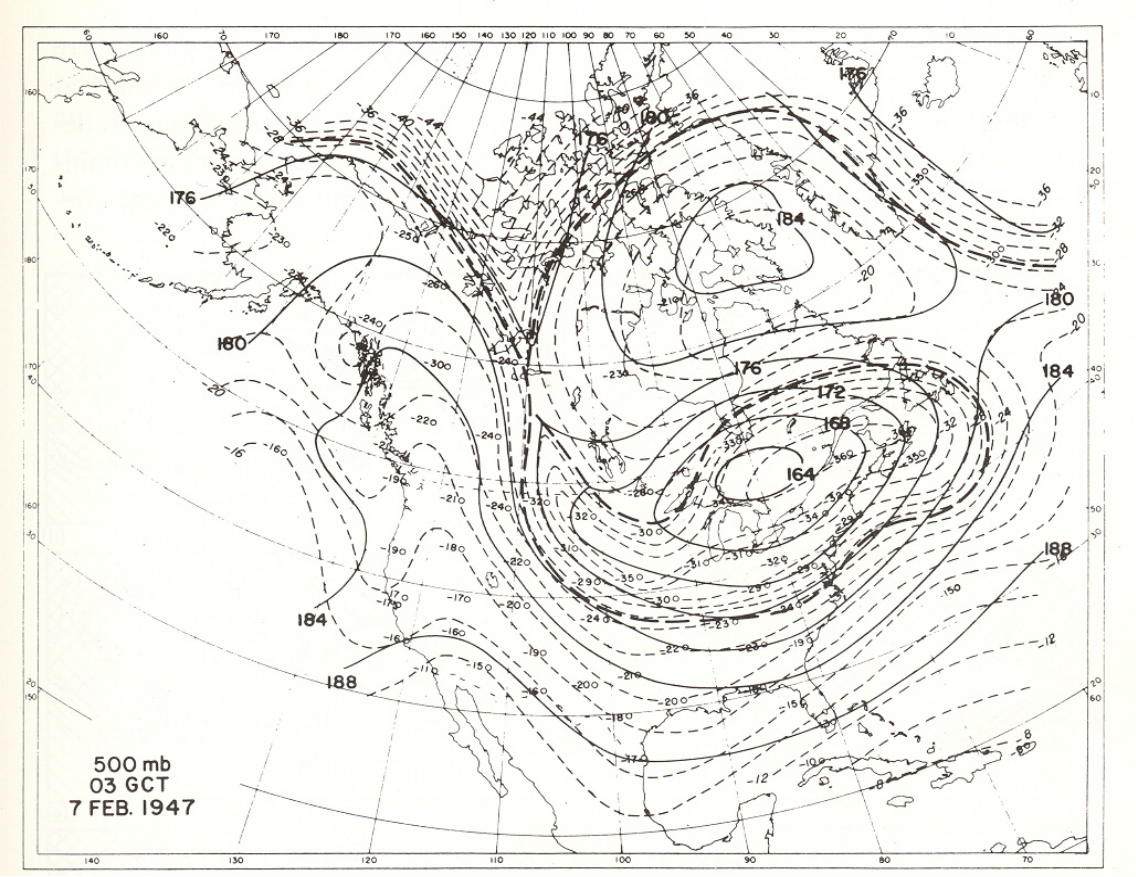

Fig. 1.4. 500 hPa isotherms (dashed lines, contour interval 2°C), upper-front boundary (heavy dashed line), and geopotential height (solid lines, contour interval 200 ft), for 0300 UTC 7 February 1947. Source: Palmén and Newton (1969), Fig. 10.1.

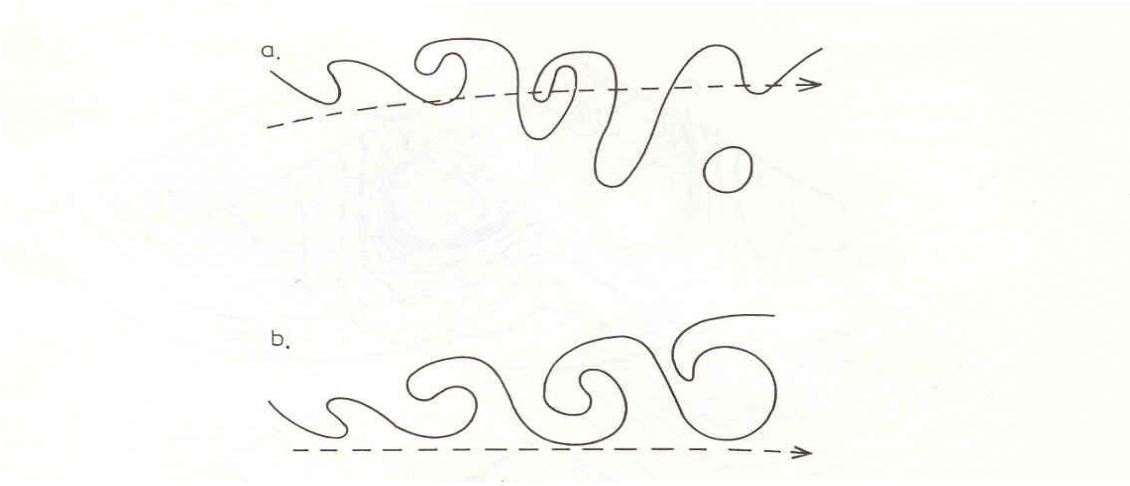

Figs. 1.5a–b. Schematic of a PV-θ contour (solid line) in the Atlantic storm track sharing its main characteristics with (a) an LC1-type life cycle and (b) an LC2-type life cycle. Dashed arrows represent the mean jet. Source: Thorncroft et al. (1993), Figs. 12a–b.

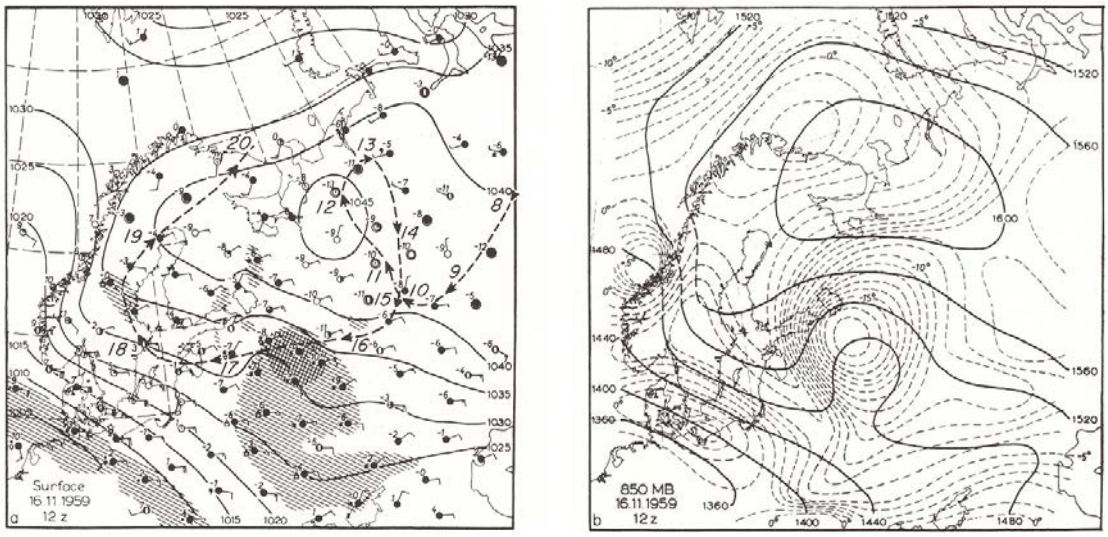

(a) (b)

Figs. 1.6a–d. (a) surface, (b) 850 hPa, (c) 500 hPa, (d) 300 hPa for 1200 UTC 16 November 1959. In (a), temperatures are in °C; precipitation areas are hatched, with areas exceeding 1 mm/12 h cross-hatched. In other charts, isotherms are at 1°C intervals and height intervals are at 40 m intervals. Heavy line in (c) and (d) is the "tropopause intersection." The path of the 500 hPa low center is shown in (a) with the arrowheads indicating its location at 0000 UTC on the dates given. Source: Palmén and Newton (1969), Figs. 10.7a–d.

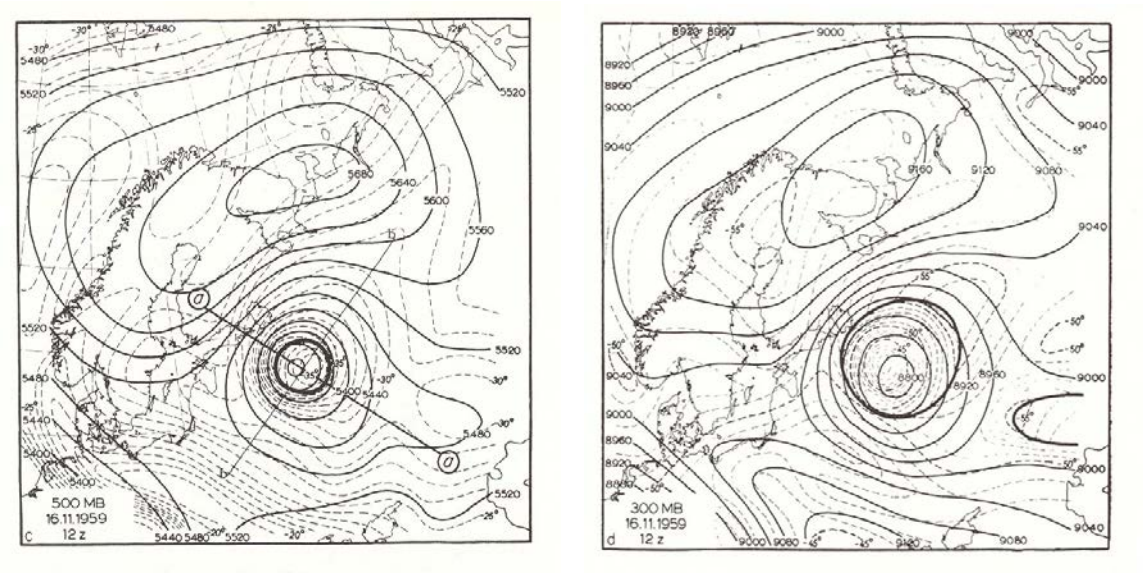

(c) (d)

Fig. 1.6. *Continued*

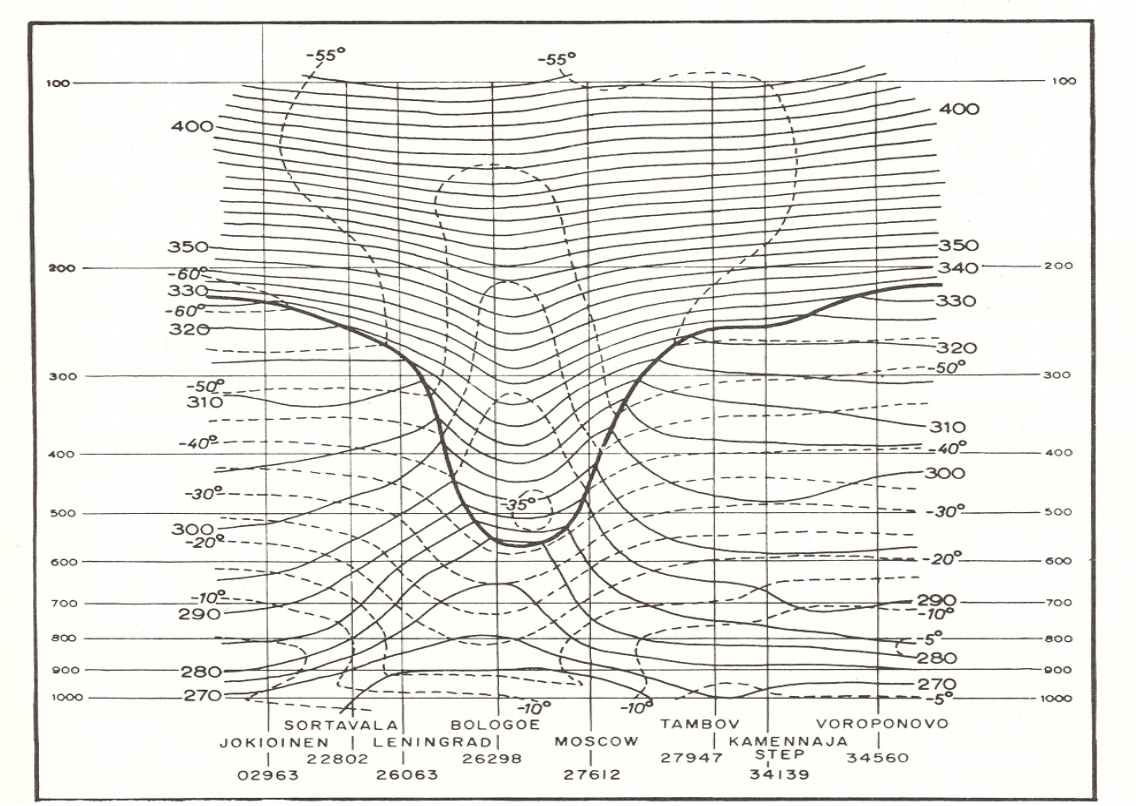

Fig. 1.7. Vertical cross section along line *a—a* in Fig. 1.6c. Left to right along the x-axis is equivalent to northwest to southeast in Fig. 1.6c. Shown is the tropopause (heavy solid line), isotherms (dashed lines, contour interval 5°C), and isentropes (solid lines, contour interval 5 K). Source: Palmén and Newton (1969), Fig. 10.8.

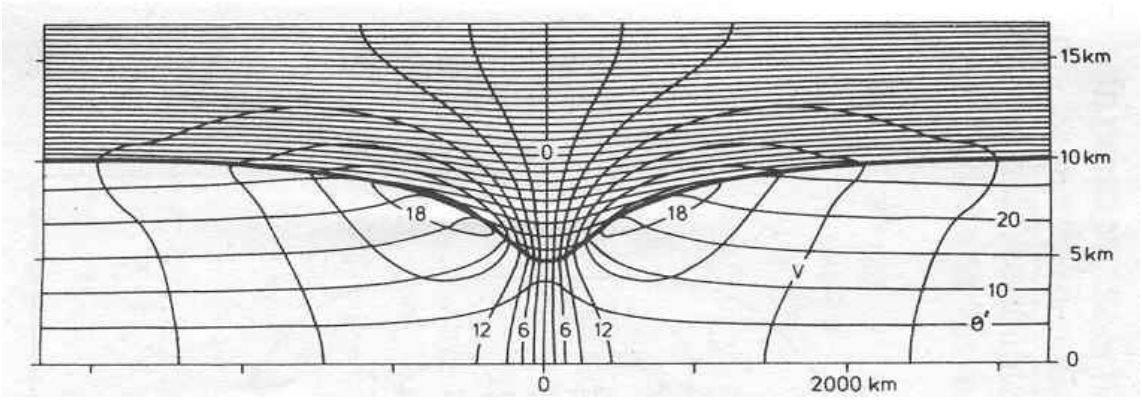

Fig. 1.8. Idealized vertical cross section of a cold-core, upper-level cyclone. Shown are isotachs (v, solid lines, contour interval 3 m s^{-1}), isentropes (θ', solid lines, contour interval 5 K), the tropopause (heavy solid line), and the axis of symmetry (represented by the "0" label on the horizontal axis). Source: Thorpe (1986), Fig. 1.

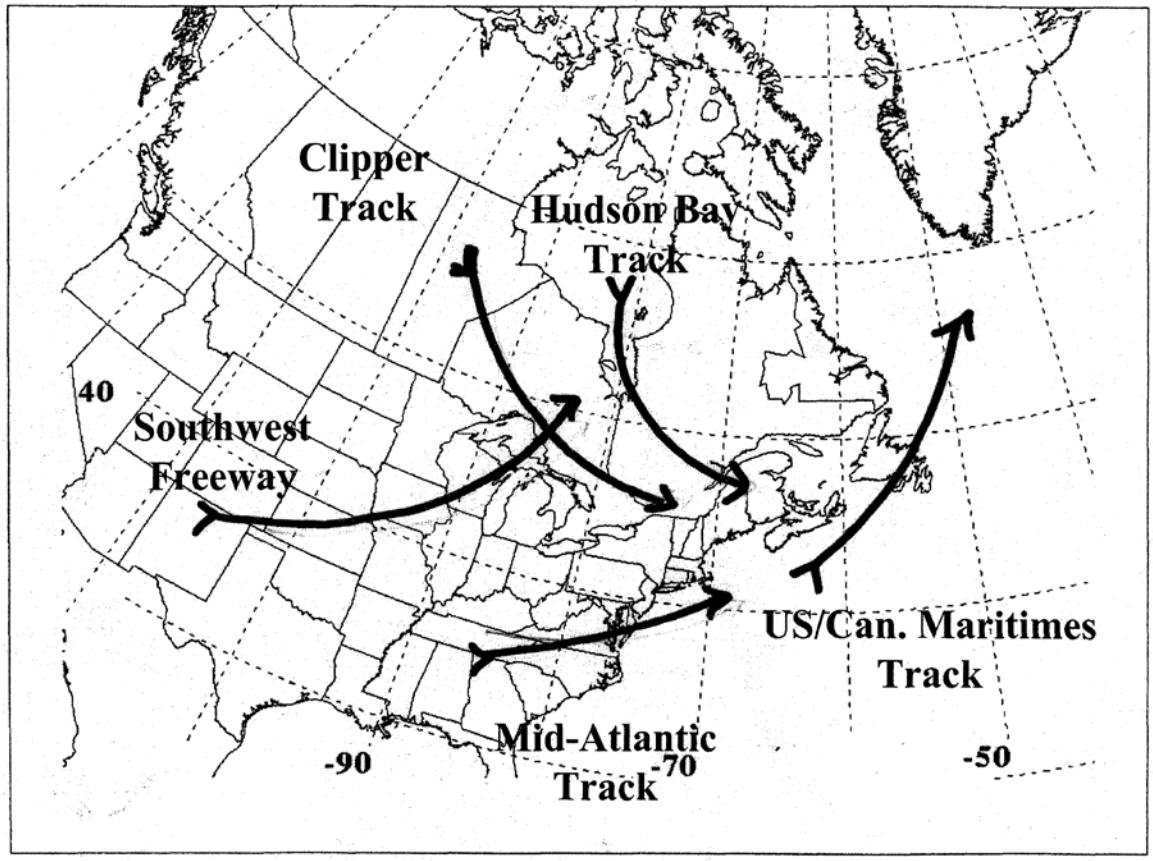

Fig. 1.9. Subjective cool-season mean cutoff cyclone tracks impacting eastern North America. Source: Smith (2003), Fig. 3.84.

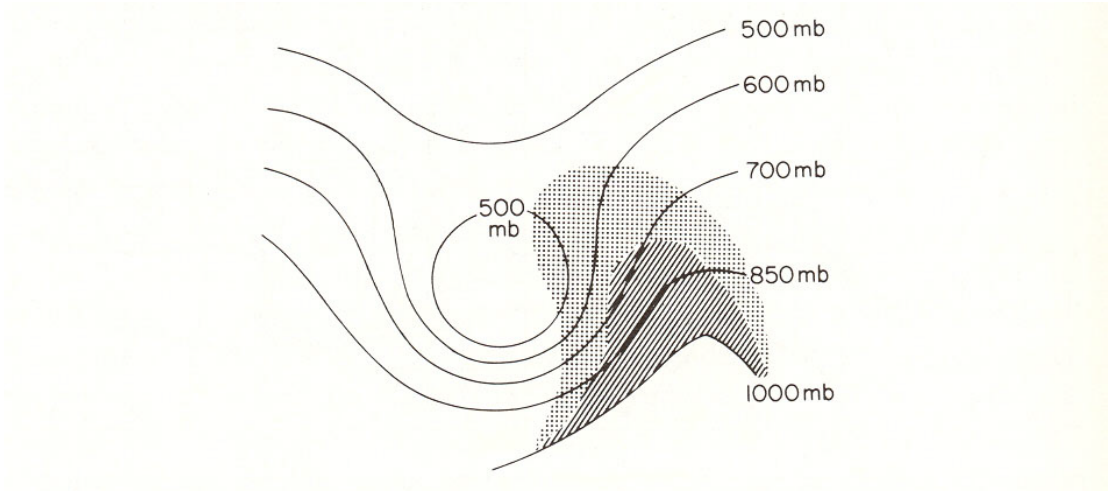

Fig. 1.10. Schematic representation of precipitation relative to upper-level geopotential height contours (solid lines). Heavier precipitation is hatched; lighter precipitation is stippled. Source: Hsieh (1949), Fig. 13.

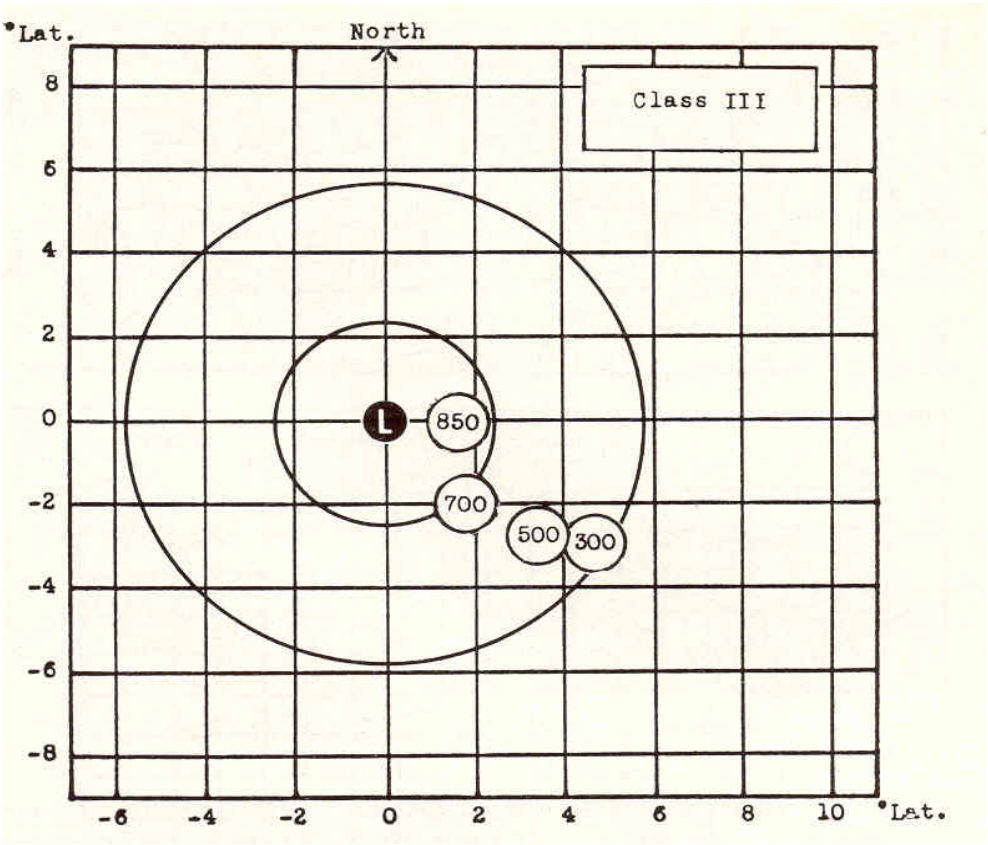

Fig. 1.11. Areas of maximum frequency of occurrence of measurable precipitation associated with the most intense (Class III) lows, centered at the origin for 850, 700, 500, and 300 hPa. Symmetrical circles represent idealized contours about the low center at any level. Source: Klein et al. (1968), Fig. 8.

2. Data and Methodology

2.1 Data Sources

2.1.1 Climatology

The National Centers for Environmental Prediction (NCEP)/National Center for Atmospheric Research (NCAR) reanalysis (Kalnay et al. 1996; Kistler et al. 2001) was used in conjunction with the NCEP Climate Prediction Center (CPC) US Unified Precipitation dataset (UPD) (Higgins et al. 1996). The NCEP/NCAR global reanalysis dataset has 2.5° latitude-longitude spatial resolution and 6 h temporal resolution. Four times daily 500 hPa geopotential height grids for the period 1 January 1948 through 31 December 1998 were used to construct the climatologies. The UPD dataset has a 0.25° latitude-longitude spatial resolution over the continental US and a 24 h (1200 UTC–1200 UTC) temporal resolution. The data are derived from National Climatic Data Center (NCDC) daily co-op stations (1948–2002), River Forecast Centers' data (1992–2002), and daily accumulations from the NCDC Hourly Precipitation Data (HPD) (1948–2002). The UPD is provided by the National Oceanic and Atmospheric Administration (NOAA)-Cooperative Institute for Research in Environmental Sciences (CIRES) Climate Diagnostics Center (CDC), Boulder, Colorado, available at http://www.cdc.noaa.gov/. Plots for the period 1 January 1948–31 December 1998 were used for the climatologies. Throughout the majority of this research, the UPD was only available through 1998. Currently, it has been extended through 31 December 2002.

2.1.2 Case Studies

For all case studies, locally archived NCEP 80 km Eta model 00 h forecasts were used at 12 h intervals for horizontal maps and cross-sectional analyses. When available, 40 km Eta grids at 6 h intervals were also used in analyses for more spatial and temporal detail. Surface observations from the archived National Weather Service (NWS) Automated Surface Observing System (ASOS) and cooperative reporting station data in the Northeast states were used in the development of surface potential temperature (θ) and mixing ratio maps. Radar reflectivity data from NCAR were also used in the case studies. Additional insight was gained from the use of the NWS Weather Event Simulator (WES) at the Binghamton, NY, NWS Forecast Office on the 23–31 May 2003 case study. UPD and locally generated and archived 6- and 24-hourly precipitation maps (derived from ASOS observations) were also used for verification over the Northeast, in conjunction with Co-op reports available through NCDC.

2.2 Methodology

2.2.1 Objective Climatology

The program used to identify and catalog cutoff lows over the 51-year (1948–1998) period was identical to the one used by Smith (2003). It is similar to the methodology used in Bell and Bosart (1989), which defined a cutoff to be at least a 30 m height rise in all directions from a grid point. Figures 2.1a–b show an example of (a) a

cutoff and (b) an open circulation, determined by extending radial arms from grid point "A," (see Smith 2003, section 2.2.1 for a detailed explanation of how the program explicitly determines a cutoff). In this study, as well as in Najuch (2004), only cutoffs that were within an outer domain (Fig. 2.2) bounding the Northeast were considered. The date and location of each cutoff was cataloged and was used as input with the UPD into another program. Precipitation amounts (both zero and nonzero) on days (1200 UTC–1200 UTC) with a cutoff present within the outer domain were summed and subsequently divided by the number of days used. After some consideration of the original output maps, it was decided to make the further requirement that only days with nonzero precipitation (i.e., 0.01" or more) would be counted. It was believed that the following scenario would arise often enough to warrant the change: a cutoff could be in a far corner of the outer domain with an associated precipitation distribution. However, in one corner of the inner domain (to be defined in Chapter 3) it could be dry but the other could have measurable precipitation. In other words, a cutoff in Tennessee could produce rain in southern Pennsylvania but not likely in Maine. On the contrary, this eliminated the possibility of counting a "dry" cutoff. However, after examining multiple maps of precipitation versus cutoff occurrence, this dry situation was virtually nonexistent. The resultant average daily precipitation maps by month for the cool season (October–May) are presented in Chapter 3.

Using the summed total precipitation on days with a cutoff in the outer domain divided by the climatological precipitation at that grid point, monthly maps of the percent of climatology of precipitation were produced. Each map shows the average monthly percentage of precipitation that is associated with cutoff lows in the outer domain.

2.2.2 Subjective Tracking of Cutoffs

Due to the finer scale of this study as compared to Smith (2003), it was deemed necessary to abandon the objective tracking program (see Smith 2003, section 2.2.2) and instead complete a subjective hand analysis of cutoff tracks. A 19-year (1980–1998) subset was used that balanced research time constraints with a significant sample size. Four times daily 500 hPa geopotential height maps were produced for all days in the cool season over the 19-year period (nearly 20,000 maps). Tracks of each cutoff within the outer domain were hand plotted by month, with usually two to three years plotted on a single map for clarity. In this way, cyclones that are initially closed, then "open up," then close again can be counted as one entity, a scenario that was ignored in both Bell and Bosart (1989) and Smith (2003). The individual tracks were then traced with a fine point pen onto tracing paper to fit cutoffs over all or half of the 19 years (depending on how many cutoffs there were that month over the 19 years) on a single map to identify common tracks by month.

From this subset of cutoffs, in conjunction with the mean tracks found earlier and in Smith (2003), a subjectively chosen smaller subset of cutoffs was used for analyses within four of the favored tracks. Precipitation from lows that were deemed close enough to the mean tracks was averaged and used in the track analysis portion of this research. Furthermore, in order to generate the track-relative precipitation distribution, cutoffs that were far enough away from the US border were further eliminated. In general, the 1200 UTC location of the cutoff had to be within one grid point of a grid point that was located

on or very close to US land. Precipitation fields were shifted to a centroid position (the average 1200 UTC ending location) and averaged.

2.2.3 Case Studies

The case studies were chosen based on their recent occurrence as well as their overall impact on the Northeast. The main case study was a multifaceted cutoff with three distinct phases over the period 23–31 May 2003. Several other cases (25–27 December 2002, 3–5 January 2003, and 11–15 May 2003) were used to gain insight into cutoffs of other flavors. The maps produced and their purpose are as follows:

1) 500 hPa geopotential heights and absolute vorticity in order to track the cutoff and its associated vorticity features.
2) 1000 hPa geopotential heights and 1000–500 hPa thickness (ΔZ) in order to assess the cutoff's surface reflection and its role.
3) 850 hPa geopotential heights, temperature, and warm air advection in order to investigate the lower-tropospheric factors conducive to precipitation.
4) 300 hPa geopotential heights and wind speed to examine the jet stream's interaction with the cutoff.
5) 700 hPa geopotential heights, relative humidity, and, as needed, Miller 2-D frontogenesis to document the available lower-tropospheric moisture.
6) Vertical cross sections of potential temperature (θ), normal wind component, vertical velocity (ω), relative humidity, frontogenesis (when applicable), and

absolute vorticity at critical times to investigate the vertical circulation and structure of the cutoff and associated features.

7) Maps of surface potential temperature (θ), mixing ratio, and wind velocity in order to evaluate the existence and possible effects of surface boundaries.
8) Radar reflectivity to verify and supplement surface observations, as well as the evolution of each cutoff's precipitation shield.
9) Precipitation verification maps from the UPD (or, in 2003, CPC's equivalent dataset) and the NWS Taunton, MA, River Forecast Office daily precipitation maps.

The General Meteorology Package (GEMPAK) (e.g., desJardins et al. 1991) was used to produce most of the aforementioned maps. Additional hand-drawn maps were used as necessary to illustrate key features of certain cutoffs.

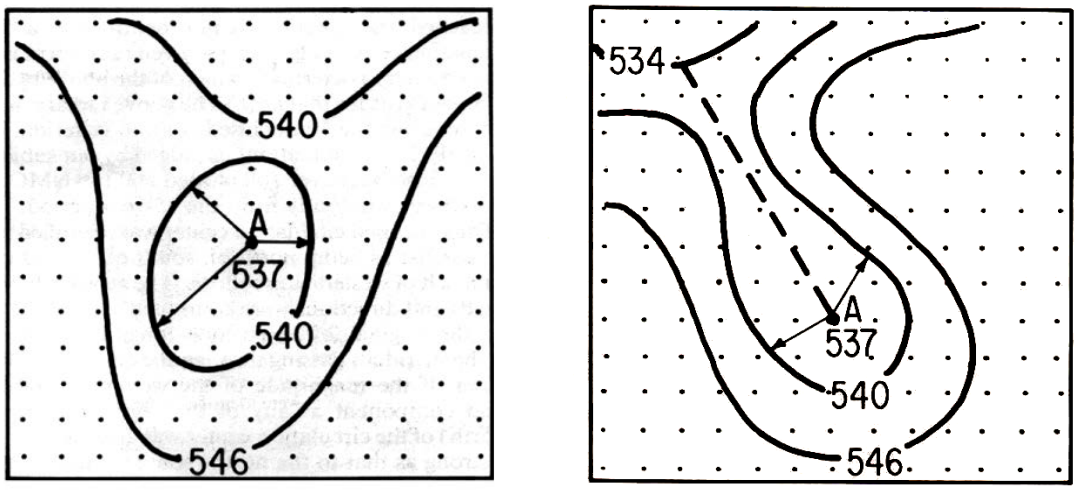

(a) (b)

Figs. 2.1a–b. Sample 500 hPa geopotential height analysis illustrating the objective method used to identify cutoff cyclones: (a) Three sample radial arms out of the actual 20 used to identify a 30 m closed contour around the center grid point of a cutoff cyclone. A geopotential height rise of at least 30 m occurs before a decrease along all arms. (b) As in (a) except that geopotential heights along the dashed radial arm do not exceed 30 m higher than at point A before decreasing. Source: Bell and Bosart (1989), Figs. 1a–b.

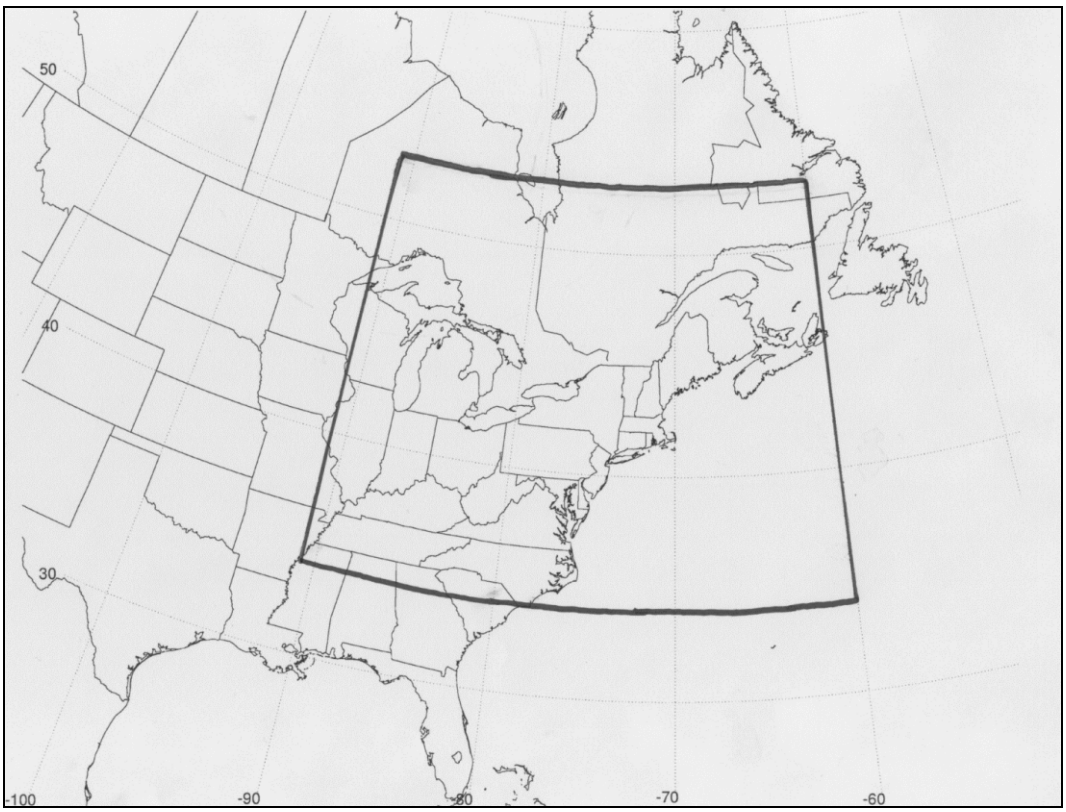

Fig. 2.2. Outer domain bounding the northeast US. Only cutoffs within this box are counted in the climatologies.

3. Results

3.1 Northeast Climatology (1948–1998)

Using the methodology described in Chapter 2 over the period 1 January 1948 through 31 December 1998, a list of cutoff lows with the date and position within the outer domain (Fig. 2.2) was obtained. Figure 3.1 shows a graphical depiction of the percent of observations (0000, 0600, 1200, and 1800 UTC observations define a given day) in which a cutoff low was present in the outer domain on a given day (a "cutoff day") over the year. The graph clearly shows a seasonal swing, with a maximum (minimum) in cutoff activity in mid-spring (late summer). The maximum occurs on 9 April, when nearly 60% of the time a cutoff was observed in the outer domain. This maximum is followed by a marked decrease in cutoff occurrence toward the minimum on 18 July, with a cutoff present in the outer domain less than 10% of the time. Cutoff activity varies slightly between 20% and 40% during fall and winter. On an annual basis, cutoff cyclones are present near the Northeast on 28.6% of the days. The subsequent precipitation maps (Figs. 3.2–3.17) that follow show the inner domain of study. All precipitation maps (Figs. 3.2–3.25) are derived from the aforementioned list of lows.

3.1.1 Average Daily Precipitation by Month

Monthly maps were created that show the average daily precipitation (hereafter, ADP) when a cutoff low was observed within the outer domain and when precipitation

was observed at a given grid point over the period 1948–1998. Figures 3.2–3.9 show the cool season months of October–May, respectively. It is important to note that only data over the US were used; i.e., values over the oceans and Canada are a result of the smoothing program and are not representative of actual data. In the months of October and November (Figs. 3.2–3.3), cutoff lows are associated with about 4–8 mm day^{-1} of precipitation over the Northeast, increasing (decreasing) toward the southeast (northwest). Noted is the area of absolute maximum along coastal Maine. Relative maxima stretch from Connecticut and Rhode Island into Maine. Topographic features show up quite well, especially in November (Fig. 3.3). Local maxima are located over and just to the east of higher elevations, such as the Tug Hill Plateau, Catskills, Berkshires, and Green Mountains. Local minima are generally collocated with lower elevations, such as the Hudson, Mohawk, and Connecticut River valleys. However, it is important to observe that the highest ADP values occur right along the coast at the lowest elevations.

Figures 3.4–3.9 show the months of December–May. Note that the contour interval has changed from 1 mm day^{-1} to 0.5 mm day^{-1} in order to bring out more detail over the area of study in the relatively drier months of December–May. December (Fig. 3.4) shows a similar pattern to October–November (Figs. 3.2–3.3), with the highest values (between 7 mm day^{-1} and 8 mm day^{-1}) along the coast, especially in Maine. Noted are the local maxima just east of Lakes Ontario and Erie, evidence of the onset of the lake-effect snow season. The lowest ADP amounts in December occur in western New York and Pennsylvania (except for east of Lakes Erie and Ontario) and along the Canadian border in northern New York and New England. This pattern is also evident in

January (Fig. 3.5), but with lower amounts area-wide. In fact, January has the lowest area-wide ADP values of all the cool season months.

February and March (Figs. 3.6–3.7) show a slight increase in ADP values across the area, with little change in the overall distribution. Local maxima occur slightly east of higher elevations, while local minima are nearly collocated with lower elevations. Areas of absolute maxima (greater than 7 mm day^{-1}) still occur along the coast, appearing along coastal Massachusetts in February (Fig. 3.6). The area east of Lake Erie has its lowest ADP values in February, likely due to the lake freezing over by this month. In March (Fig. 3.7), the highest values appear in Rhode Island and also along coastal southwestern Maine. Previous months showed a dual maximum in coastal southwestern and eastern Maine, but March values over eastern Maine are markedly lower than those over southwestern Maine. Nearly all areas show an increase in ADP values in March over February, except for the eastern portions of Maine and Massachusetts.

Figures 3.8–3.9 show April and May, respectively, the last two months of the cool season. Values of ADP are lower than the two previous months over the eastern portion of the Northeast, but higher over the western portion of the area (i.e., western New York and Pennsylvania). The area of ADP greater than 5 mm day^{-1} shifts smartly inland by May (Fig. 3.9), along with a considerable decrease in gradient across the area. Areas of absolute maxima during April (Fig. 3.8) are located in coastal southwestern Maine and in Rhode Island, similar to March (Fig. 3.7), but with values only over 6 mm day^{-1} rather than over 7 mm day^{-1}. By May (Fig. 3.9), the absolute maximum occurs right over Mount Washington in northern New Hampshire, with local maxima in southwestern Maine, the Berkshires in northwestern Massachusetts, and eastern central Pennsylvania.

The effect of topography appears to diminish by May, with less contrast (~1 mm day^{-1}) between higher mountain elevations and lower river valley elevations.

3.1.2 Percent of Climatology by Month

Based on the methodology described in section 2.2.1, maps showing the percentage of precipitation in association with cutoff lows with respect to the monthly climatological average were created. The months of October through May are shown in Figs. 3.10–3.17, respectively. Note that the shading does not extend over the ocean or Canada. This was a result of a different plotting program that confined the data to within the US land boundary. The data tended toward either zero or over 100% at the edges, so it was deemed more eye-pleasing to restrict the plotted data to land only.

October and November are shown in Figs. 3.10 and 3.11, respectively. Nearly the entire area shows that greater than 50% of the precipitation in these months is in association with cutoff lows. The gradient follows an east–west orientation, with the highest values (65%–70%) near the coastline. In both months, distinctions between higher and lower elevations are muted, compared to the ADP maps. In fact, the only easily recognizable features are the Catskills. However, with a finer contour interval (2.5%, not shown), the Berkshires appear as slight local maximum.

The months of December and January (Figs. 3.12 and 3.13, respectively) show an overall decrease in values over the area. The gradient of values (from lower to higher) now has a southwest–northeast orientation, with the highest values in Maine (55%–60% in December and 50%–55% in January). Again, orographic features are not well-defined,

except perhaps for the Catskill and Berkshire Mountains. Note that January shows the lowest values over the area, with roughly one third to one half of the precipitation in association with cutoff lows.

Figures 3.14 and 3.15 show a substantial increase in values during February and March, respectively. The gradient is still present in its southwest–northeast orientation. By March, nearly all of the area is again over 50% (similar to October and November) and roughly half of the area is over 60%, with the highest values still primarily located in Maine. Orographic features are essentially indistinguishable in both months, with the Catskills the exception.

April and May (Figs. 3.16 and 3.17, respectively) show a similar pattern of values compared to February and March. April shows that the entire area is over 50%, and about 75% of the area is over 60%. Local maxima are evident just west of the Connecticut River in Vermont and Massachusetts, and also near the Catskill Mountains. May values decrease slightly overall, but remain almost entirely above 50% across the Northeast.

3.2 Cutoff Track Climatology (1980–1998)

Based on four of Smith's (2003) five favored tracks impacting eastern North America (Fig. 1.9), a subset of cutoff lows, separated by track, from the period 1980–1998, was chosen. The precipitation data on cutoff days were then used in a similar manner as the monthly ADP maps to show ADP for cutoffs of each track. A further subset was then used, based on the proximity of the cutoffs' 1200 UTC ending location to

US land, to produce track-relative ADP maps. Note that geography is meaningless in these maps when related to ADP values, but is displayed for scale. The contour interval is not consistent among the maps, since using the smallest contour interval can show the greatest detail.

Figure 3.18 shows ADP for cutoff days with Mid-Atlantic type tracks for 41 closed lows over 80 days, contoured at a 1.5 mm day^{-1} interval. Clearly evident is a coastal preference, especially in southeast New England in Massachusetts. An orographic signal is more pronounced away from the immediate coastline, as noted by the locally higher (lower) values in the higher (lower) elevations such as the Catskills, Berkshires, and Green Mountains (Hudson and Connecticut River valleys). Overall, values tend to increase from northwest to southeast, but increase more rapidly approaching the area of highest ADP values. Mid-Atlantic track lows produce the highest grid-point maximum value of precipitation for the four tracks.

The storm-relative precipitation distribution from Mid-Atlantic track cutoffs is shown in Fig. 3.19, contoured at a 1 mm day^{-1} interval. A subset of 60 days was used from the initial 80 days of Mid-Atlantic track cutoffs. The average starting and ending positions for each of the 60 days, as shown by the solid circle and "X," respectively, were connected to obtain an average track (black line). The area of heaviest ADP values occurs just to the north and northeast of the cutoff's 24 h ending position by about 400 km. From the perspective of the cutoff, the heaviest precipitation occurs directly out in front and just to the left of its path. Values decrease steadily and at similar rates on either side of the plotted track, as well as on either side of an extrapolated track to the northeast of the indicated average ending position.

The Southwest track ADP map is shown in Fig. 3.20. This includes 59 cutoff days and 37 individual cutoff lows. Again evident is a coastal preference for the area of maximum precipitation, extending from southwestern Maine to Connecticut and Rhode Island, as well as northern New Jersey. Higher (lower) elevations are vividly represented by higher (lower) values in the Adirondacks, Berkshires, Catskills, and Poconos (Hudson, Mohawk, and northern Connecticut River valleys). Also notable is a sizable area of locally higher values in the northern portions of lower Michigan. The ADP amounts decrease quickly near the areas of local maximum values, then decrease steadily outside of the inner domain (thinly boxed area).

Figure 3.21 shows the storm–relative ADP values for Southwest track cutoffs, plotted similarly to Fig. 3.19. The precipitation data from 48 cutoff days (37 individual cutoffs) were used to obtain this result. A striking finding is that the area of maximum ADP values occurs well to the east of the cutoff's 24 h ending position. The areal extent of greater than 1 mm day^{-1} is quite large—roughly 2000 km in either the east–west or north–south direction. If the plotted track is extrapolated towards the northeast, it can be imagined that the heaviest precipitation is preferentially located just to the right of the cutoff's track. Cutoffs following the Southwest track are also quite wet, similar to Mid-Atlantic track cutoffs, with many areas averaging over 9 mm day^{-1}.

The ADP from 58 cutoff days (30 individual cutoffs) following the Clipper track is shown in Fig. 3.22. Note that the contour interval has changed to 0.8 mm day^{-1} to show more detail for these comparatively drier systems. The distribution shows a wet bias towards New England, with the heaviest amounts in eastern New Hampshire and southeastern Massachusetts. These areas of absolute maxima are again located near the

coast in the lowest elevations. The area of greater than 1.6 mm day^{-1} appears to fan out from Lake Erie to the northeast and southeast with the highest values in the center. The higher (lower) elevations of the Berkshires, Green and White Mountains, and the Catskills (Hudson and Connecticut River valleys) show locally higher (lower) values. In New York, the Tug Hill plateau features a stark local maximum, suggestive of a strong lake–effect signal, and is centered over and just to the west of the highest elevation. To the east of Lake Erie, south of Buffalo, is another local maximum of similar area, but lower maximum value, also suggestive of lake–effect precipitation in the higher elevations in southwestern New York.

Figure 3.23 shows the storm-relative ADP distribution over 35 cutoff days (24 individual cutoffs) for lows following the Clipper track. The contour interval is now 0.5 mm day^{-1}, again to show more detail. The area of highest values occurs just ahead of the average 24 h ending position, decreasing at similar rates on either side of the track. From the cutoff's perspective, the area of maximum precipitation is located along and just to the left of the track; again, ahead of the cutoff, similar to Southwest Track cutoffs. Another area of locally higher values (for reference only, located north of Lake Ontario) occurs just to the west of the cutoff's average 24 h ending position, with ADP values up to 5 mm day^{-1}.

Cutoff lows following the Hudson Bay track produce the ADP map shown in Fig. 3.24. Here, precipitation data from 75 cutoff days (51 individual cutoffs) were used. Note that the contour interval has lowered to 0.4 mm day^{-1} since cutoffs following this track are drier than cutoffs from the previous track. The area of highest ADP values occurs in northeastern Maine, but other local maxima occur elsewhere. Mount

Washington, Mount Mansfield in Vermont, and the area just southeast of Lake Ontario (just to the southwest of the Tug Hill plateau) stand out as favored areas for precipitation in association with Hudson Bay cutoffs. The first two areas are related to topography, but the third is located just south of the highest elevations, indicating that this area is perhaps a result of the typical wind trajectory over the lake associated with cutoffs of this track. The Hudson and Connecticut River valley local minima show up in northern New York State and New England, respectively. Other notable local maxima are on Cape Cod (perhaps a response to ocean–effect precipitation), and in West Virginia (a topographic signature).

Figure 3.25 shows the storm-relative ADP for 39 cutoff days (35 individual cutoffs), with a lower contour interval (0.25 mm day^{-1}) than the Clipper Track. Precipitation in association with Hudson Bay cutoffs tends to closely follow the track of the cutoff, with the area of highest values along the track, decreasing at similar rates on either side away from the track. In addition, the most precipitation occurs directly in front of the cutoff's average track. Note that data near the average starting point cannot be taken as zero since these cutoffs originate in Canada, far outside the domain of the UPD.

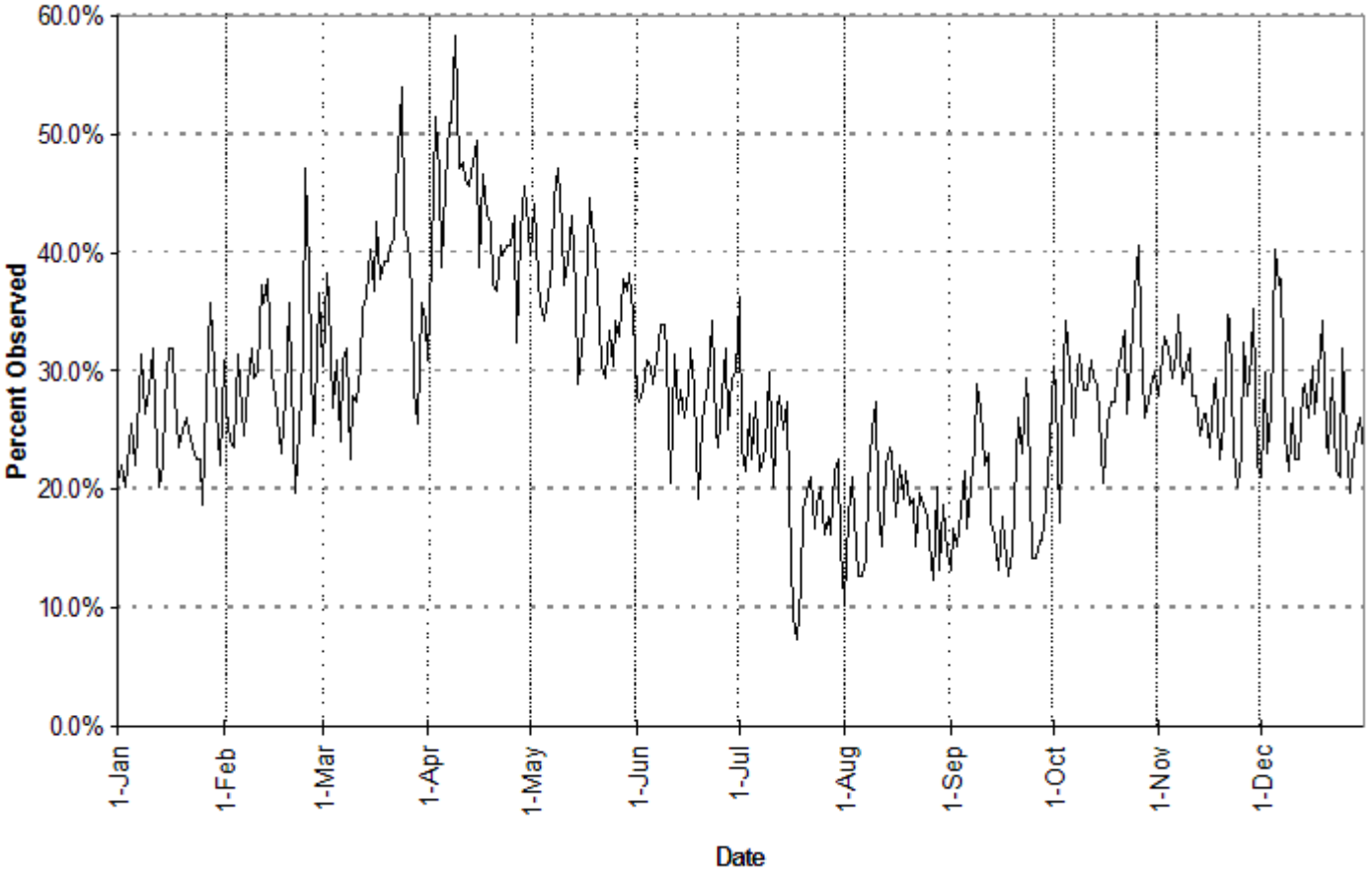

Figure 3.1. Daily percent of observations from 1 January through 31 December with at least one cutoff low detected in the outer domain (Fig. 2.2) averaged over the period 1948–1998.

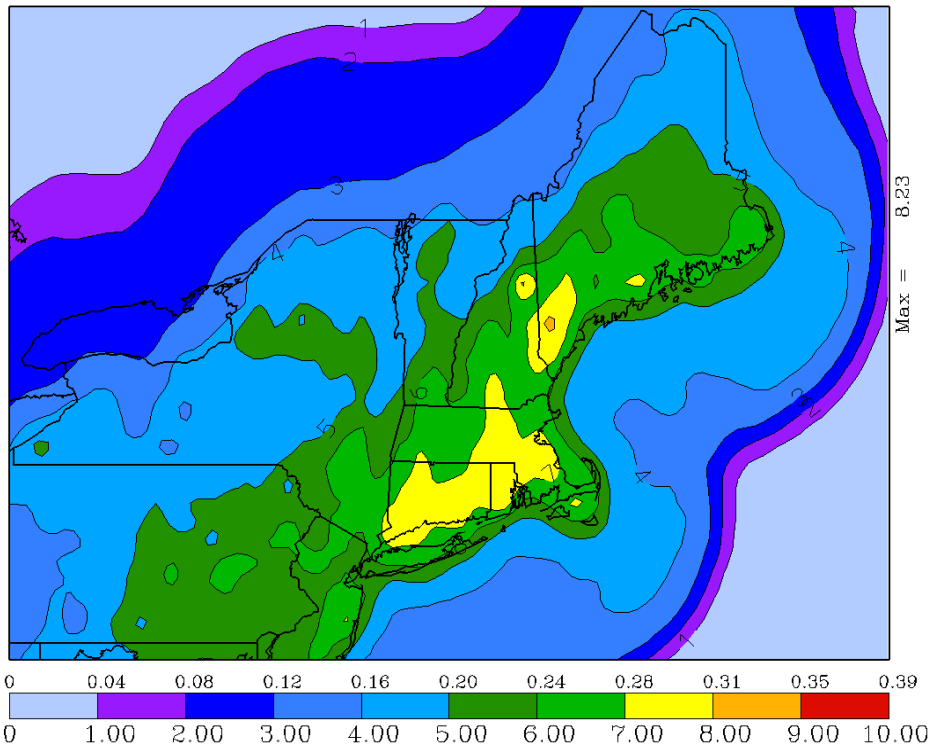

Fig. 3.2. Average daily October precipitation for 1948–1998 where a cutoff low was present in the outer domain and precipitation was observed. Amounts are contoured every 1 mm day^{-1} (shown on the bottom of the color bar) or ~ 0.04 in day^{-1} (on the top).

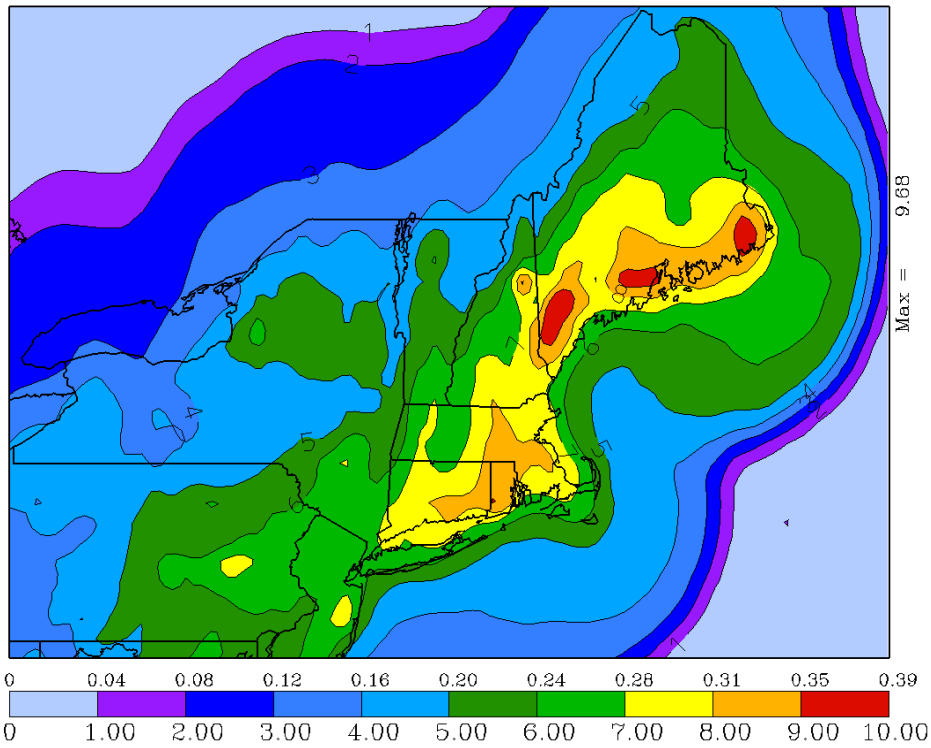

Fig. 3.3. As in Fig. 3.2 but for November.

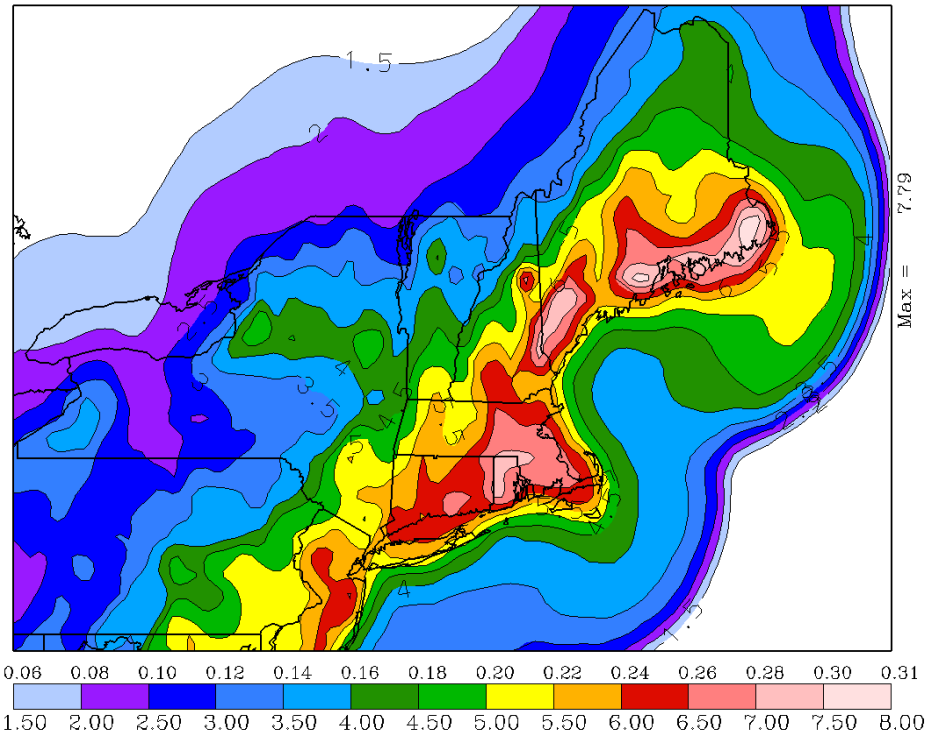

Fig. 3.4. As in Fig. 3.2 but for December. Contour interval is 0.5 mm day^{-1} (on the bottom of the color bar) and ~ 0.02 in day^{-1} on the top.

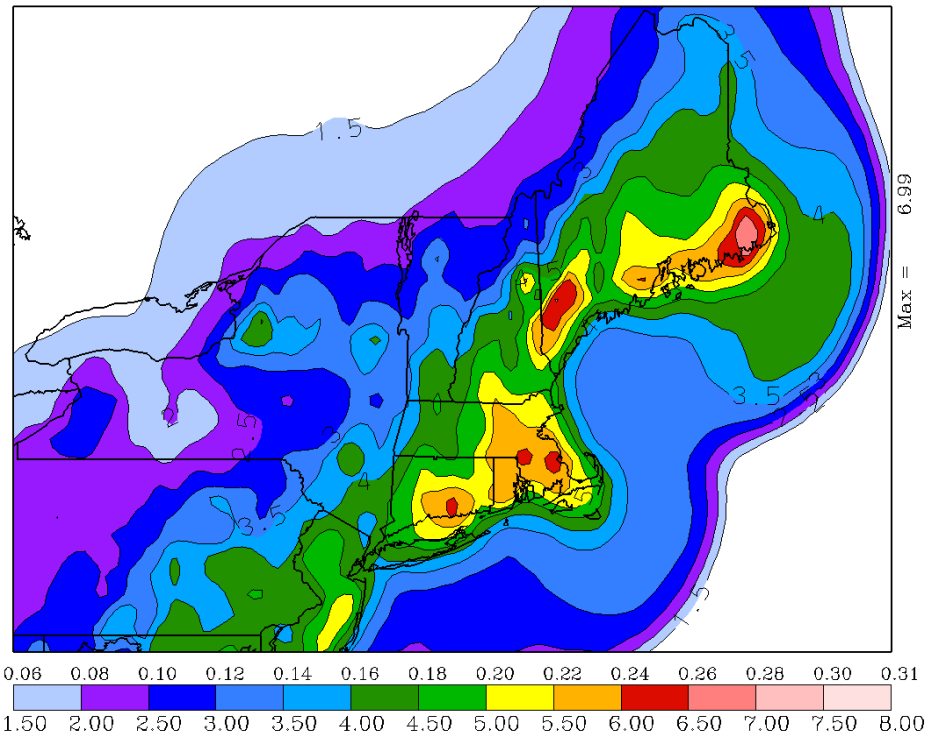

Fig. 3.5. As in Fig. 3.4 but for January.

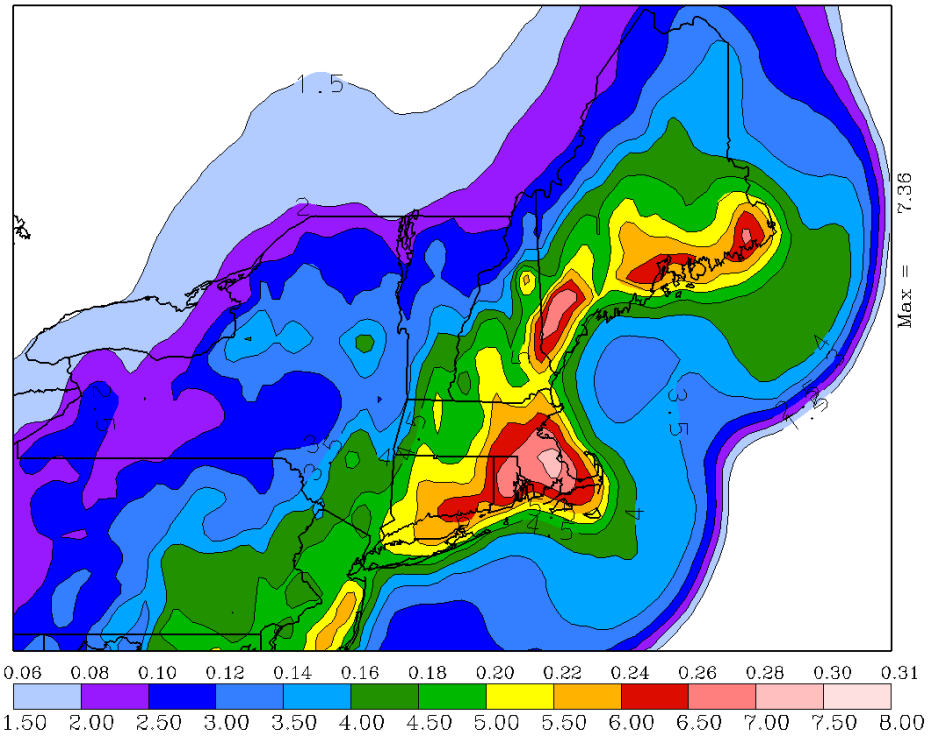

Fig. 3.6. As in Fig. 3.4 but for February.

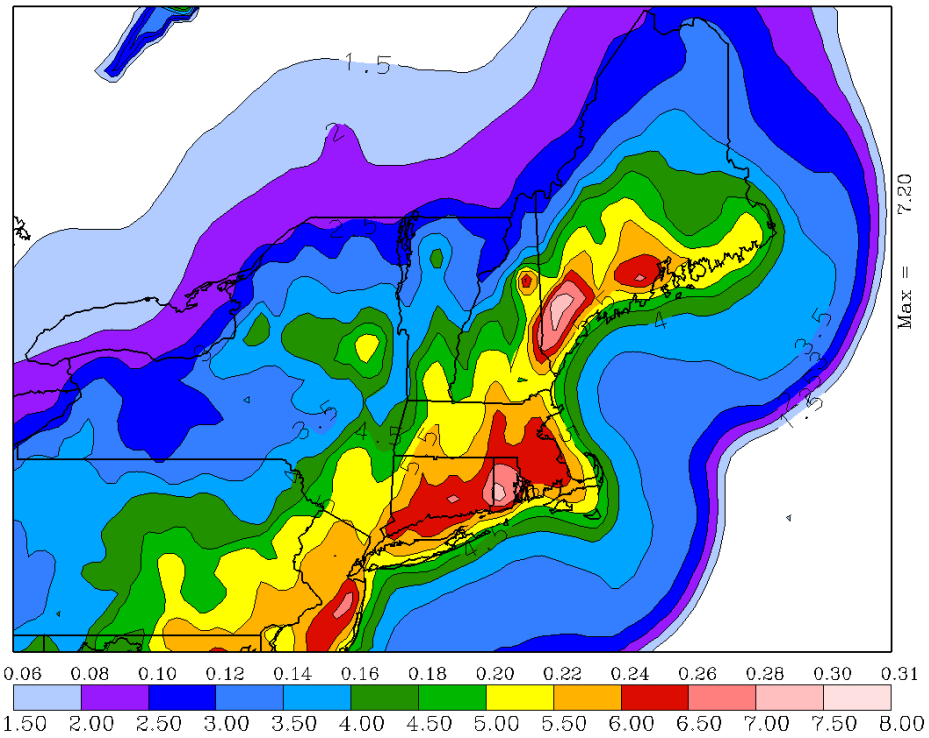

Fig. 3.7. As in Fig. 3.4 but for March.

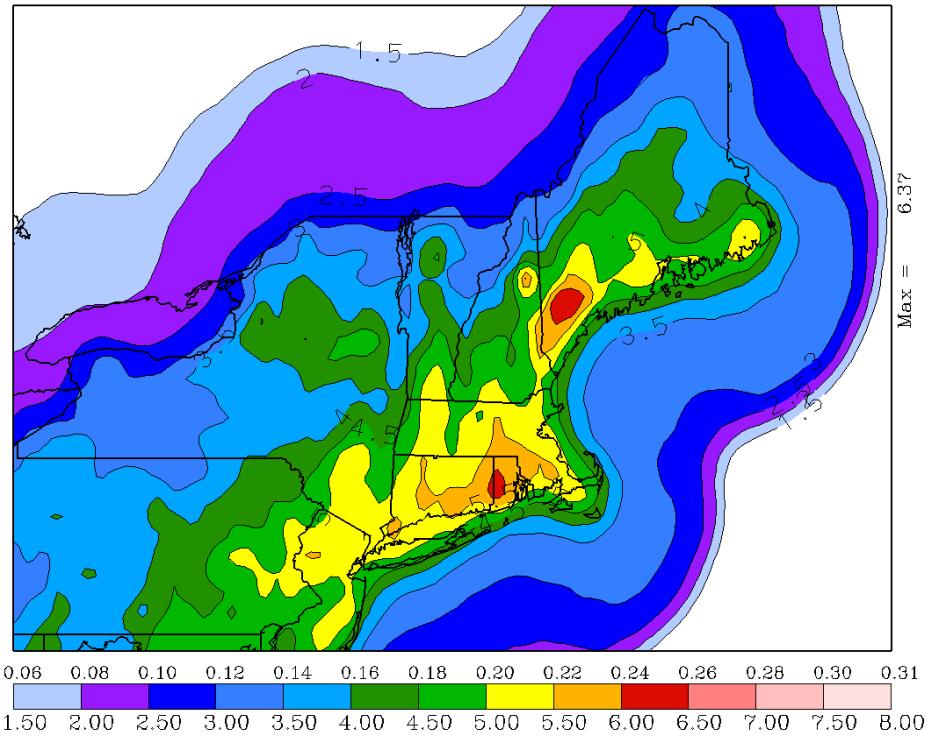

Fig. 3.8. As in Fig. 3.4 but for April.

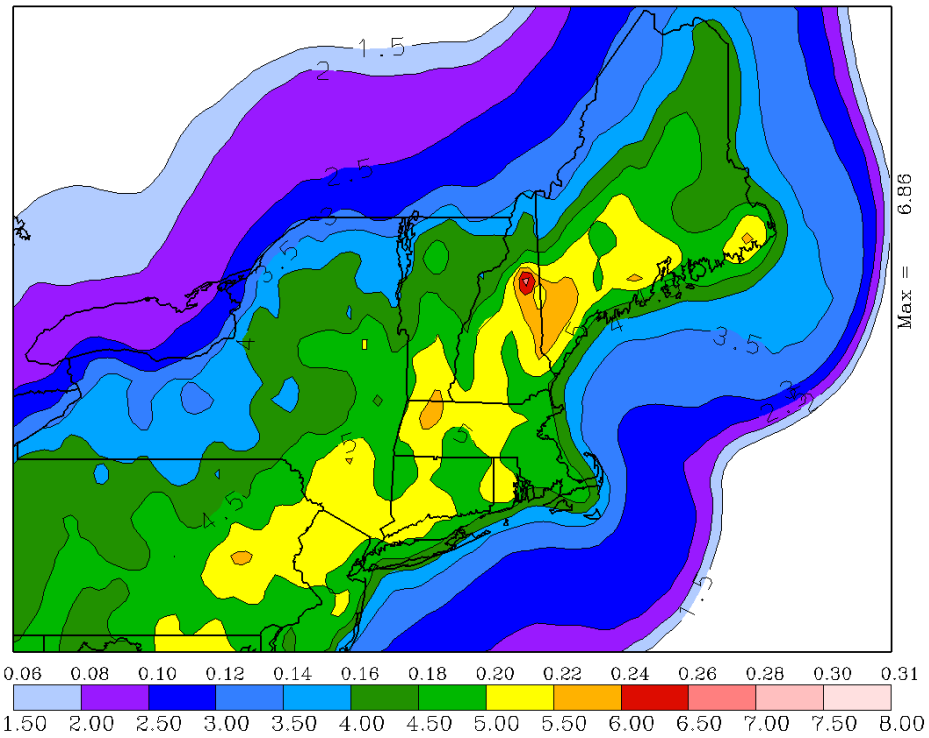

Fig. 3.9. As in Fig. 3.4 but for May.

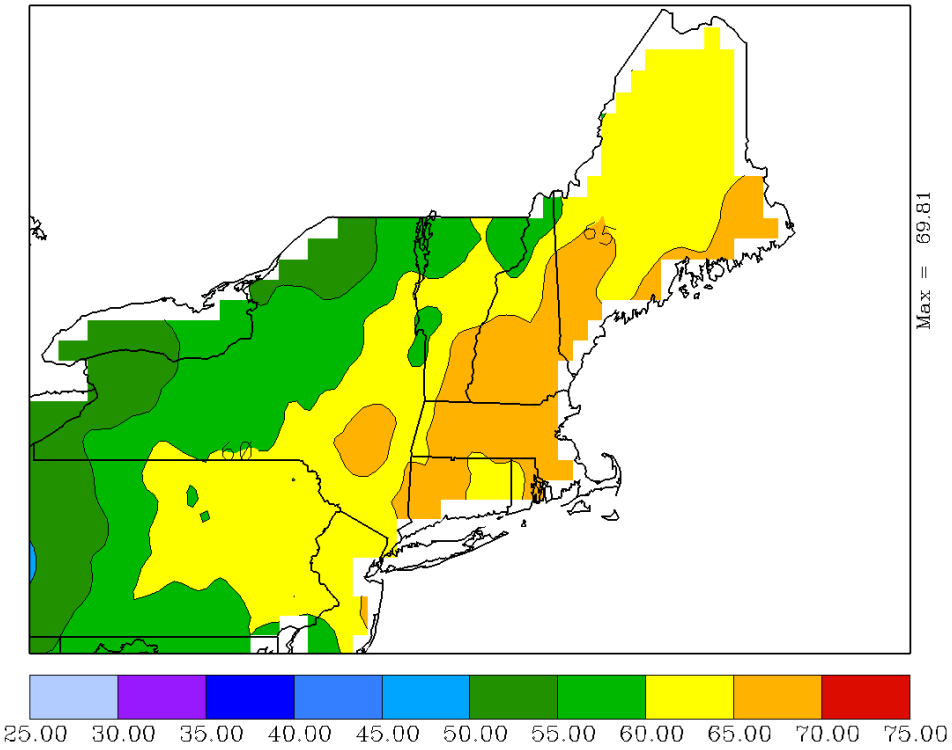

Fig. 3.10. Average percent of the climatological precipitation in association with cutoff lows for October. Contour interval 5%.

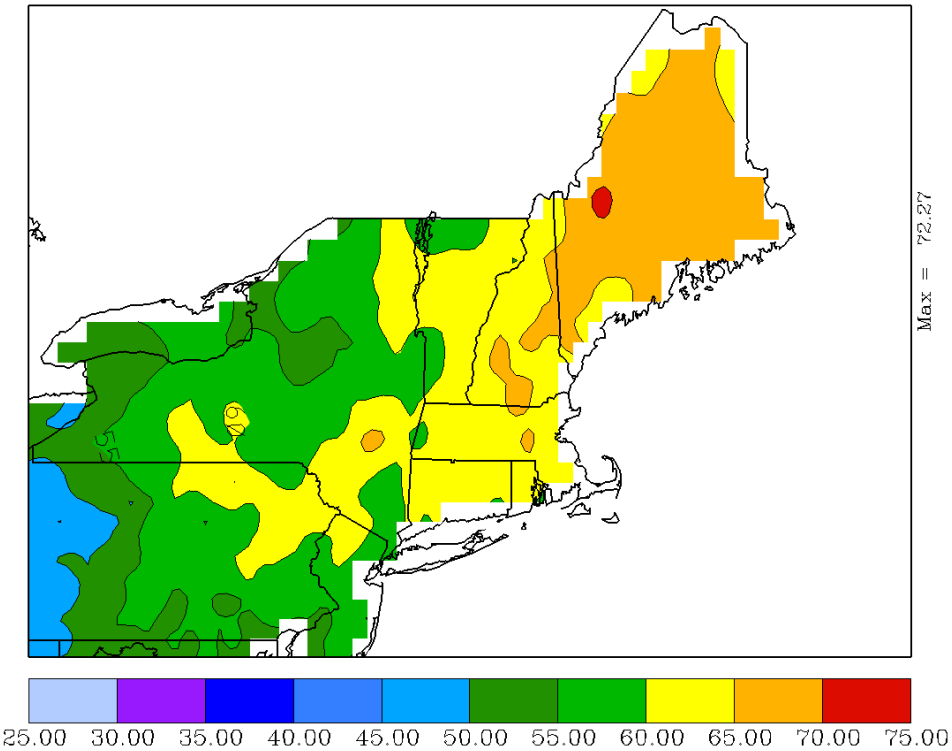

Fig. 3.11. As in Fig. 3.10 but for November.

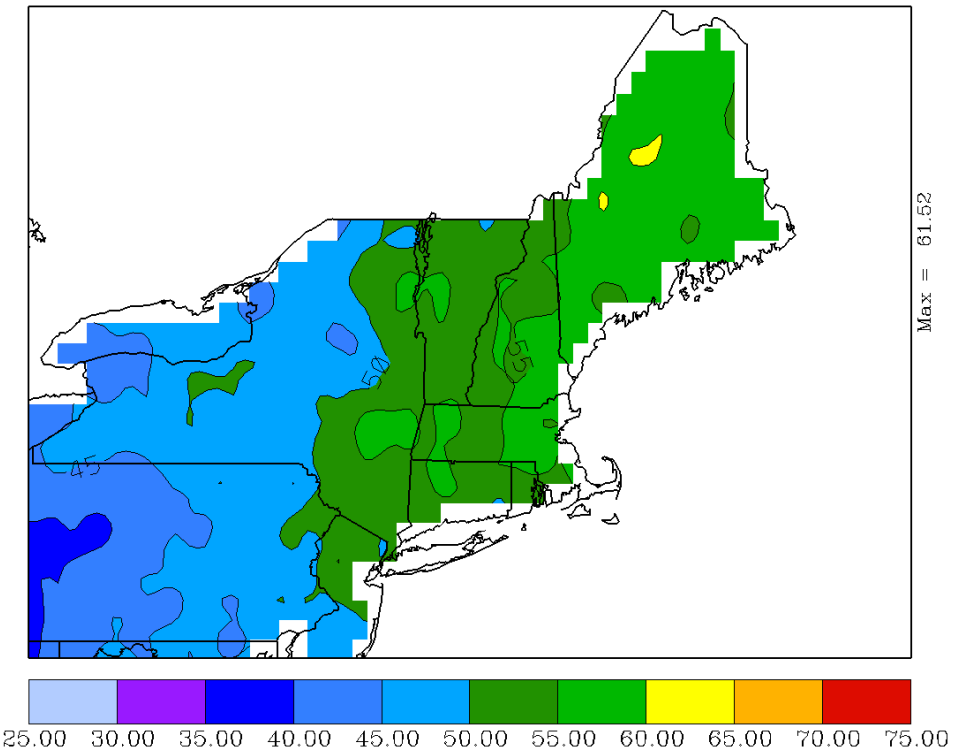

Fig. 3.12. As in Fig. 3.10 but for December.

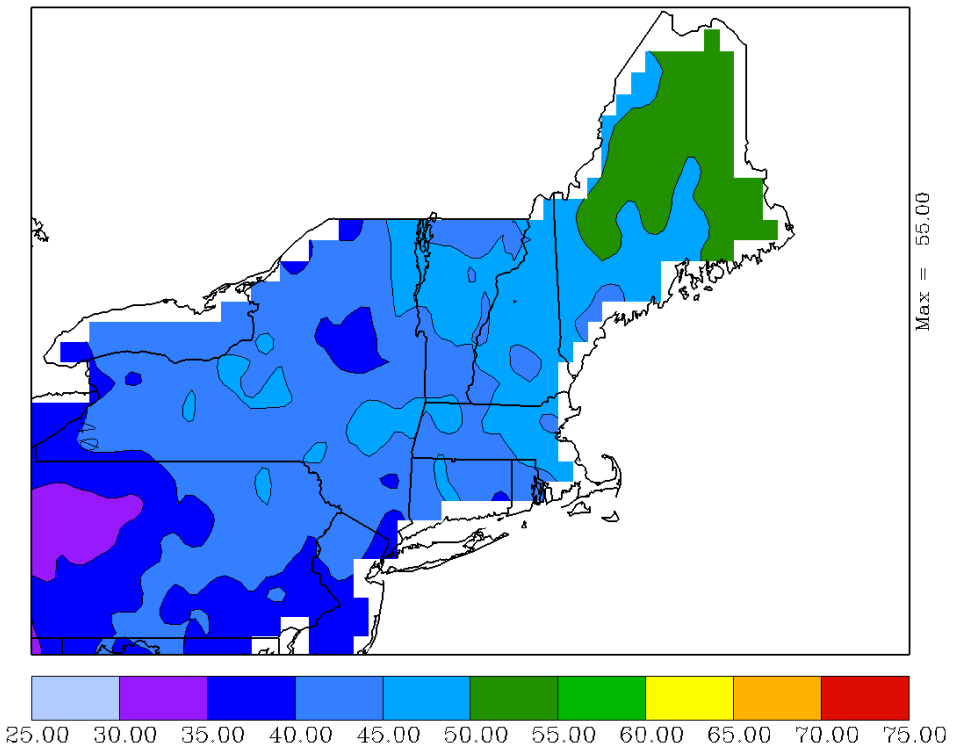

Fig. 3.13. As in Fig. 3.10 but for January.

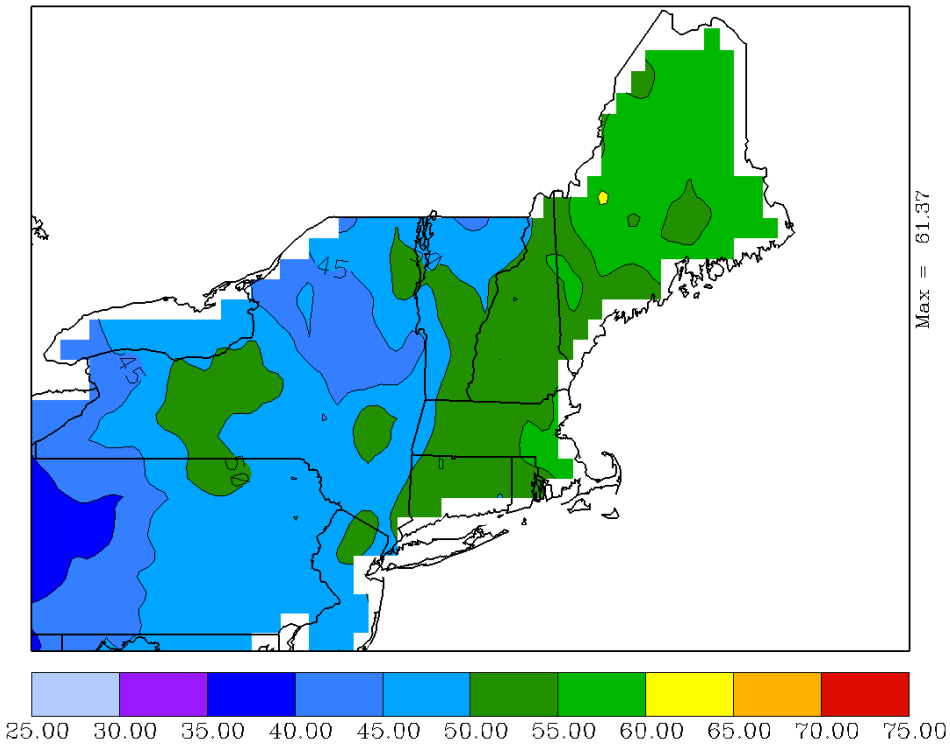

Fig. 3.14. As in Fig. 3.10 but for February.

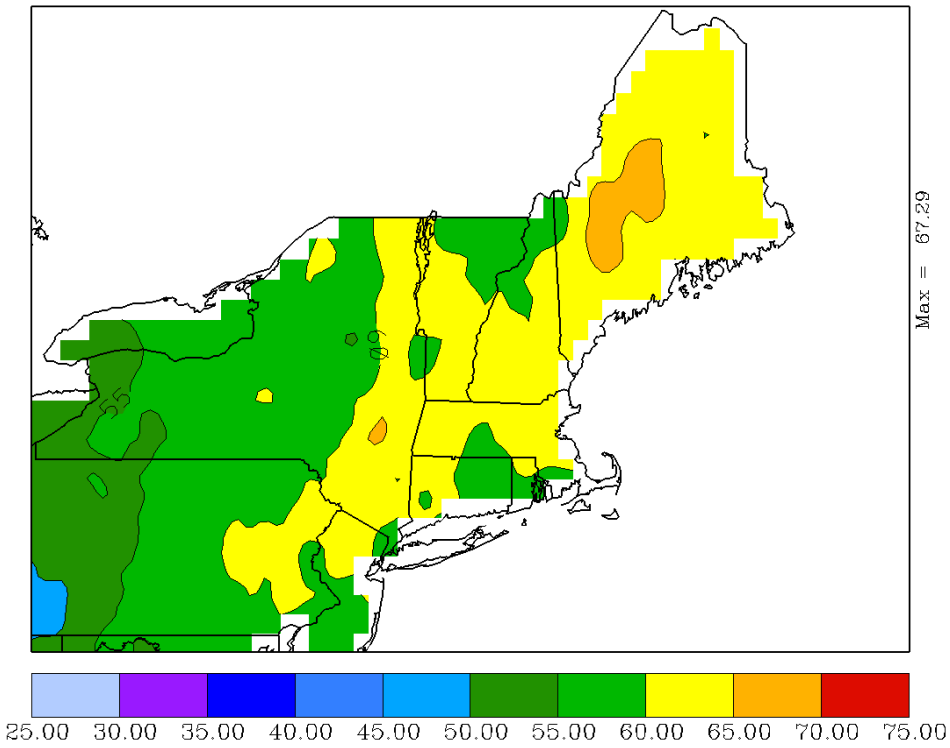

Fig. 3.15. As in Fig. 3.10 but for March.

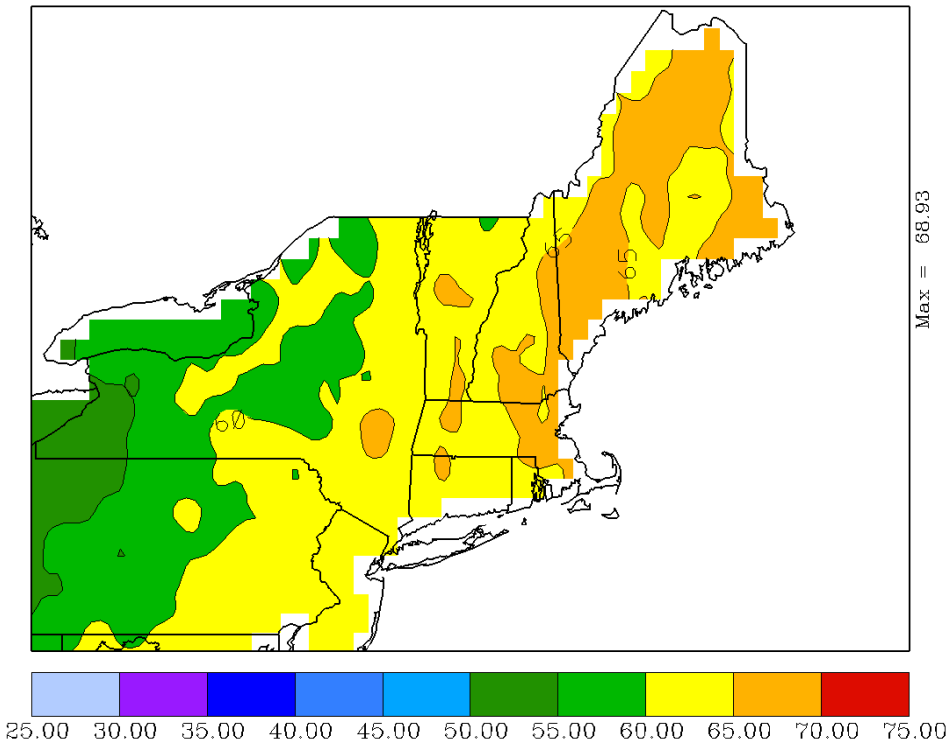

Fig. 3.16. As in Fig. 3.10 but for April.

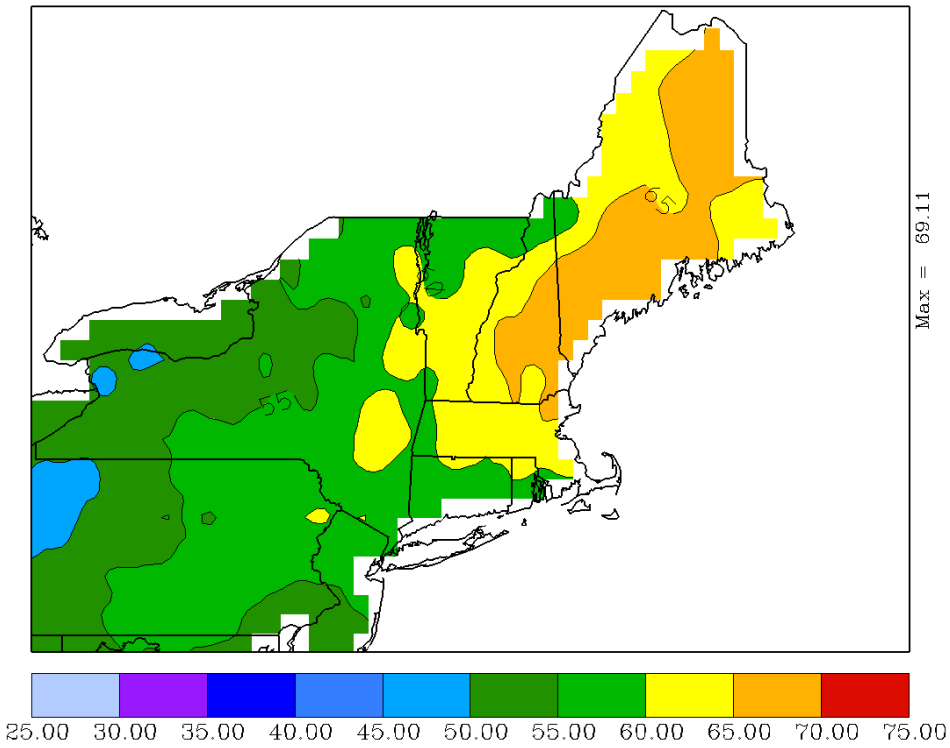

Fig. 3.17. As in Fig. 3.10 but for May.

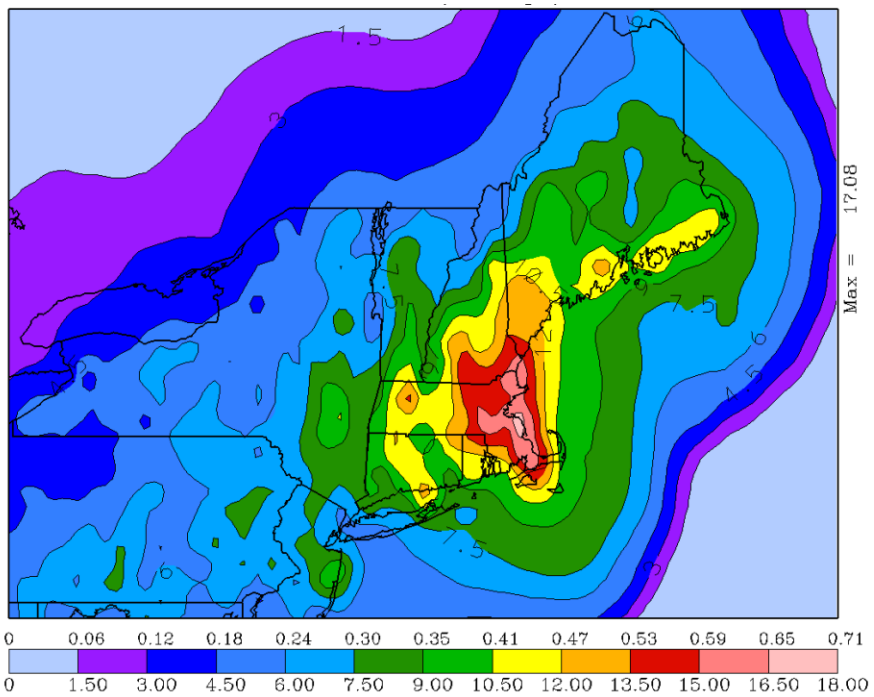

Fig. 3.18. Average daily precipitation over 80 cutoff days for lows that followed the Mid-Atlantic track. Contour interval is 1.5 mm day^{-1} (~0.06 in day^{-1}).

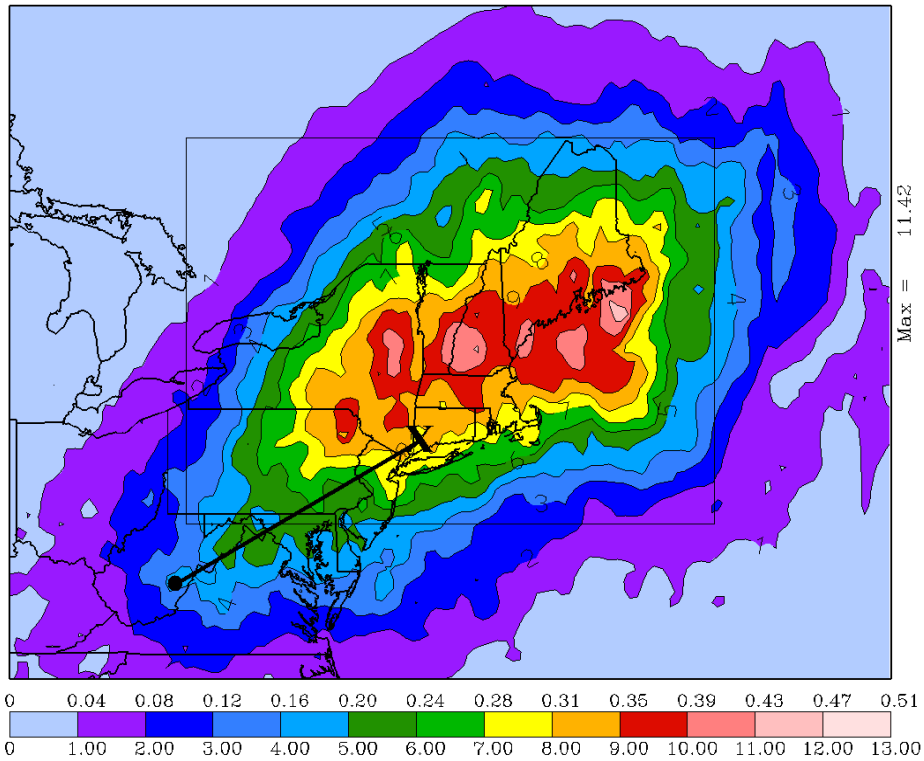

Fig. 3.19. Storm-relative average daily precipitation over 60 cutoff days for lows that followed the Mid-Atlantic track. Average starting and ending positions are represented by the solid circle and "X," respectively, along with the resultant average track. Contour interval is 1 mm day^{-1} (~0.04 in day^{-1}).

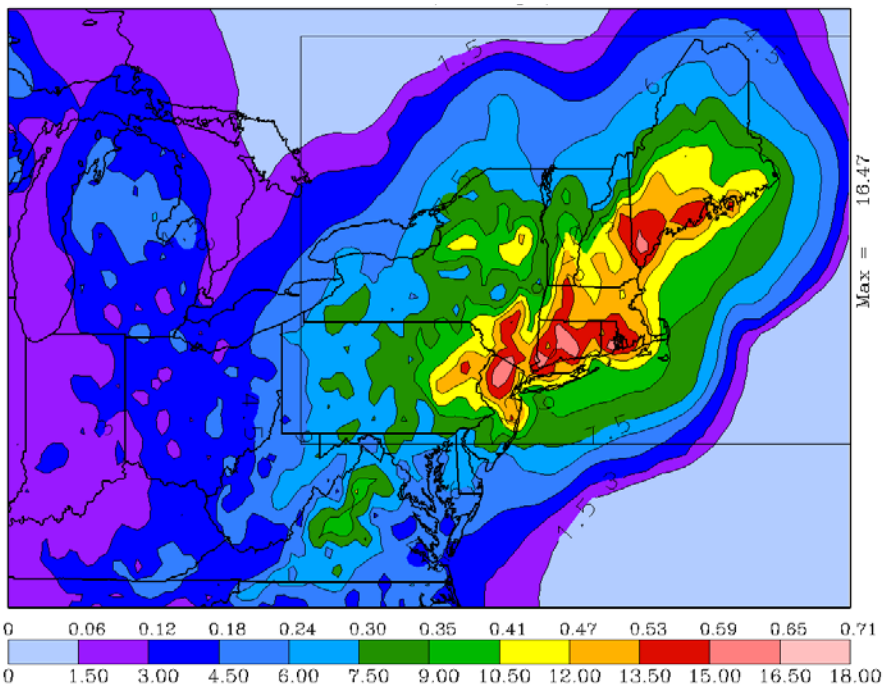

Fig. 3.20. Average daily precipitation over 59 cutoff days for lows that followed the Southwest track. Contour interval is 1.5 mm day^{-1} (~0.06 in day^{-1}).

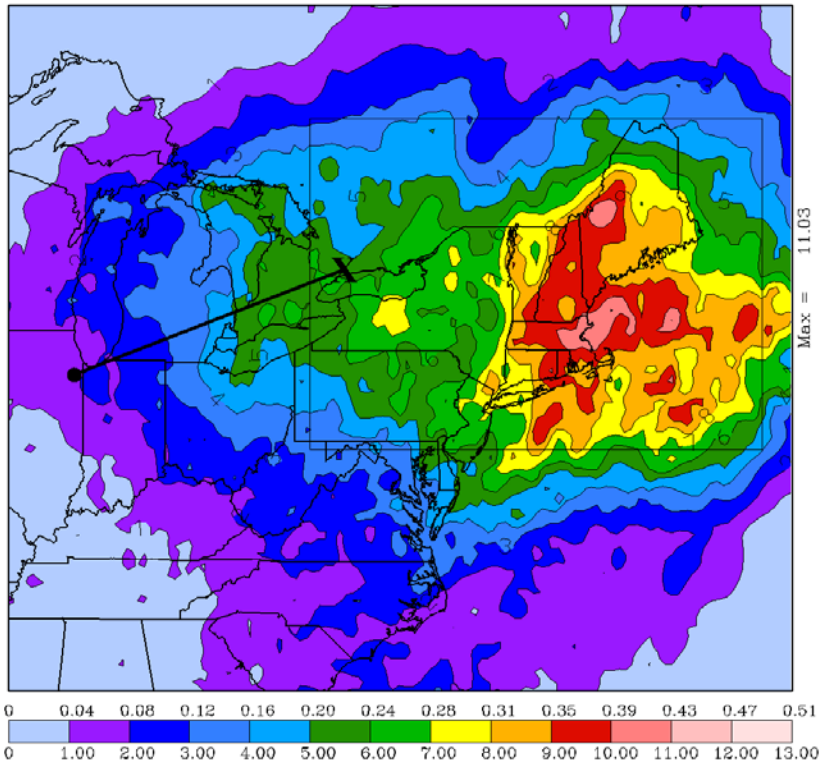

Fig. 3.21. Storm-relative average daily precipitation over 48 cutoff days for lows that followed the Southwest track. Average starting and ending positions are represented by the solid circle and "X," respectively, along with the resultant average track. Contour interval is 1 mm day^{-1} (~0.04 in day^{-1}).

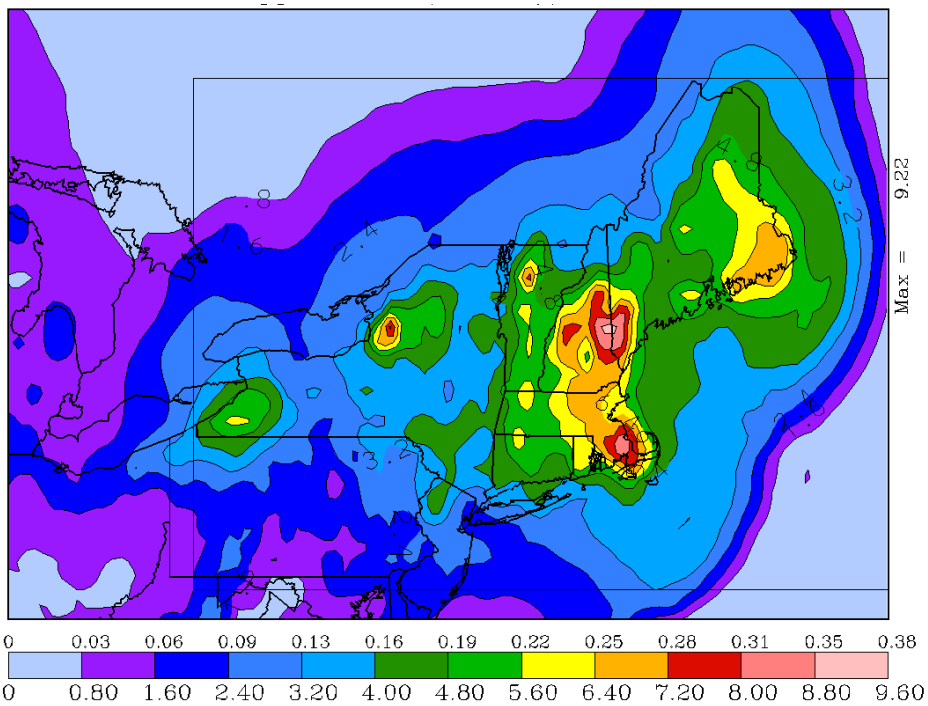

Fig. 3.22. Average daily precipitation over 58 cutoff days for lows that followed the Clipper track. Contour interval is 0.8 mm day^{-1} (~0.03 in day^{-1}).

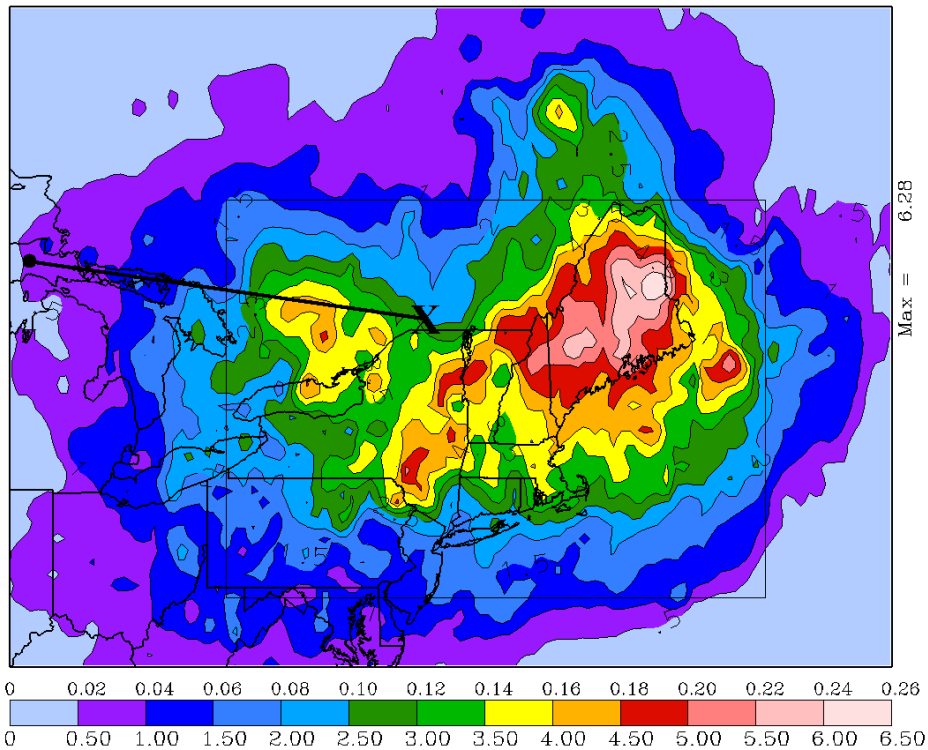

Fig. 3.23. Storm-relative average daily precipitation over 35 cutoff days for lows that followed the Clipper track. Average starting and ending positions are represented by the solid circle and "X," respectively, along with the resultant average track. Contour interval is 0.5 mm day^{-1} (~0.02 in day^{-1}).

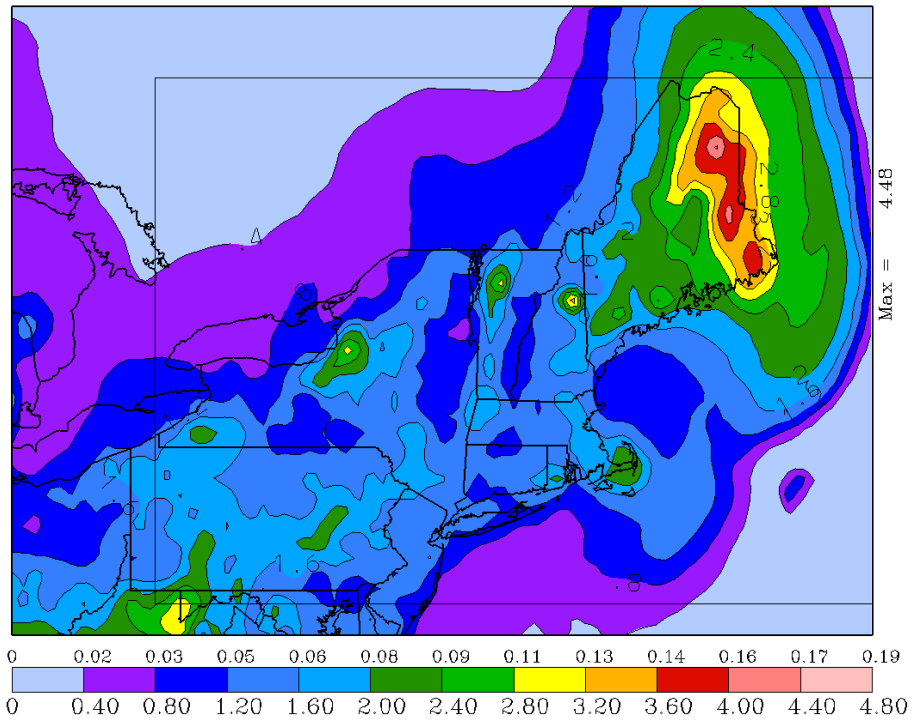

Fig. 3.24. Average daily precipitation over 75 cutoff days for lows that followed the Hudson Bay track. Contour interval is 0.4 mm day^{-1} (~0.16 in day^{-1}).

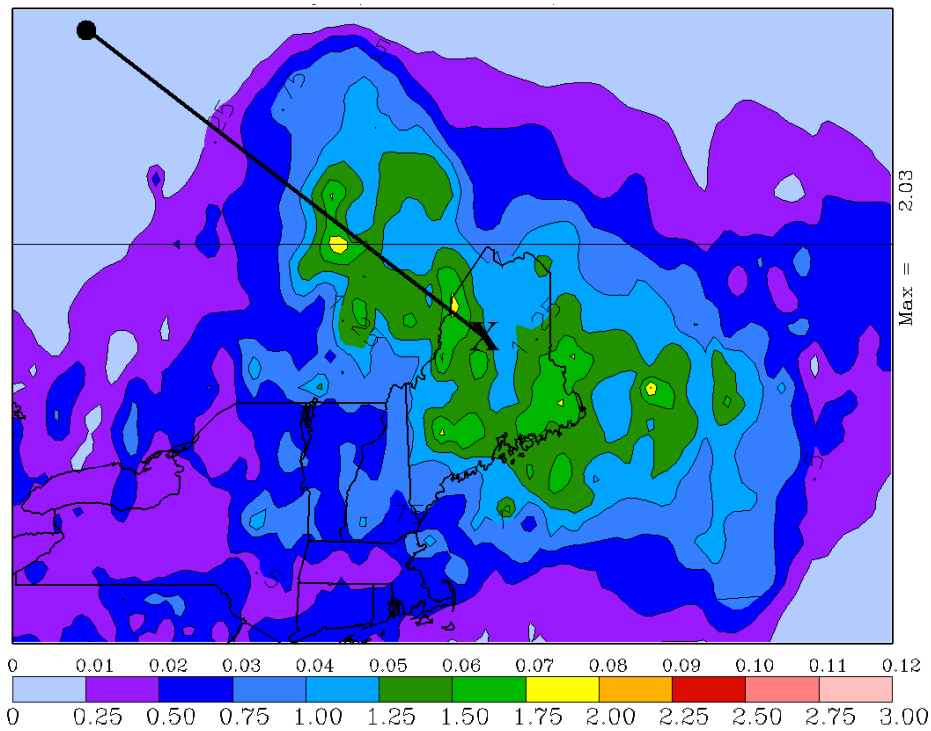

Fig. 3.25. Storm-relative average daily precipitation over 39 cutoff days for lows that followed the Hudson Bay track. Average starting and ending positions are represented by the solid circle and "X," respectively, along with the resultant average track. Contour interval is 0.25 mm day^{-1} (~0.01 in day^{-1}).

4. Case Studies

4.1 Overview

As previously mentioned in sections 1.3 and 2.2.3, one multifaceted case along with several other cutoff cases were examined. These cases were chosen to illustrate the difficulty in cutoff prediction and variability. The 23–31 May 2003 cutoff case was a typical example of a spring cutoff with an atypical progression. It produced close to 100 mm of rain in some locations, yet the amount of precipitation a given location received was not proportional to its proximity to the location of the cutoff; i.e., locations near the cutoff's track did not necessarily receive the most precipitation. The other cases provide a concise overview of some of the many "flavors" that cutoffs may assume. These include cutoffs associated with powerful nor'easters (25–27 December 2002 and 3–5 January 2003) and another springtime cutoff of a more progressive nature (11–15 May 2003). All of these systems were associated with significant amounts of precipitation across the Northeast; yet each develop and progress through the area in different environments, leading to varied distributions of the resultant precipitation.

4.2 Case 1: 23–31 May 2003

4.2.1 Precipitation Distribution and Progression

Figure 4.1 shows a four–day (96 h) precipitation plot ending at 1200 UTC 27 May 2003. Note for this and future plots similar to this one that precipitation values outside the US land border are a result of the smoothing program used to plot the data, and should be ignored. The dark line is the track of the 500 hPa cutoff, with its 1200 UTC locations denoted by the inserted day. The initial track of this cutoff follows a Southwest track (compare Fig. 1.9 with Fig. 4.1) (Smith 2003) in its first stage, but then stalls and slowly heads south in its second stage by 27 May. The cutoff's third stage is its exiting phase, looping through Pennsylvania before headed out of the Northeast (Fig. 4.2). The precipitation pattern in Fig. 4.1 reveals the first two stages of this cutoff's three-stage progression. First, in northern lower Michigan, there is an area of precipitation directly associated with the cutoff as it moved eastward into southwestern Ontario. The precipitation along the East Coast is associated with the cutoff's second stage, when it slows its progression and becomes nearly stationary just north of Toronto. This area of precipitation is much farther away from the cutoff, has a greater areal extent, and has higher overall values than the precipitation over Michigan associated with the cutoff's first stage. Higher elevations did not necessarily receive more precipitation than lower elevations, but the upper Hudson and Connecticut River Valleys do represent slight local minima in the distribution, with a muted signal near the coast.

The third stage of the cutoff denotes its slow progression toward the Northeast, taking a wide turn over Pennsylvania before heading away from the Northeast via northern Maine. Figure 4.2 shows the resultant precipitation associated with this third stage, which is markedly lighter than the previous stage. Values in the Northeast are all less than 25 mm and are somewhat proportional to elevation. Some higher amounts are

observed over higher elevations, but this relationship is not ubiquitous. Note that precipitation near the western Great Lakes is associated with the last two of the five total vorticity maxima rotating around the cutoff as well as another cutoff moving into the area. The track of the cutoff appears to have a direct association with the location of the heaviest precipitation, with locally higher values located right along the cutoff's track. However, since the data over the ocean and in Canada are not real, it is difficult to totally validate the aforementioned statement.

Figures 4.3a–f show the national radar composite (Level 1; 0.5º elevation angle) at 24 h intervals starting at 0000 UTC 24 May 2003 and ending at 0000 UTC 29 May 2003. These figures, along with Figs. 4.4–4.9, will be used to assess the forcing for precipitation and the resultant effect on observed precipitation. In each figure, an "X" denotes the center of the cutoff, while the letters "A," "B," "C," "D," and "E" are used to locate five 500 hPa vorticity maxima centers that migrate around the cutoff. A continuity map showing each vorticity maximum's track, to be thoroughly discussed later, is shown in Fig. 4.10.

Figure 4.3a shows the precipitation at 0000 UTC 24 May 2003, with the cutoff located over southwestern lower Michigan. An area of precipitation is located to the north and east of the cutoff, along the Mid–Atlantic coast (associated with vorticity maximum "A"), and also in North and South Dakota (associated with vorticity maximum "B"). As the cutoff drifts to the northeast by 25 May (Fig. 4.3b), the area of precipitation once located to the northeast of the cutoff has diminished in size and moved into northern New York, although the US Radar may not pick up precipitation far into Canada. The area of precipitation associated with vorticity maximum "B" has moved southeastward

into Missouri and Illinois, ahead of the center of the vorticity maximum. The area of precipitation along the East Coast associated with vorticity maximum "A" has diminished in both size and area as it moved northeastward.

By 26 May (Fig. 4.3c), the cutoff has become essentially stationary north of Toronto, and nearly all precipitation in the immediate area of the cutoff has dissipated. The precipitation associated with "B" is moving through the Ohio River Valley while another vorticity maximum ("C") is seen in Minnesota with no precipitation. At 0000 UTC 27 May (Fig. 4.3d), an area of heavy rain associated with "B" is exiting New England, while "C" has traveled south in a similar path as "B," but still with no precipitation. The cutoff itself is still in the same general area as it was 24 h prior, with only some precipitation to its east.

At 28 May (Fig. 4.3e) the cutoff is again in motion, traveling southward over Lake Erie. It now has a small area of precipitation southwest of its center over northern Ohio. Vorticity maximum "B" has moved just north of New Hampshire, but its associated precipitation has all moved offshore. Vorticity maximum "C" now has some associated precipitation over the Delmarva Peninsula as it rotates around the cutoff center, while vorticity maximum "D," located over North Dakota, has some precipitation to its southeast. Figure 4.3f shows the cutoff on 29 May moving through New England out to sea, with most of the precipitation in Maine northeast of the cutoff's center near vorticity maximum "C." Light and scattered precipitation can be seen over the rest of New England and in Canada. Vorticity maximum "D" has now split off "E," with both associated with some precipitation across the Ohio River Valley.

4.2.2 *Synoptic Overview*

The large-scale pattern over the Northeast is displayed in 24 h intervals starting at 0000 UTC 24 May 2003 through 0000 UTC 29 May 2003 in Figs. 4.4–4.9, respectively. These correspond to the US radar images (Figs. 4.3a–f) previously discussed. These figures will serve to illustrate the synoptic environment surrounding the cutoff over the 5-day period, clearly showing its three-stage life cycle.

Figure 4.4 shows the eastern half of the US at 0000 UTC 24 May 2003. The cutoff of concern is shown in Fig. 4.4d, located over southwestern Michigan, with its associated area of isolated cool air in the lower troposphere (Fig. 4.4a) denoted by an area of less than 546 dam thickness. The strongest vorticity maximum is located just to the southeast of the cutoff's center, but vorticity maximum "B" lies upstream in North Dakota (compare Fig. 4.3a and Fig. 4.4d). Little surface reflection of the upper low is apparent as no closed 1000 hPa contour appears in the area of the cutoff (Fig. 4.4a). Little warm air advection exists except for offshore from Virginia (Fig. 4.4b). There is ample moisture in the mid-levels of the atmosphere (Fig. 4.4c) both to the north of the cutoff and also well to the east and southeast of the cutoff, with areas of vigorous ascent located along the coast [associated with a 250 hPa jet streak (Fig. 4.4e)] as well as to the north of the cutoff. These areas correspond quite well to the areas of precipitation in Fig. 4.3a.

At 0000 UTC 25 May 2003 (Fig. 4.5), the cutoff has moved slightly east into extreme southwestern Ontario (Fig. 4.5d) and has strengthened, as noted by an additional closed contour as well as an increase in the areal extent of its associated values of

absolute vorticity above 28 x 10^{-5} s^{-1}. The distribution of absolute vorticity is now more symmetric about the center of the cutoff as compared to 24 h prior. The 1000 hPa plot (Fig. 4.5a) reveals a surface low pressure system off the Northeast coast, well removed from the cutoff, but no such surface reflection beneath the cutoff low. An embedded 250 hPa jet streak (Fig. 4.5e) within the jet stream is seen over the Ohio River Valley, with the surface low located near the poleward exit region of the jet. Figure 4.5c reveals that the available mid-tropospheric moisture is located all to the east of the cutoff over the Northeast and adjacent Atlantic Ocean. The area of most vigorous ascent is located in eastern New York State, with little significant rising motion near the cutoff at this time. Correspondingly, the area where the heaviest precipitation was falling at this time is eastern New York, seen in Fig. 4.3b. In addition, some precipitation is noted in southeast Massachusetts, associated with weak vorticity maximum "A" and weak 850 hPa warm air advection (Fig. 4.5b). The aforementioned vorticity maxima, "B," previously located in North Dakota, has now traveled southward into South Dakota and Iowa (Fig. 4.5d), but has little moisture associated with it (Fig. 4.5c) and also no detectable precipitation at the surface (Fig. 4.3b).

Twenty-four hours later, at 0000 UTC 26 May 2003 (Fig. 4.6), the cutoff has now become stationary north of Toronto (Fig. 4.6d), with a nearly symmetric distribution of absolute vorticity with respect to the cutoff's center. The closed contours are also nearly symmetric, but seem to be elongated toward the vorticity maximum ("B," see Fig. 4.3c) located to the southwest of the cutoff. Also noted is the third vorticity maximum ("C," see Fig. 4.3c) in Minnesota, beginning its rotation around the cutoff. A long extended jet is located to the southeast of the cutoff (Fig. 4.6e), with two embedded jet streaks—one

to the east of Maine and the other in Tennessee. The latter is in association with vorticity maximum "B" (see Fig. 4.3c) (and perhaps a small–scale cutoff as well) rotating around the cutoff, which has ample moisture (>90% relative humidity) and lift (< -8×10^{-3} hPa s^{-1}) (Fig. 4.6c). Accordingly, an area of precipitation is noted over southern Ohio (Fig. 4.3c) while precipitation near the cutoff's center is spotty at best. The precipitation associated with the surface low pressure system has moved offshore with that system (Fig. 4.6a), along with any significant warm air advection (Fig. 4.6b), leaving the rest of the area characterized by neutral temperature advection at 850 hPa.

Figure 4.7 shows the environment at 0000 UTC 27 May 2003, with the cutoff drifting slowly southward (Fig. 4.7d). Vorticity maximum "B" (see Fig. 4.3d) has now rotated to the east of the cutoff over northern New England with its accompanying moisture and lift (Fig. 4.7c), surface low pressure system (Fig. 4.7a), and location in the poleward jet exit region of a small jet streak (Fig. 4.7e). Consequently, an area of heavy rain was moving offshore from New England (Fig. 4.3d) and was responsible for precipitation amounts between 25 mm and 50 mm across southern New England. An area of slight warm air advection (values between 0.2ºC day^{-1} and 0.4ºC day^{-1}) is located offshore of New England (Fig. 4.7b), perhaps connected to the heavy precipitation along the Northeast coast. However, since the radar does not extend that far offshore, it is difficult to validate this connection. Vorticity maximum "C" has now rotated to just south of St. Louis, Missouri, with a small area of moisture (Fig. 4.7c) and even less precipitation (Fig. 4.3d). Also evident is the lack of precipitation near the cutoff center (Fig. 4.3d), partly due to a lack of available moisture in the immediate area (Fig. 4.7c).

With a symmetric distribution of absolute vorticity (Fig. 4.7d), the cutoff is dynamically dead.

At 0000 UTC 28 May 2003 (Fig. 4.8), the cutoff has now increased its forward motion to the south and becomes "alive" as it has precipitation directly associated with it in northern Ohio (Fig. 4.3e). While the distribution of absolute vorticity is still primarily symmetric, it is now off-center (Fig. 4.8d) and is coupled with an area of moisture (Fig. 4.8c). This moisture was actually in association with vorticity maximum "B," (see Fig. 4.3e) now located north of New Hampshire, but was subsequently advected cyclonically around the northern side of the cutoff. Vorticity maximum "C" is now located over New Jersey (Fig. 4.8d), along with a small area of light–to–moderate precipitation (Fig. 4.3e). The jet stream to the south of the cutoff (Fig. 4.8e) remains lengthy, but overall is stronger by about 10 m s^{-1} than 24 h prior (compare Figs. 4.7e and 4.8e). No surface low pressure system exists in the area (Fig. 4.8a) nor does any significant warm air advection at 850 hPa (Fig. 4.8b), leaving the precipitation in the Northeast primarily attributable to cyclonic vorticity advection.

Figure 4.9 shows the cutoff near the end of its life at 0000 UTC 29 May 2003, located over northern New England (Fig. 4.9d), with a large lower–tropospheric cold pool over the Northeast (Fig. 4.9a). The absolute vorticity, once symmetric about the center, has become disrupted as vorticity maximum "C" (see Fig. 4.3f) rotates on the east side of the cutoff. The area near "C" in eastern Maine is the only region of concentrated precipitation in the Northeast (Fig. 4.3f), with spotty precipitation over the rest of New England. At 850 hPa (Fig. 4.9b), the isotherms are somewhat parallel to the isoheights, leading to a lack of warm or cold air advection. The lack of significant 700 hPa upward

motion, in part, precludes more precipitation, despite ample moisture (Fig. 4.9c). Vorticity maxima “D” and “E” (see Fig. 4.3f) are noted over Illinois, located in the poleward exit region of a jet streak diving south from Canada (Fig. 4.9e).

4.2.3 *Mesoscale Aspects*

Figure 4.10 shows the progression of the five vorticity maxima during the event at 12 h intervals. Referring back to the precipitation amounts during the first half of the event (Fig. 4.1), note that the areas of heaviest precipitation occur near the track of vorticity maxima “A,” “B,” and “C” along the coastal sections of the Northeast. A second maximum occurs near St. Louis, near where both “B” and “C” traveled. It is these smaller–scale vorticity features that appear to be a key factor for predicting heavier precipitation amounts.

The internal structure of the cutoff observably changes characteristics during its lifetime. Figures 4.11a and 4.11b show observed soundings from Detroit, MI (DTX) at 1200 UTC 24 May 2003 and Buffalo, NY (BUF) at 1200 UTC 27 May 2003, respectively. At these times, the cutoff center was serendipitously close to these upper-air stations, allowing a close look at the structural changes of the cutoff.

At DTX at 1200 UTC 24 May (Fig. 4.11a), an area of rain had pushed through the area and was off to the east, while another area of rain was situated off to the north (not shown). The cutoff itself was moving slowly east into Canada and would soon stall. The sounding reveals a moist and cool lower and middle troposphere, with the air temperature and dewpoint temperature quite close from the surface up to about 500 hPa. The 1000–

500 hPa thickness is about 541 dam, which is quite cool for late May. Light winds (below 20 kts), apparent of a cutoff overhead, exist from the surface up to 200 hPa, first veering from west to northeast in the moist layer, and then backing to northwest above 500 hPa. The tropopause is also markedly low at about 400 hPa.

The conditions at BUF at 1200 UTC 27 May were free of any precipitation. The cutoff was coming out of its meandering stage and was now increasing its forward speed toward the south, just west of BUF. Figure 4.11b shows numerous differences from the DTX sounding 72 h prior. The lower troposphere is no longer saturated below 500 hPa, but has a dry layer between 900 hPa and 950 hPa and also above 600 hPa to the tropopause, which is higher up than at DTX at around 300 hPa. The 1000–500 hPa thickness has risen to about 546 dam, which is still quite cool for late May, but not as cool as it was at DTX three days earlier. Winds are again light, but only from the surface up to 550 hPa, above which they are between 40 kts and 50 kts up to 300 hPa. Winds veer from southerly at the surface to west–southwesterly at 800 hPa, back slightly from 800 hPa to 500 hPa, and then remain nearly unidirectional to 200 hPa, much different from the earlier DTX sounding.

Another glimpse into the changing structure of the cutoff is afforded by two cross sections, shown in Figs. 4.12 and 4.13. The first cross section (Fig. 4.12a), from Chicago, IL (ORD) to Burlington, VT (BTV), is valid at 0000 UTC 25 May. The cutoff is depicted in the center of the cross section by the rise (dip) in the isentropes below (above) about 300 hPa. The cyclonic circulation is maximized between 300 hPa and 400 hPa with south–southeasterly (north–northwesterly) flow to the east (west) of the cutoff at about 25 m s^{-1} (15 m s^{-1}). The absolute vorticity generally increases upward, but is

maximized between 400 hPa and 500 hPa near the center of the cutoff (Fig. 4.12a), decreasing in either direction away from the cutoff (compare with Fig. 4.5d). Figure 4.12b shows an abundance of moisture away from the cutoff, especially to its east, all below about 550 hPa. However, any rising motion is confined to the area near Burlington, with sinking motion throughout the troposphere to the cutoff's west.

Figures 4.13a–b, valid at 0000 UTC 28 May 2003, depict slightly different characteristics. Note that this cross section is from northwest to southeast, from Green Bay, WI (GRB) to 37ºN, 70ºW, so the vantage point into the paper is to the northeast, different from the previous figure. The distribution of absolute vorticity still increases upward, but is much narrower (note that the x-axis covers slightly more distance in Fig. 4.13 than in Fig. 4.12). The rise (dip) in the isentropes bends toward the east (west), unlike in Fig. 4.12a, where they are aligned vertically on top of each other. The circulation, now centered higher at about 300 hPa, is off-center compared to Fig. 4.12a, with the "0" line to the southeast of the area of maximum absolute vorticity. The distribution of moisture is still concentrated to the east of the cutoff, but has spread farther up into the troposphere, with relative humidity values greater than 70% observed above 500 hPa. Note that such values were all observed below about 550 hPa in Fig. 4.12b. The magnitude of the rising motion has decreased while staying primarily to the east of the cutoff (Fig. 4.13b), but to the west of the cutoff the air motion is neither rising nor sinking.

4.3 Case 2: 25–27 December 2002

4.3.1 Precipitation Distribution

Figure 4.15 shows a three–day (72 h) precipitation plot for the period 1200 UTC 24 December through 1200 UTC 27 December 2002, with the overlaid 500 hPa cutoff track. The cutoff did not acquire a closed contour until 0000 UTC 25 December; hence the line starts near St. Louis and not farther west. There is an extensive area of greater than 25 mm of precipitation from Florida northeastward to the Northeast, with a small area of over 50 mm of precipitation in east central New York. This cutoff did not follow any particular track, but instead started as a Southwest track cutoff that transitioned to a Mid-Atlantic track. The pattern reveals higher amounts closer to the coast and light amounts in the cutoff's initial stage, as well as a rather swiftly moving cutoff (roughly 1300 km in 24 h or about 15 m s^{-1}).

Snowfall observations plotted by NWS Binghamton (BGM) are shown in Fig. 4.15. Here, all precipitation fell as snow. The northeast portion of the blue-outlined area shows amounts over 20 inches, with a maximum of 39 inches in northeast Otsego county. This area corresponds well with the liquid precipitation maximum shown in Fig. 4.14.

4.3.2 Synoptic Overview

The synoptic pattern during this case featured a rapidly developing surface cyclone with an accompanying 500 hPa cutoff to its west, a signature of a classic nor'easter winter storm. Figure 4.16 shows a six–panel plot at 0000 UTC 25 December 2002, showing a weak cutoff at 500 hPa (Fig. 4.16d) with its area of absolute vorticity

mainly to its south. (Note that for this and the next two cases the 500 hPa geopotential heights are contoured using the conventional 6 dam in order to illustrate the cutoff's relative insignificance compared to other features.) One surface low pressure system is observed over Kentucky while a coastal redevelopment near North Carolina is evident (Fig. 4.16a), each with minimal 850 hPa warm air advection to their northeast (Fig. 4.16b) and 700 hPa frontogenesis farther northeast (Fig. 4.16c). Figures 4.16e and 4.16f show the East Coast between a 300 hPa polar jet streak and 200 hPa subtropical jet streak, respectively.

Figure 4.17 reveals a rather weak cutoff at 500 hPa (Fig. 4.17d) at 1200 UTC 25 December, with ample absolute vorticity around its center and also to it south. The primary surface cyclone is beginning to develop near the Delmarva peninsula (Fig. 4.17a), while a lower–tropospheric warm front is evident at 850 hPa (Fig. 4.17b), depicted by warm air advection over the Atlantic Ocean westward to the Mid-Atlantic. The Northeast is still situated near the intersection of the poleward exit region of the subtropical jet (Fig. 4.17f) and the equatorward entrance region of a weaker polar jet (Fig. 4.17e), aiding in the surface cyclone's development. Significant 700 hPa frontogenesis is primarily located offshore, well away from surface and upper level cyclones, with a smaller area of frontogenesis located in central Pennsylvania (Fig. 4.17c).

By 12 h later at 0000 UTC 26 December, the surface cyclone has "bombed" out and is located just southeast of New England (Fig. 4.18a). Intense warm air advection at 850 hPa is noted from southern New England eastward (Fig. 4.18b), south of an area of vigorous 700 hPa frontogenesis (Fig. 4.18c). The 500 hPa cutoff has also deepened, but

with a similar distribution of vorticity (Fig. 4.18d) as 12 and 24 h prior. The 300 hPa and 200 hPa jet streaks (Figs. 4.19e,f, respectively), located to the south and to the north of the cyclone are exiting the region as the whole system departs the area over the next day or so.

Figure 4.19 shows the Albany, NY (KENX) radar image (0.5º elevation angle) at 0128 UTC 26 December 2002, shortly after the previous figure. Clearly evident is a band of intense reflectivity (greater than 30 dBz), corresponding to heavy snow in this case, situated over Albany and points southwest and northeast. This area coincides with the edge of the intense warm air advection at 850 hPa and is also behind the area of 700 hPa frontogenesis (Novak et al. 2004). The band was responsible for the heavy snowfalls just west of Albany (Fig. 4.15) as it remained over central New York for some duration before it moved east. Note that this area of heavy precipitation was about 300 km from the cutoff center, which was located near Long Island.

4.4 Case 3: 3–5 January 2003

4.4.1 Precipitation Distribution

A three–day (72 h) precipitation plot for the period 1200 UTC 2 January through 1200 UTC 5 January 2003 is shown in Fig. 4.20. This nor'easter and associated cutoff developed on the heels of the previous case and produced significant precipitation over a similar area (i.e., central and eastern New York). Overall amounts are less than 50 mm and the location of amounts over 25 mm appears close to the first time that the cutoff was

observed (1200 UTC 4 January). Amounts decrease in a similar manner on either side of the cutoff's track, and also decrease along the track in Maine. Figure 4.21 shows the storm total snowfall observations over central and eastern New York, with the highest amounts reported in a similar area as the 25–27 December 2002 storm (Fig. 4.15). This area of maximum snowfall aligns well with the liquid precipitation maximum observed in Fig. 4.20, with amounts between 25 mm and 40 mm. Note that snow fell outside of the area shown, but was generally lighter.

4.4.2 Synoptic Overview

Figures 4.22–4.24 show the environment at 12 h intervals, from 0000 UTC 4 January through 0000 UTC 5 January 2003. At 0000 UTC 4 January (Fig. 4.22), 12 h before the 500 hPa cutoff appears, there is a developing surface cyclone east of the Delmarva peninsula (Fig. 4.22a), ample warm air advection at 850 hPa just south of New England (Fig. 4.22b), and slight 700 hPa frontogenesis in central New England (Fig. 4.22c). The 300 hPa jet stream (likely an anomalously low subtropical jet stream) is located over the developing surface cyclone (Fig. 4.22e). The surface cyclone system is located near the equatorward jet entrance region of an anomalously high 200 hPa polar jet stream (Fig. 4.22e). One area of absolute vorticity is located near the location where the cutoff is about to form (Fig. 4.22d), with another vorticity maximum located to its south offshore of Georgia.

Twelve hours later at 1200 UTC 4 January (Fig. 4.23) the surface cyclone has intensified (note the –30 m closed contour compared to 60 m higher 12 h earlier) and

moved northeastward to a location just offshore of Cape Cod, MA (Fig. 4.23a). Its associated area of 850 hPa warm air advection (Fig. 4.23b) and frontogenesis (Fig. 4.23c) also have moved north into central and northern New England, respectively. At 500 hPa (Fig. 4.23d), a cutoff has formed just east of BGM, using the 30 m criterion, but is not evident using the conventional 60 m interval. At 300 hPa (Fig. 4.23e), the poleward exit region of the subtropical jet and implied area of divergence have also moved smartly offshore. The surface cyclone is still located in the equatorward jet entrance region of the polar jet (Figs. 4.23e,f), aiding in its intensification.

By 0000 UTC 5 January (Fig. 4.24), the system is steadily moving out of the Northeast. The surface cyclone has maintained its strength (Fig. 4.24a) while the 500 hPa cutoff is now visible at the 60 m contour interval (Fig. 4.24d). Areas of warm air advection and frontogenesis have also exited the Northeast (Figs. 4.24b,c), along with both subtropical and polar jets (Figs. 4.24e,f). It is seen that in this and the previous case that the surface cyclone and associated lower–tropospheric dynamics (850 hPa warm air advection and 700 hPa frontogenesis) affect the distribution of precipitation far more than just the track of the 500 hPa cutoff and its associated vorticity maxima.

4.5 Case 4: 11–15 May 2003

4.5.1 Precipitation Distribution and Progression

The precipitation plot for the four–day (96 h) period from 1200 UTC 11 May through 15 May 2003 is shown in Fig. 4.25. A large area of 25 mm to 50 mm of

precipitation exists across upstate New York, with over 50 mm observed over the Tug Hill Plateau and southwestern Adirondacks. Another area of locally higher values exists downwind of Lake Erie, south of Buffalo. These two areas of locally higher precipitation amounts could be a result of lake-enhanced precipitation. Along the track of the cutoff, there is an area of higher values near the cutoff's position at 1200 UTC 11 May, then a decrease in amounts, a second resurgence of precipitation amounts in New York, and finally a decrease in amounts over Maine. It is difficult to determine whether or not precipitation was evenly distributed to the north and south of the track because data in Canada are virtually useless. However, in Maine it appears that values are even on either side of the track.

Figures 4.26a–d show the progression of the precipitation as a national radar composite (Figs. 4.26a,b) and a Northeast radar composite (Figs. 4.26c,d) at 24 h intervals starting at 1200 UTC 11 May 2003. Figure 4.26a shows the precipitation associated with a surface low pressure system over Wisconsin and its cold front to the east and south. By 1200 UTC 12 May (Fig. 4.26b), the precipitation along the cold front has dissipated, and the precipitation near the weakening surface low pressure system has diminished. Twenty–four hours later (Fig. 4.26c) the precipitation is mainly oriented west–east, with enhancement along the Green Mountains in Vermont and also in central New York. Nearly all precipitation has dissipated by 1200 UTC 14 May (Fig. 4.26d), confined only to northeast Maine.

4.5.2 Synoptic Overview

The progression of the cutoff from 1200 UTC 11 May through 1200 UTC 14 May 2003 at 24 h intervals is shown in Figs. 4.27–4.30 in a similar display as the first case. The cutoff of interest is clearly seen at 500 hPa in Fig. 4.27d over Wisconsin, with five closed contours around the center. A maximum of absolute vorticity is located just southeast of the center of the cutoff, with extended "filaments" of absolute vorticity to the south and southwest of the cutoff. A surface cyclone is evident just to the northeast of the 500 hPa cutoff (Fig. 4.27a), with an impressive central geopotential height of –120 m. Absent from the structure is an isolated cold pool in the lower troposphere (no closed 1000–500 hPa thickness contour). The cutoff is located in the poleward jet exit region of the 250 hPa jet stream with significant ridging to the east (Fig. 4.27e). Ample lower tropospheric moisture exists to the west, north, and east of the center, while the most vigorous upward motion is located to the north of the cutoff in the upper peninsula of Michigan (Fig. 4.27c). In the same area, however, 850 hPa warm air advection (Fig. 4.28b) is below 0.2ºC day^{-1}, despite an easterly flow normal to the isotherms. The national radar composite (Fig. 4.26a) shows high reflectivity in this area as well, confirming the inference of heavy precipitation. Note that this area is also where greater than 50 mm of precipitation will fall while 10 mm or less will fall along the cutoff's initial track near Green Bay, WI (Fig. 4.25).

Figure 4.28, valid at 1200 UTC 12 May, reveals the swift progression of the 500 hPa cutoff, which is now located over Georgian Bay in Canada (Fig. 4.28d). The distribution of absolute vorticity is biased toward the south of the cutoff, with an accompanying vorticity maximum traveling eastward through Virginia, likely once an aforementioned filament of vorticity. The ridging at 250 hPa has moved quickly offshore

ahead of the jet (Fig. 4.28e) as the cutoff now spans the entire depth of the troposphere. At the surface (Fig. 4.28a), the original surface cyclone presently over Georgian Bay has weakened, while a new system has formed southeast of New England. Only to the northeast of this new surface cyclone is an area of 850 hPa warm air advection (Fig. 4.28b). Note that now the cutoff still has ample moisture surrounding it, but the upward motion is lost (Fig. 4.28c). The national radar composite reveals a marked decrease in precipitation echoes near the Great Lakes, with the heaviest echoes confined to eastern Ohio and western Pennsylvania. As a result, precipitation totals over eastern Michigan are also lower than those found over the upper peninsula of Michigan (Fig. 4.25).

At 1200 UTC 13 May (Fig. 4.29), the 500 hPa cutoff has now become less organized as it moved into northern New England (Fig. 4.29d). The surface cyclone has all but dissipated (Fig. 4.29a), but a large area of lower–tropospheric moisture remains in place over the northern portions of the Northeast into Canada (Fig. 4.29c). However, little upward motion exits over the area (Fig. 4.29c) as the jet is well offshore (Fig. 4.29e). Consequently, the precipitation observed over the Northeast (Fig. 4.26c) apparently occurs in response to a small vorticity maximum rotating through western New York, in the absence of 850 hPa warm air advection in the Northeast (Fig. 4.29b).

Figures 4.30 and 4.26d show that by 1200 UTC 14 May the entire system at all levels has departed the Northeast. Geopotential heights at 1000 hPa and 850 hPa are on the rise (Figs. 4.30a,b) over the Northeast as the 500 hPa cutoff has moved into the Canadian Maritimes (Fig. 4.30d). Some residual lower–tropospheric moisture is still evident over the Northeast (Fig. 4.30c), which is under northwesterly flow behind the cutoff. The 250 hPa jet is well to the south and east over the Atlantic Ocean (Fig. 4.30e).

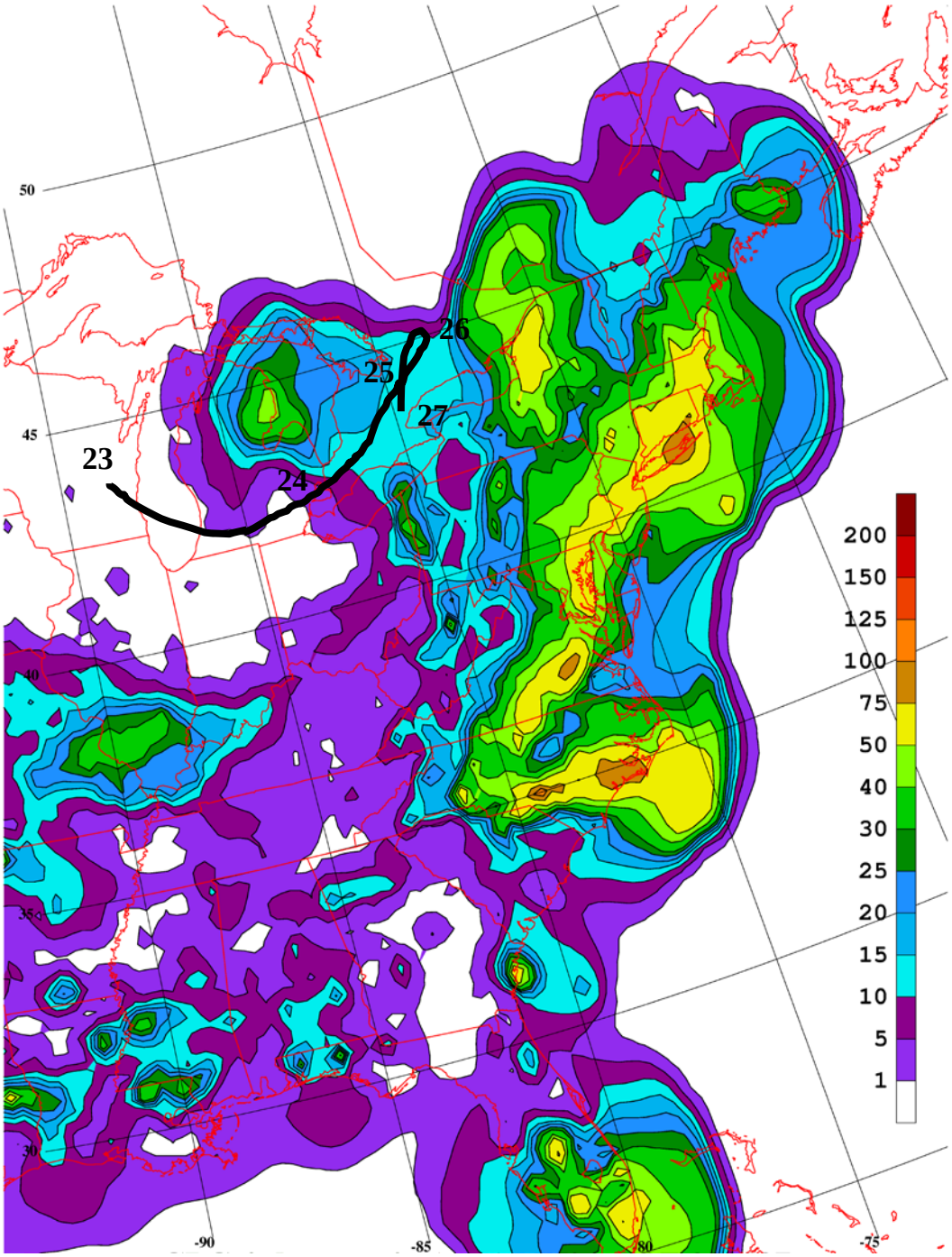

Fig. 4.1. Four–day (96 h) precipitation plot (mm) from 1200 UTC 23 May 2003 through 1200 UTC 27 May 2003. Dark solid line indicates track of 500 hPa cutoff low with indicated daily 1200 UTC locations.

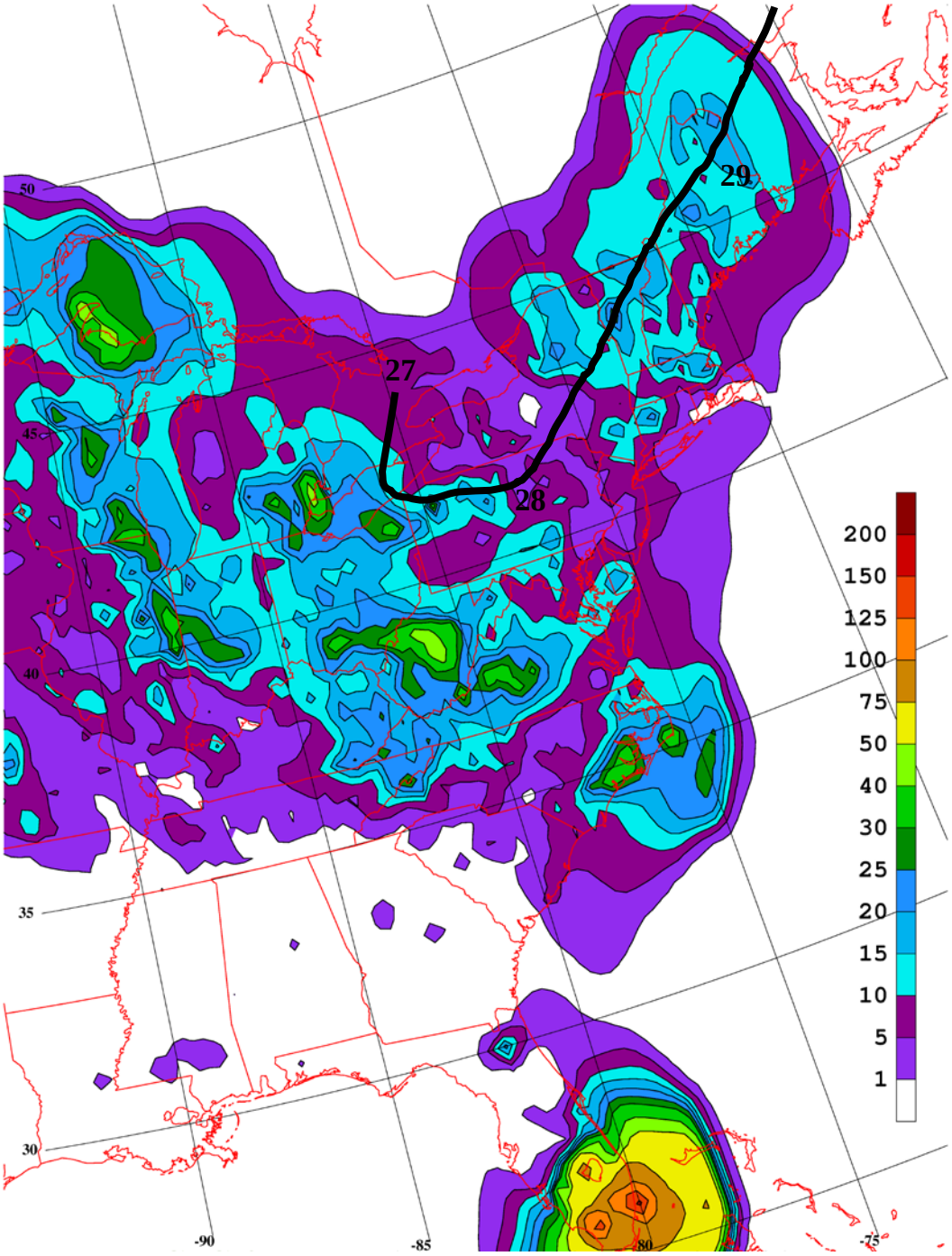

Fig. 4.2. As in Fig. 4.1, except for the period 1200 UTC 27 May 2003 through 1200 UTC 31 May 2003.

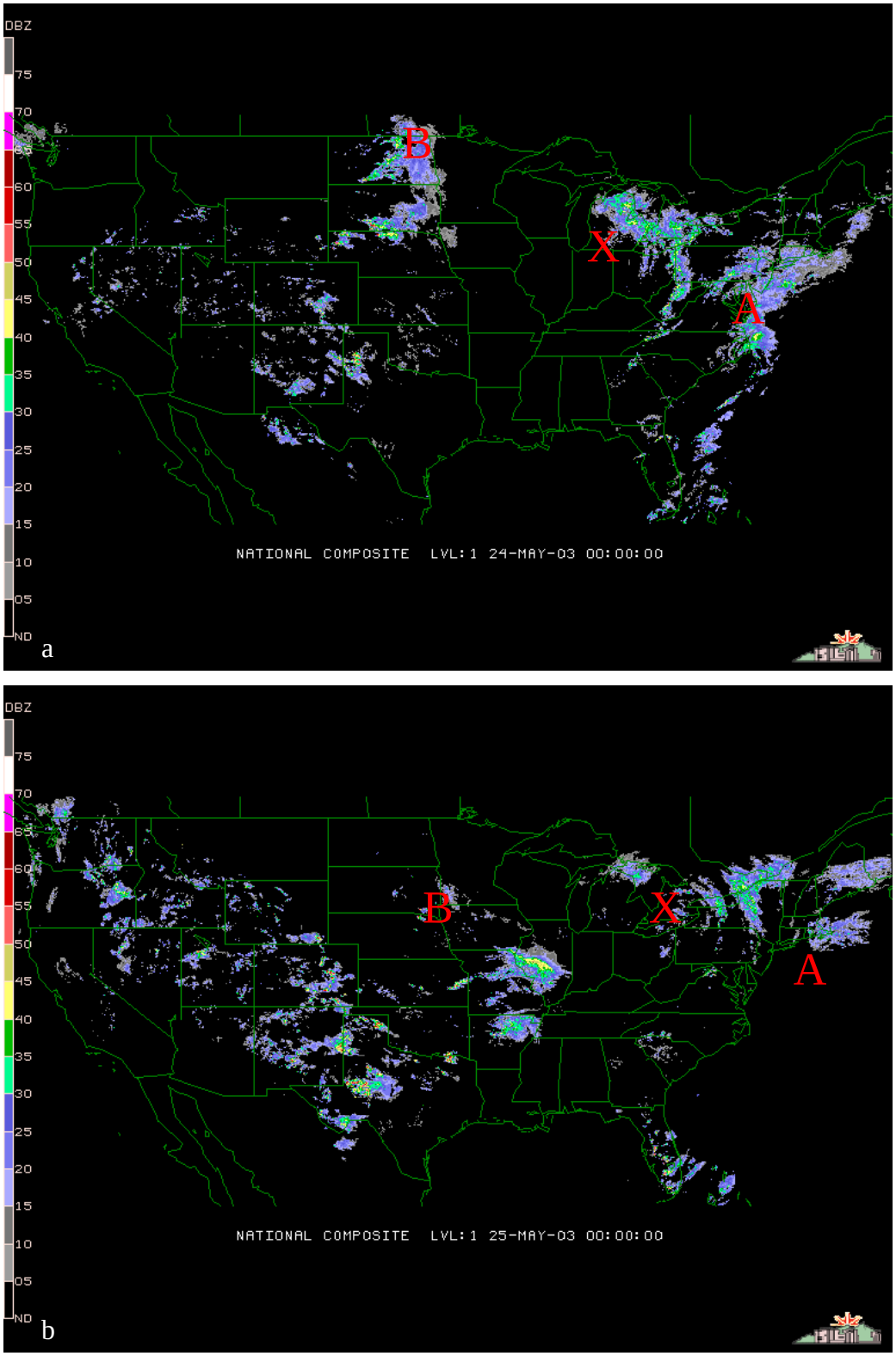

Fig. 4.3. National composite radar (Level 1) at 0000 UTC on: a) 24 May 2003, b) 25 May 2003, c) 26 May 2003, d) 27 May 2003, e) 28 May 2003, and f) 29 May 2003. A, B, C, D, and E denote the five vorticity maxima, while X denotes the center of the cutoff.

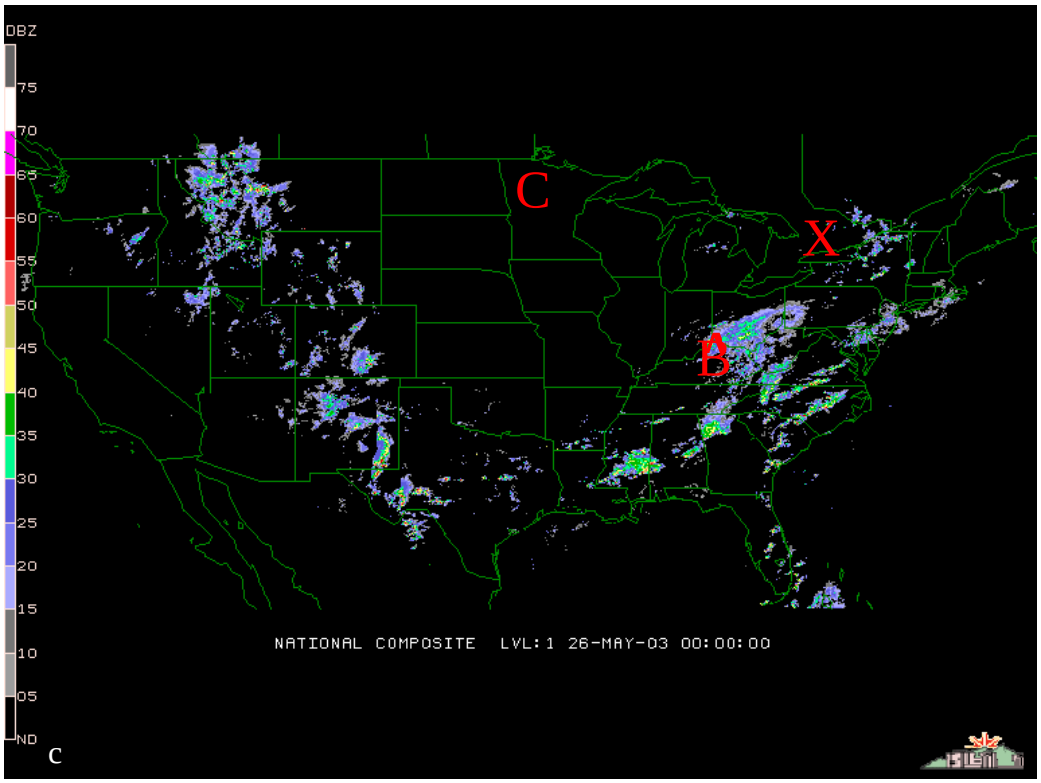

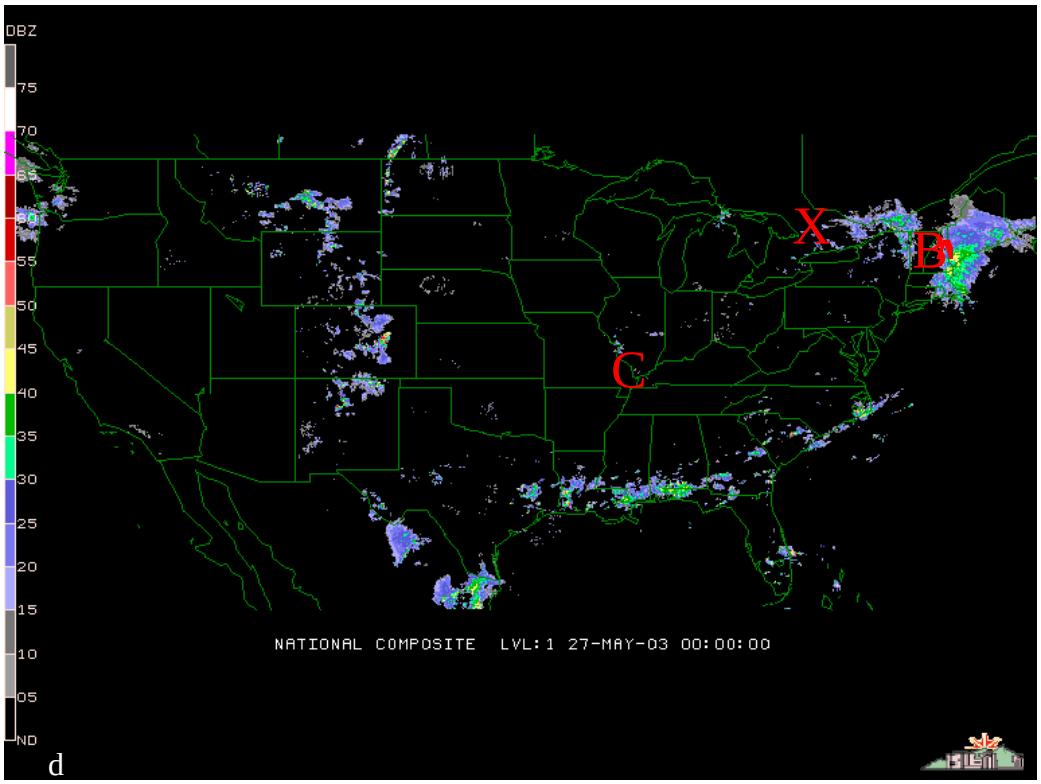

Fig. 4.3. Continued.

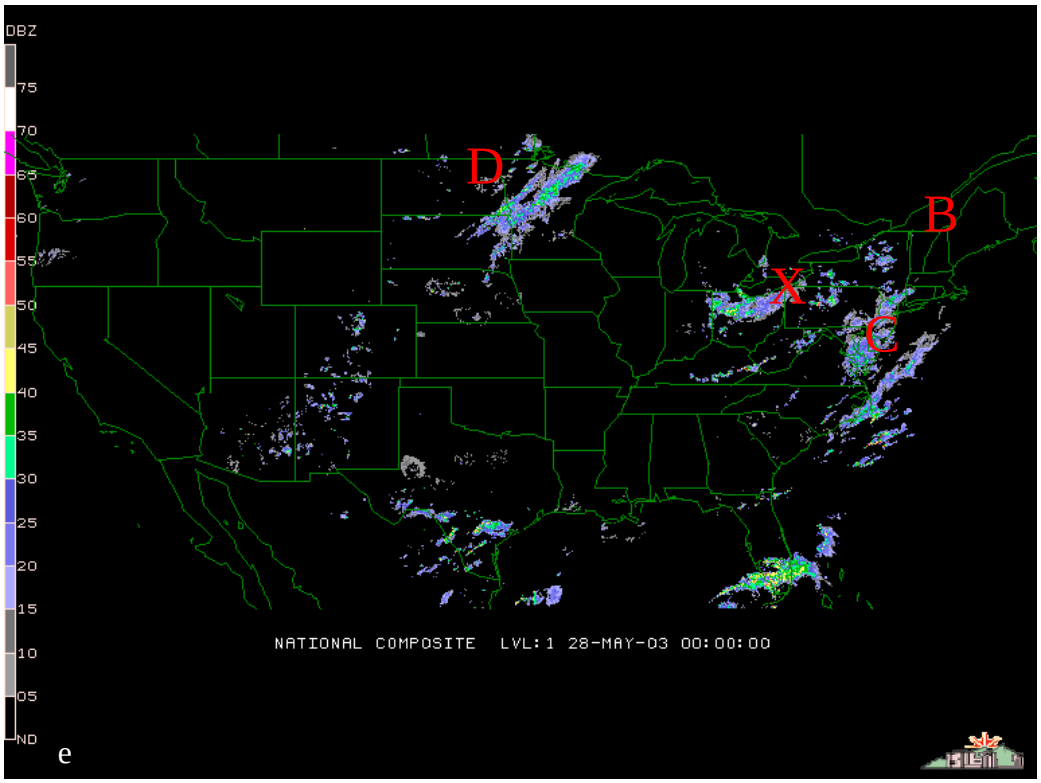

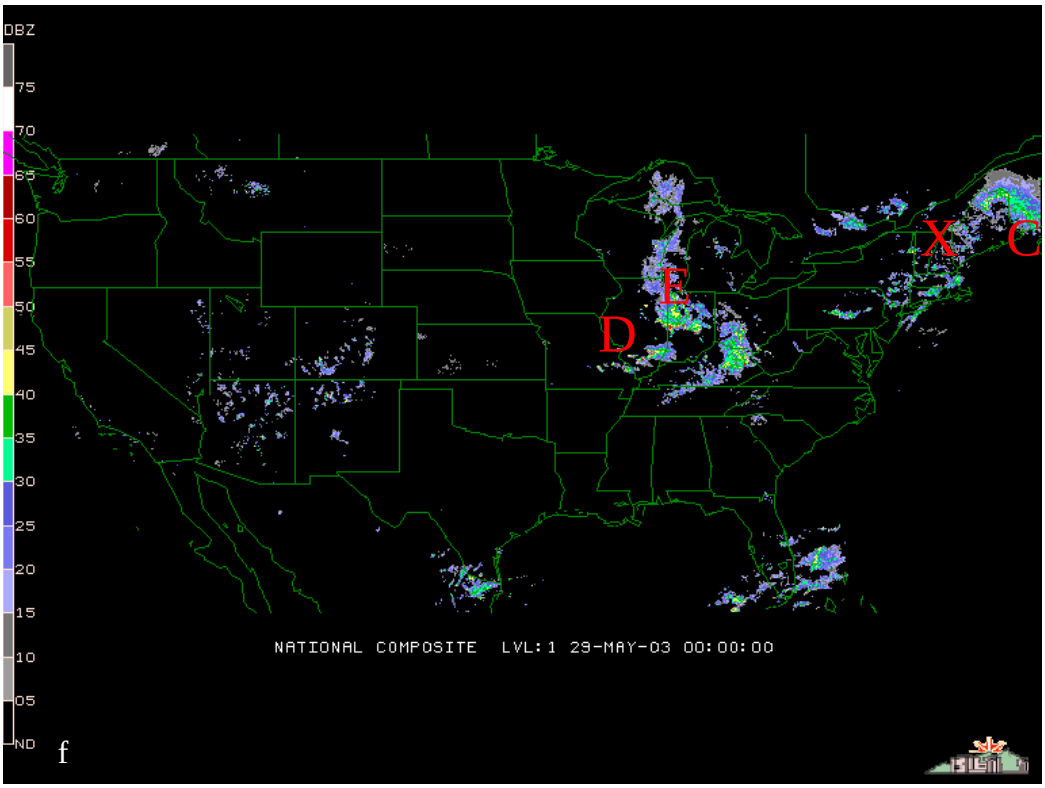

Fig. 4.3. Continued.

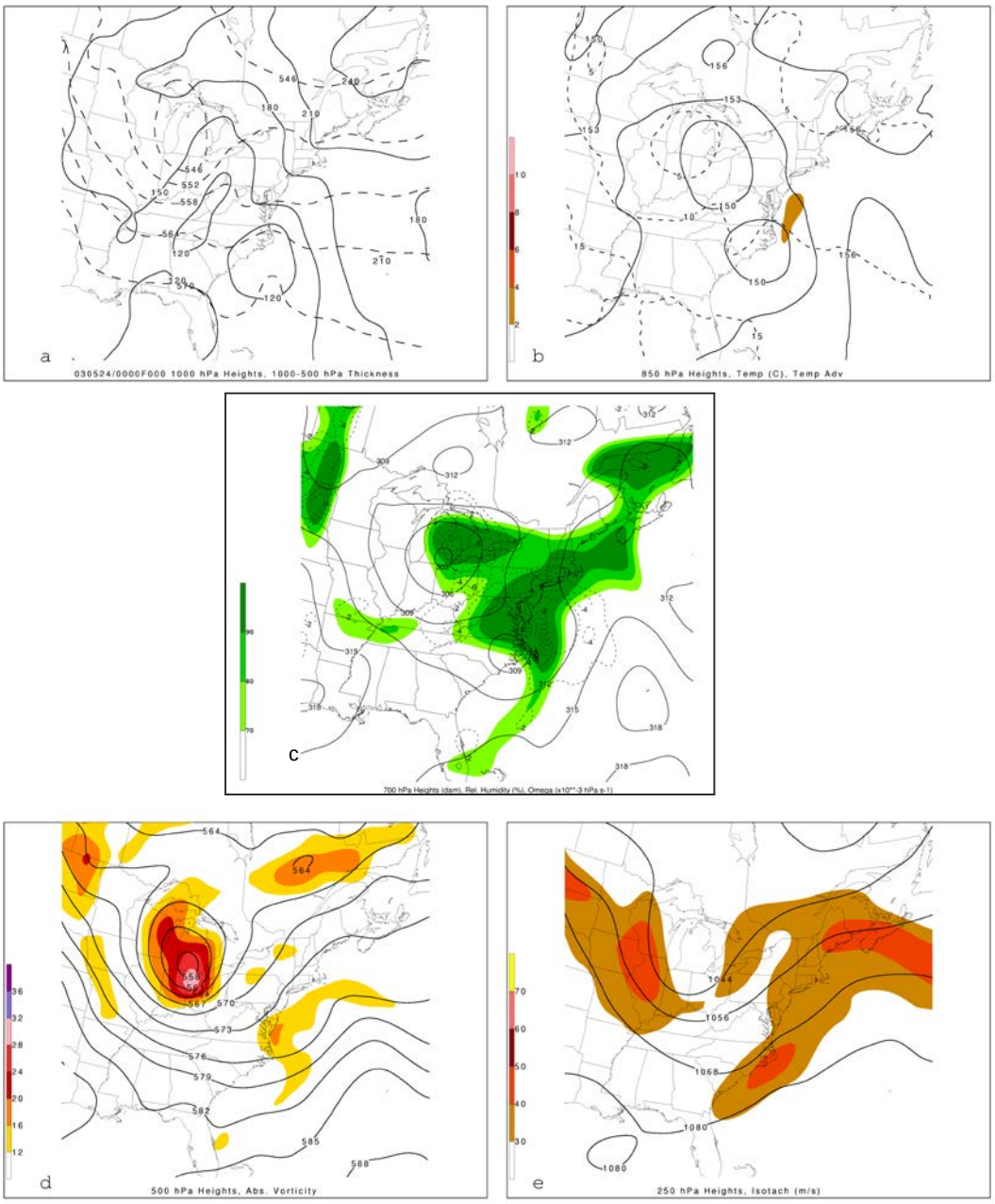

Fig. 4.4. Five–panel analysis plot valid at 0000 UTC 24 May 2003 showing: a) 1000 hPa geopotential height (m, solid) and 1000–500 hPa thickness (dam, dashed); b) 850 hPa geopotential height (dam, solid), temperature (ºC, dashed), and temperature advection ($0.1^{o}C\ day^{-1}$); c) 700 hPa geopotential height (dam, solid), relative humidity (%, shaded above 70%), and vertical velocity (10^{-3} hPa s^{-1}, dashed below -2×10^{-3} hPa s^{-1}); d) 500 hPa geopotential height (dam, solid) and absolute vorticity (10^{-5} s^{-1}, shaded above 12×10^{-5} s^{-1}); e) 250 hPa geopotential height (dam, solid) and wind speed (m s^{-1}, shaded above 30 m s^{-1}).

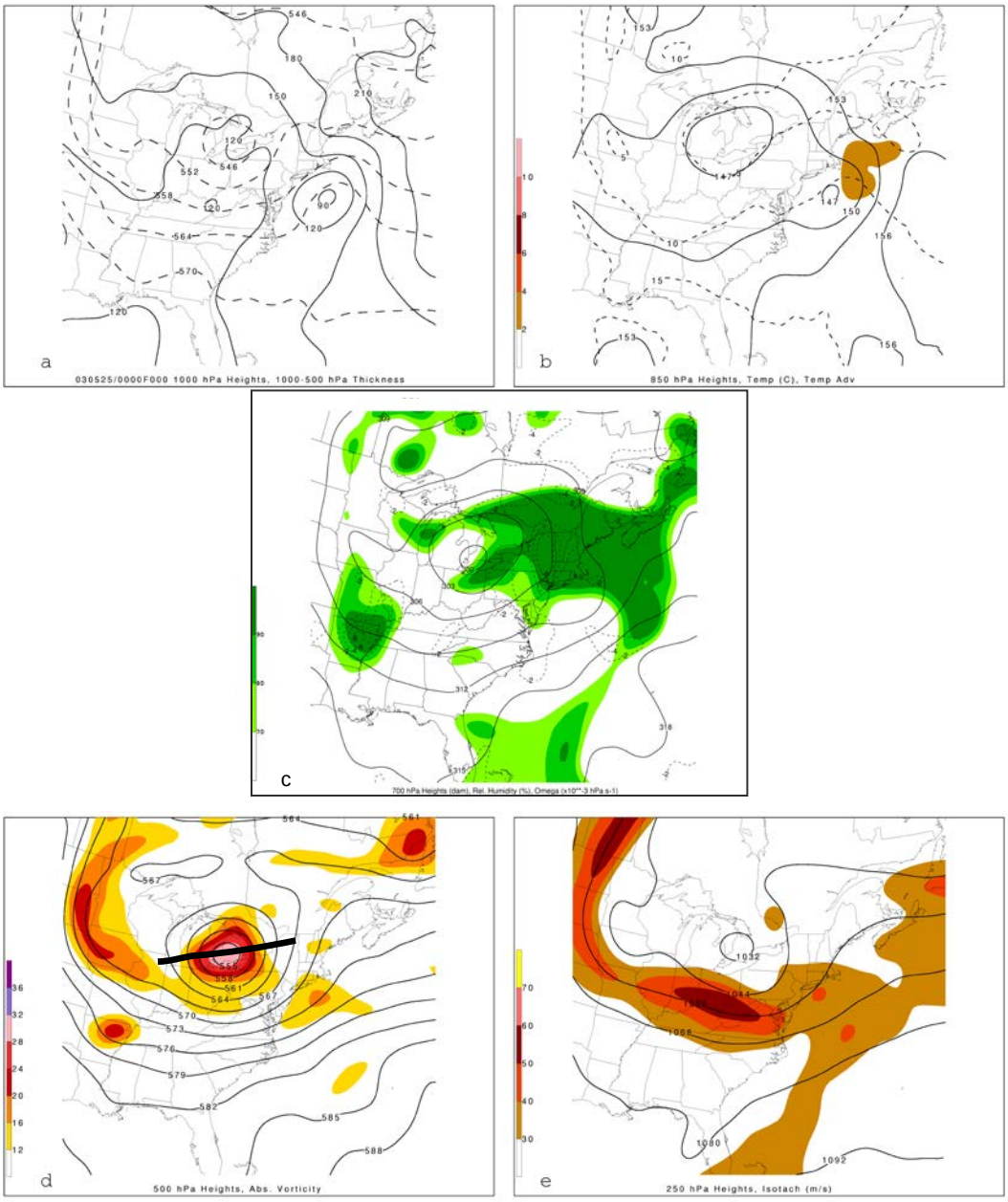

Fig 4.5. As in Fig. 4.4, except for 0000 UTC 25 May 2003. Dark solid line in panel (d) shows approximate orientation of cross section in Fig. 4.12.

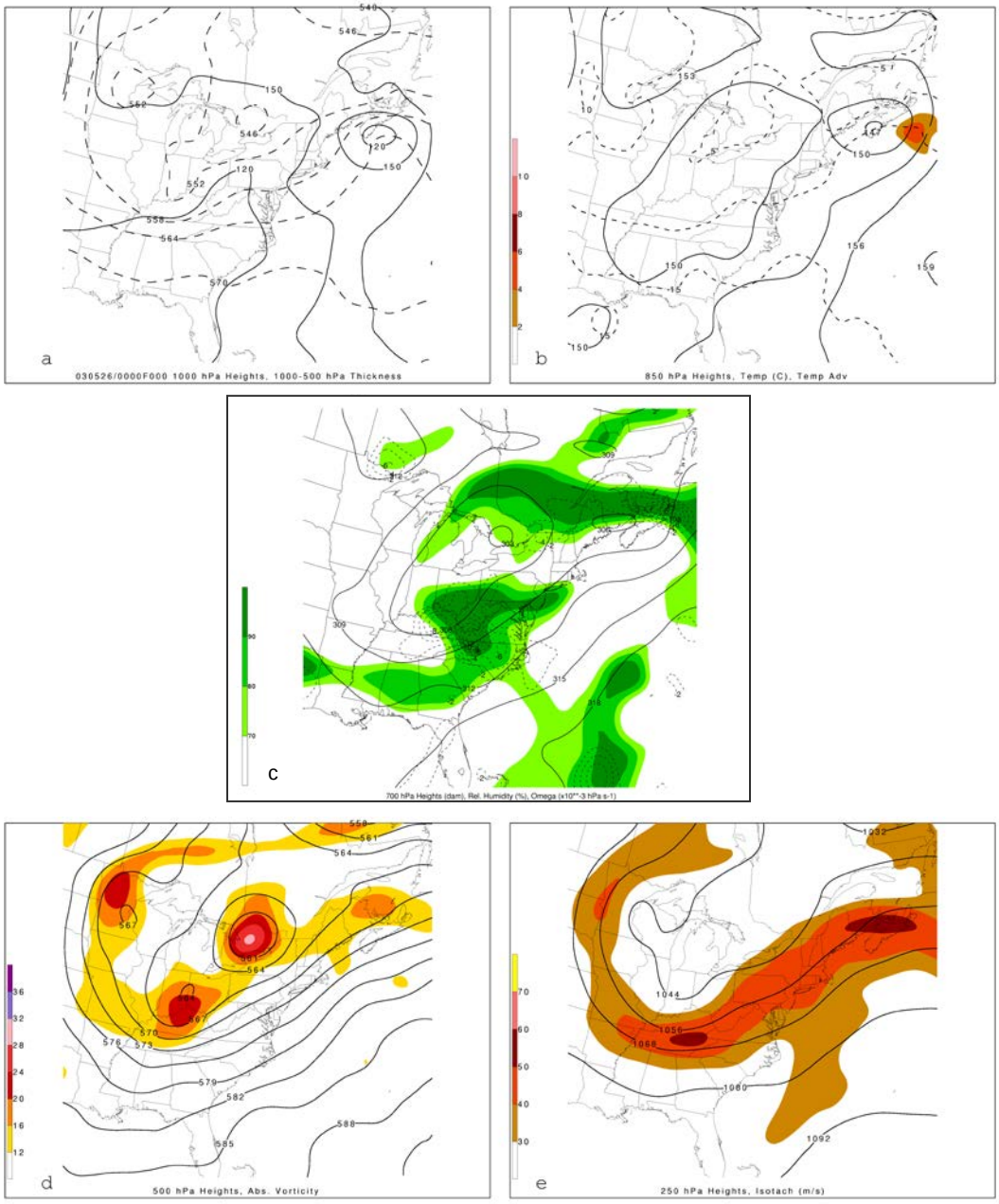

Fig 4.6. As in Fig. 4.4, except for 0000 UTC 26 May 2003.

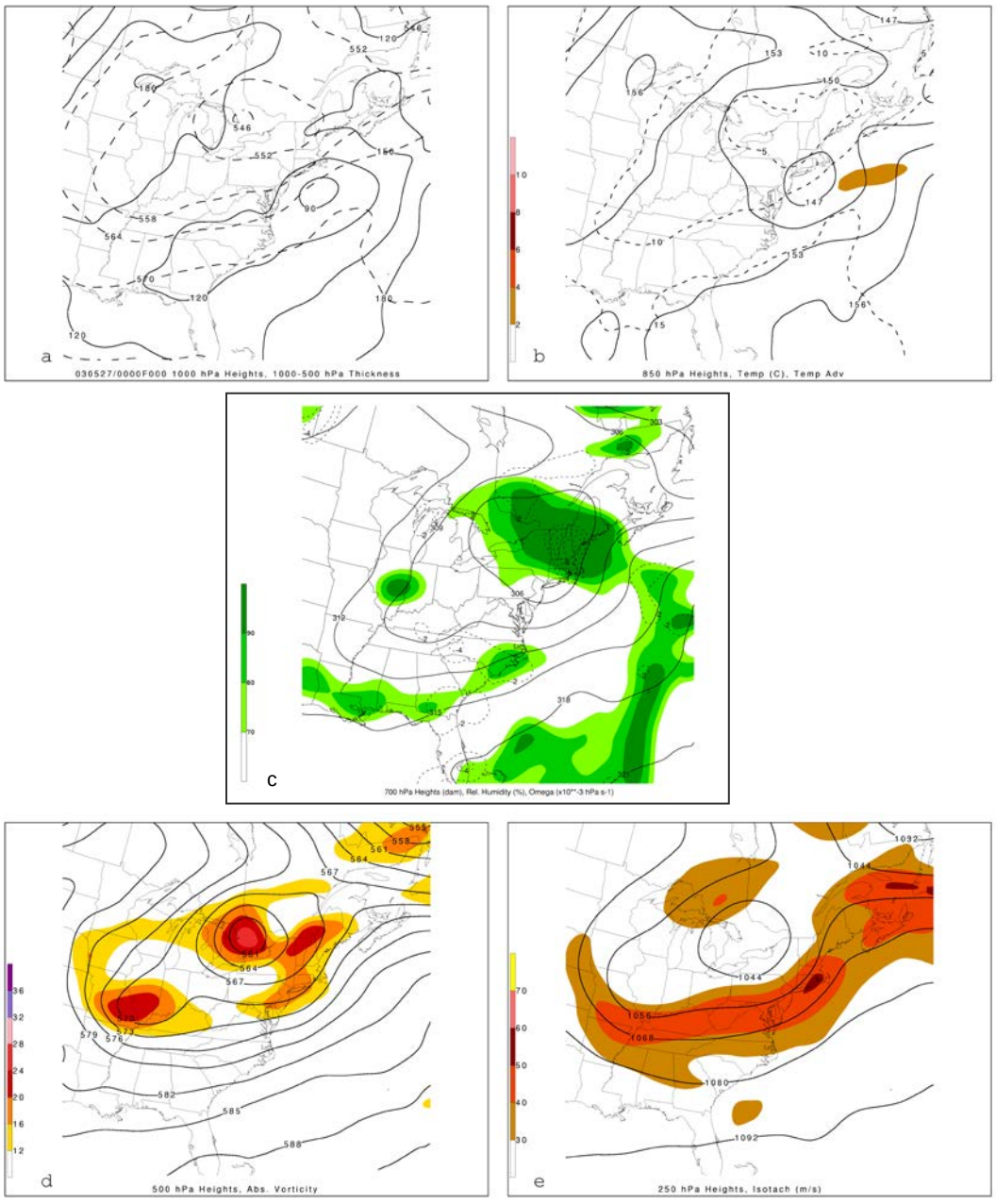

Fig 4.7. As in Fig. 4.4, except for 0000 UTC 27 May 2003.

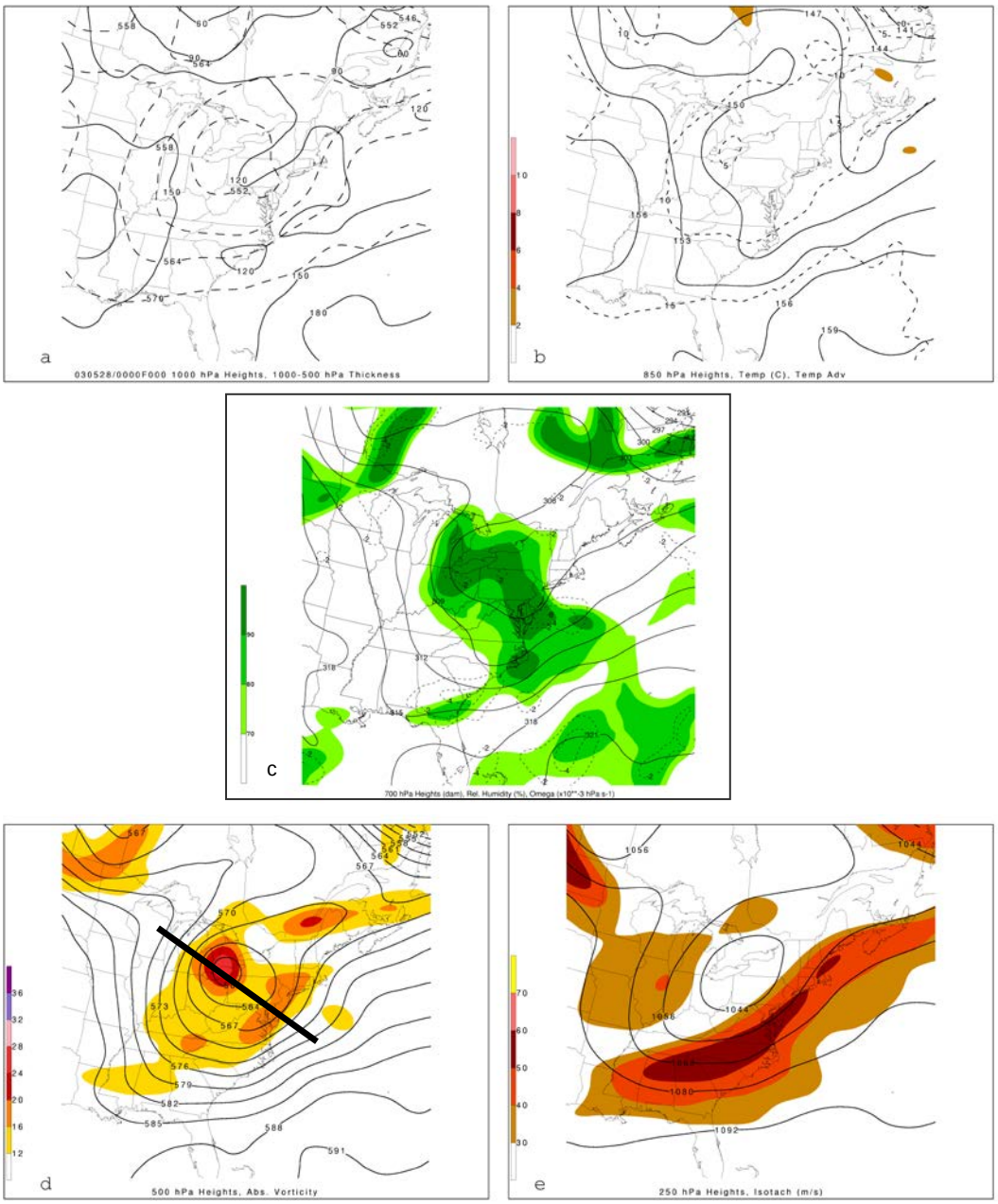

Fig 4.8. As in Fig. 4.4, except for 0000 UTC 28 May 2003. Dark solid line in panel (d) shows approximate orientation of cross section in Fig. 4.13.

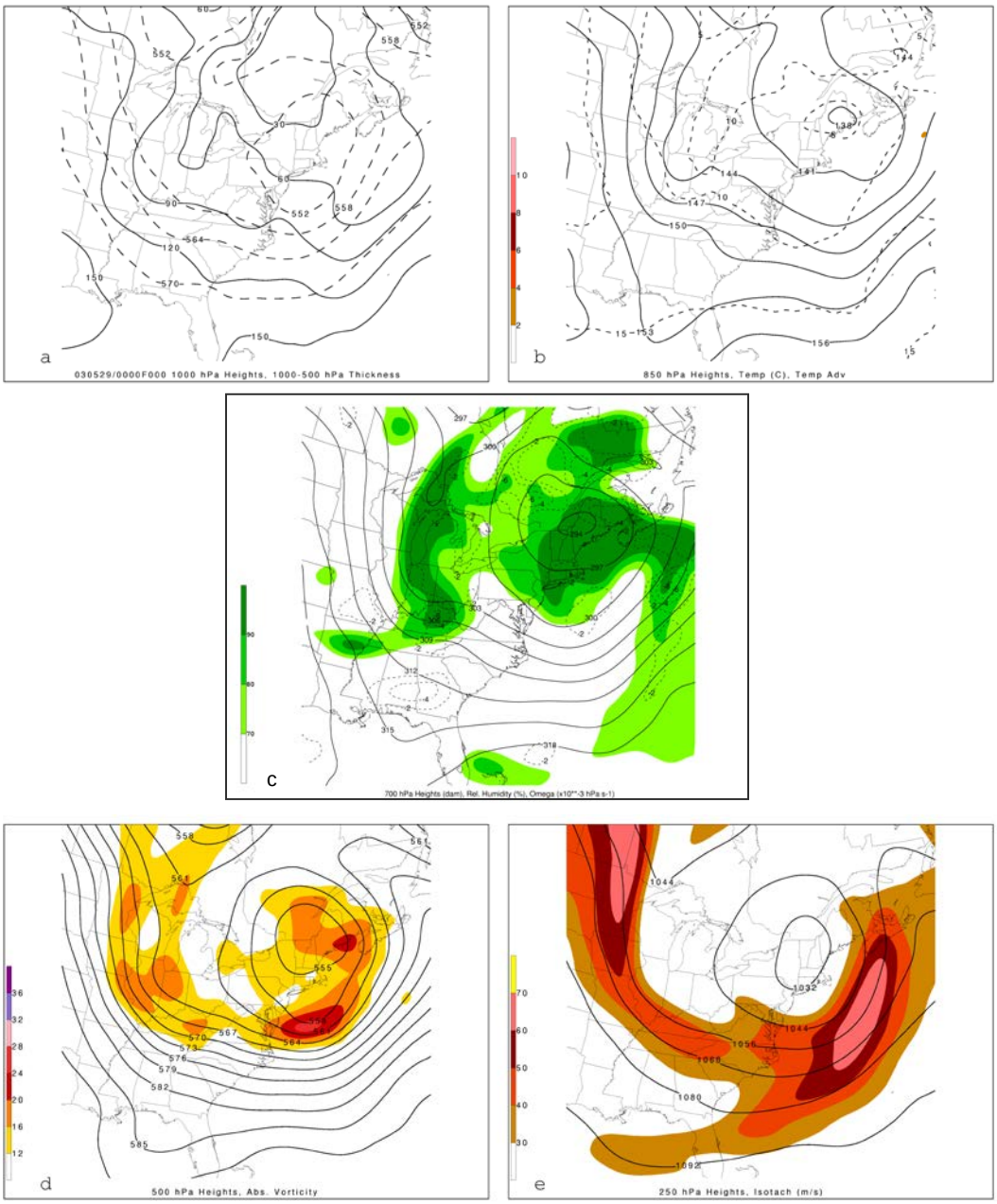

Fig 4.9. As in Fig. 4.4, except for 0000 UTC 29 May 2003.

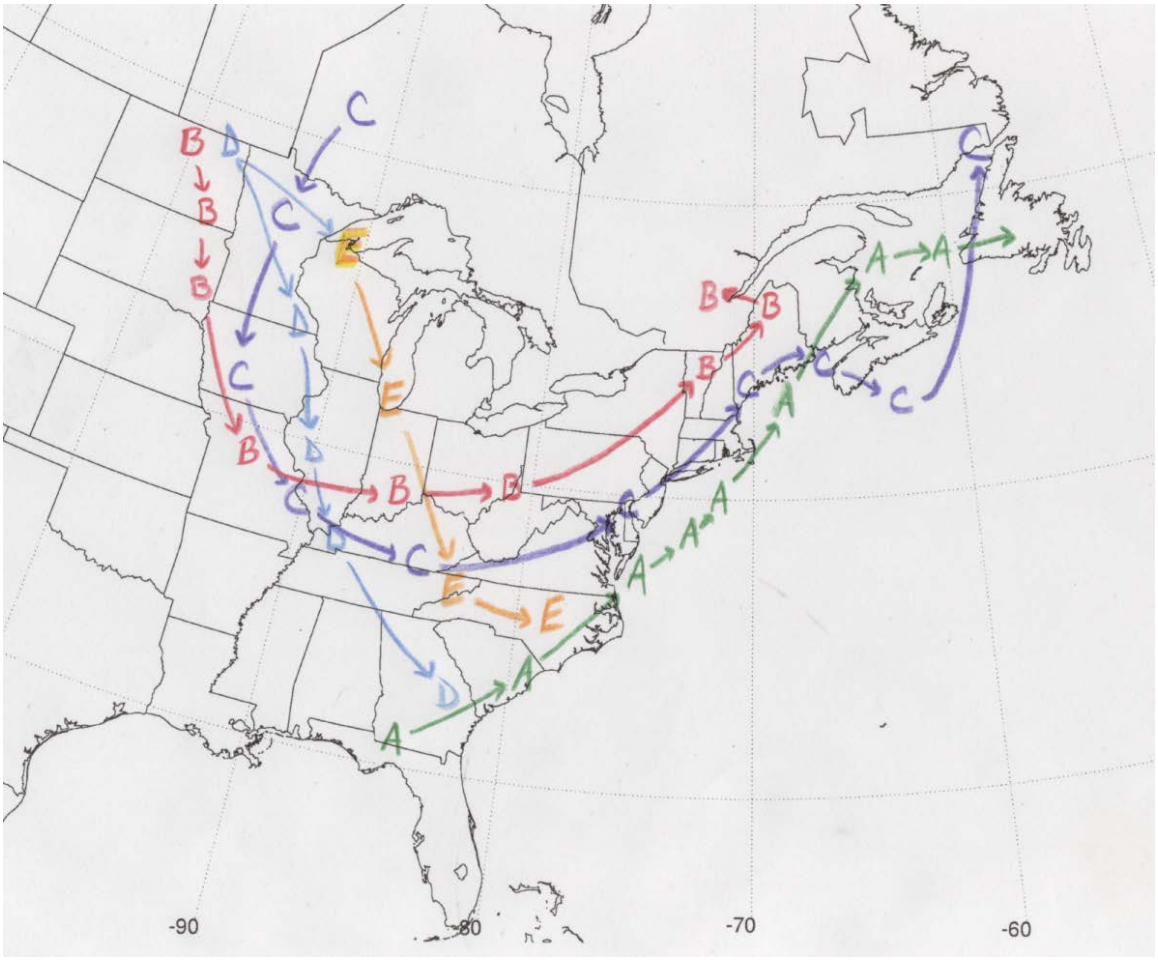

Fig. 4.10. Paths of five significant vorticity maxima centers at 12 h intervals: A (green) begins at 0000 UTC 23 May 2003 and ends at 1200 UTC 26 May 2003; B (red) begins at 0000 UTC 24 May 2003 and ends at 0000 UTC 28 May 2003; C (purple) begins at 1200 UTC 25 May 2003 and ends at 0000 UTC 30 May 2003; D (light blue) begins at 0000 UTC 28 May 2003 and ends at 0000 UTC 30 May 2003; E (light orange) begins at 1200 UTC 28 May 2003 and ends at 0000 UTC 30 May 2003.

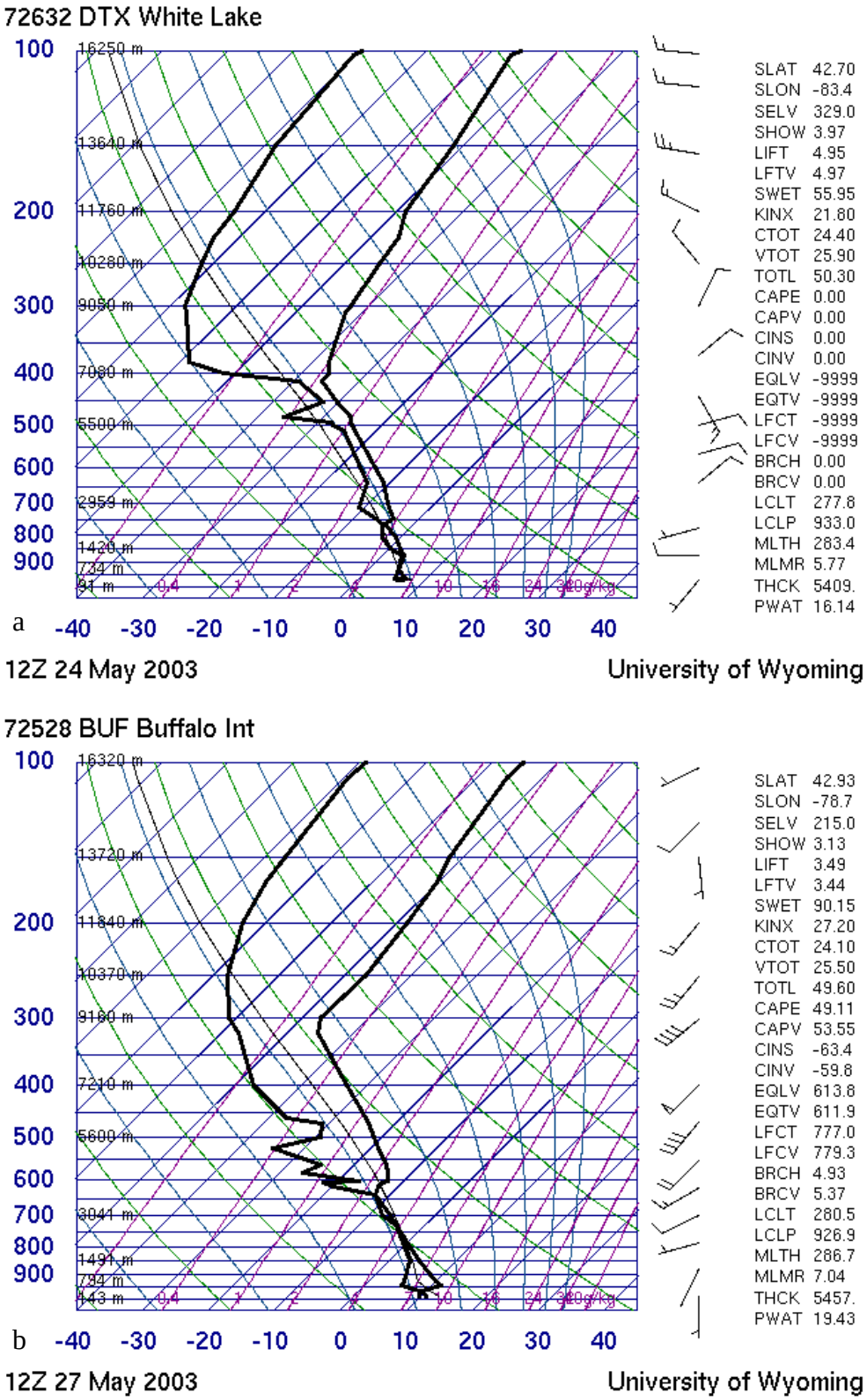

Fig. 4.11. Observed soundings from a) Detroit, MI (DTX) at 1200 UTC 24 May 2003 and b) Buffalo, NY (BUF) at 1200 UTC 27 May 2003, courtesy University of Wyoming.

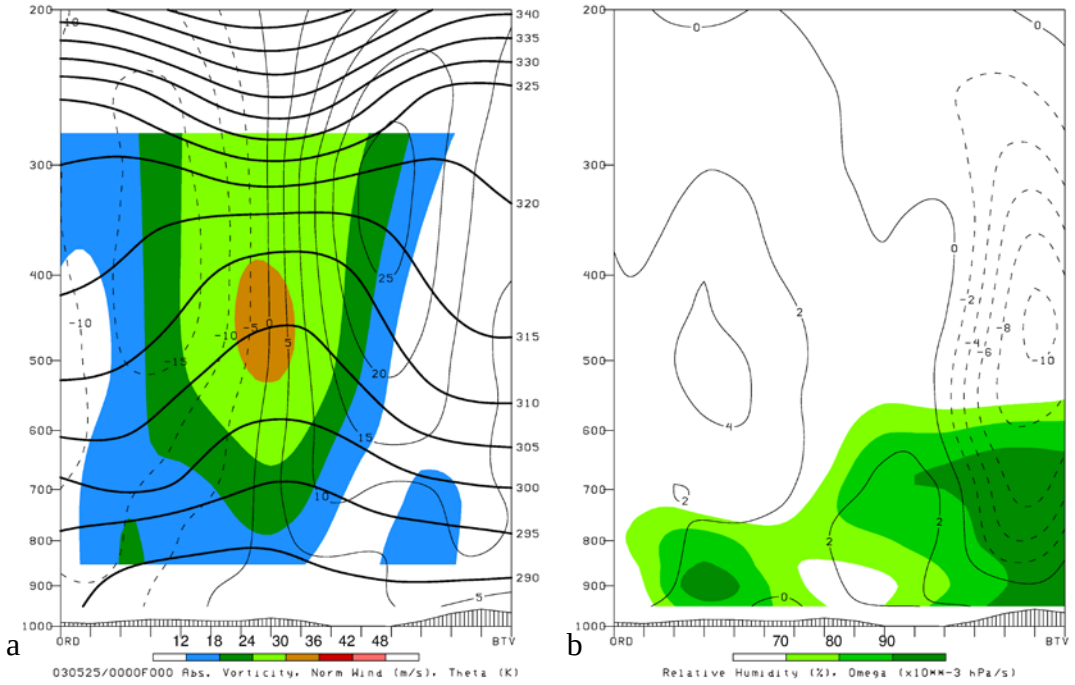

Fig. 4.12. Cross sections at 0000 UTC 25 May 2003 from Chicago, IL (ORD) to Burlington, VT (BTV) showing a) absolute vorticity (shaded every 6 x 10^{-5} s^{-1}), potential temperature (heavy solid lines every 5 K), and normal component of the wind [contoured every 5 m s^{-1}, positive (negative) light contours indicate south–southeasterly (north–northwesterly) flow] and b) relative humidity (shaded above 70%) and vertical velocity [solid (dashed) lines depict sinking (rising) motion, contoured every 2 x 10^{-3} hPa s^{-1}].

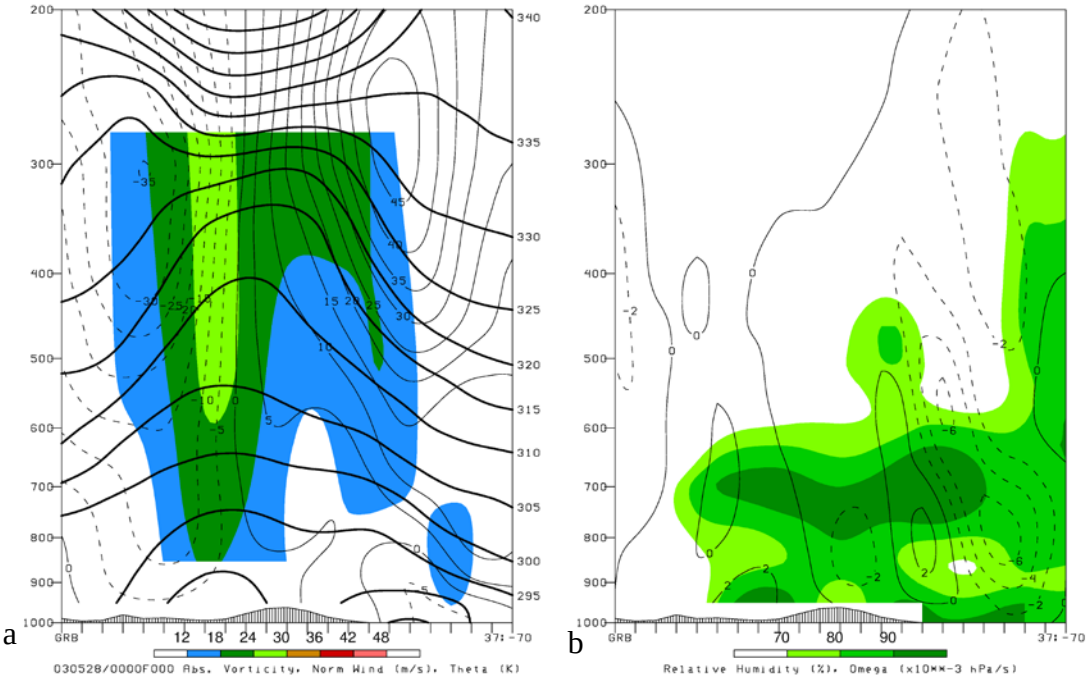

Fig. 4.13. As in Fig. 4.13, except for 0000 UTC 28 May 2003 from Green Bay, WI (GRB) to 37ºN, 70ºW (at an intersection east of Norfolk, VA and south of Cape Cod, MA) and positive (negative) light contours indicate southwesterly (northeasterly) flow.

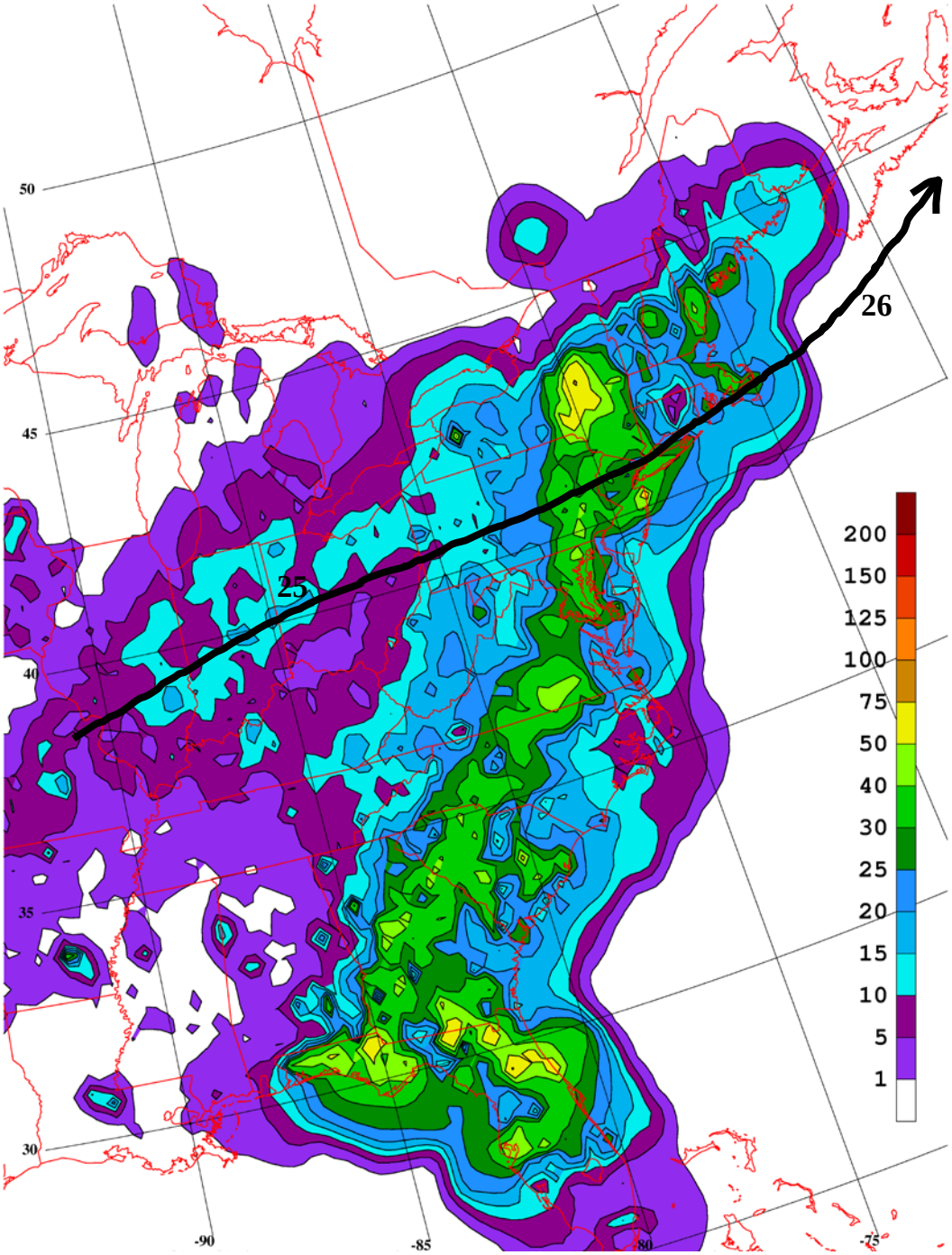

Fig. 4.14. Three–day (72 h) precipitation plot (mm) from 1200 UTC 24 December 2002 through 1200 UTC 27 December 2002. Dark solid line indicates track of 500 hPa cutoff low (beginning at 0000 UTC 25 December) with indicated daily 1200 UTC locations.

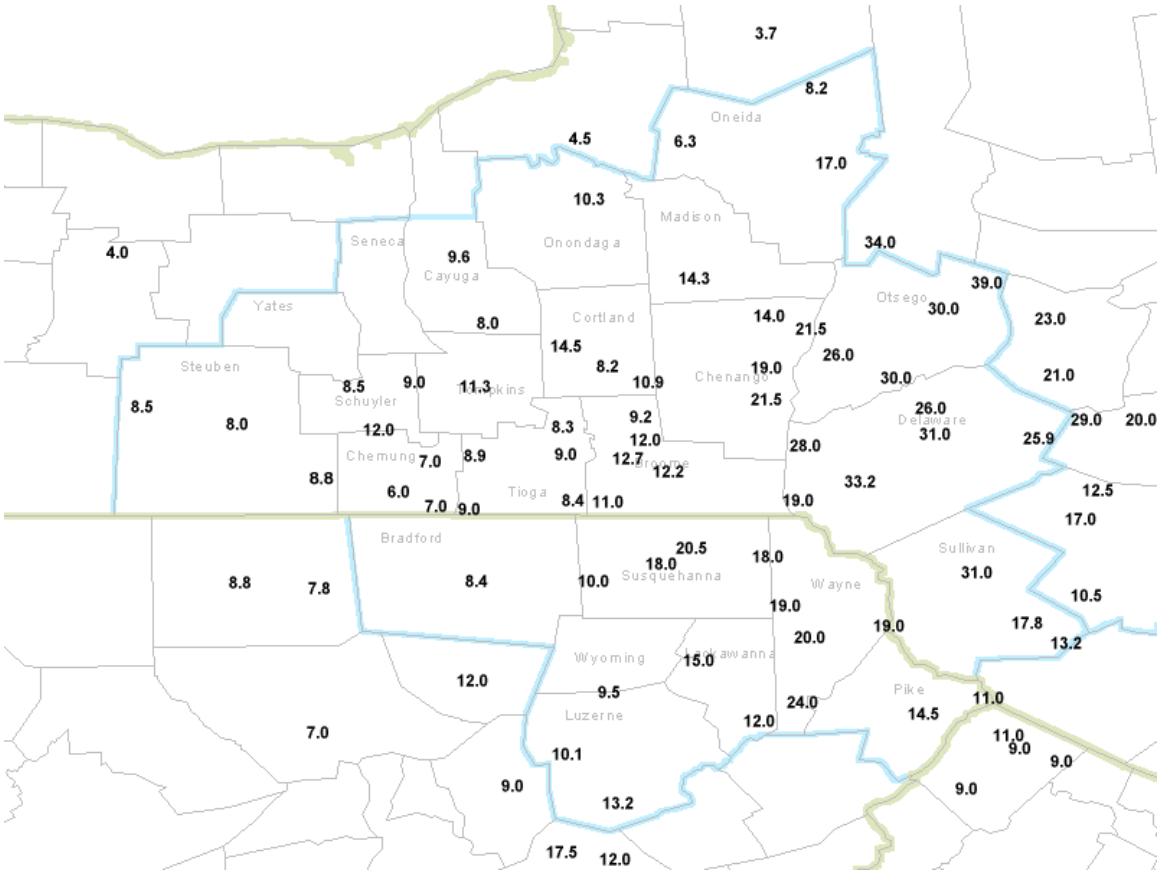

Fig. 4.15. Storm total snowfall observations (inches) over central New York for the period 24–26 December 2002, courtesy NWS BGM.

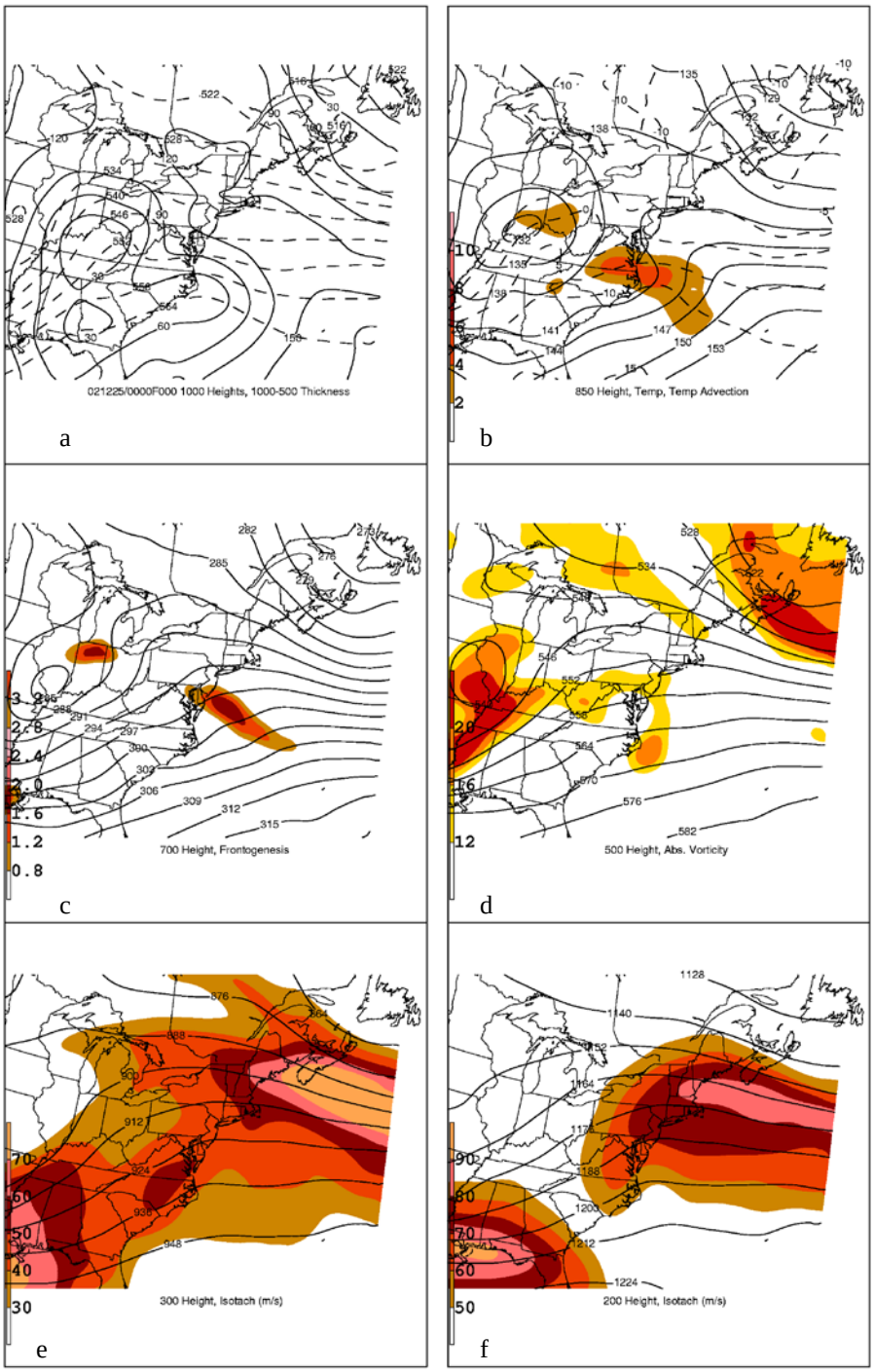

Fig. 4.16. Six–panel plot at 0000 UTC 25 December 2002 showing: a) 1000 hPa geopotential height (m, solid) and 1000–500 hPa thickness (dam, dashed); b) 850 hPa geopotential height (dam, solid), temperature (ºC, dashed), and temperature advection (0.1ºC day^{-1}, shaded); c) 700 hPa geopotential height (dam, solid) and Miller 2-D frontogenesis [ºC (100 km)$^{-1}$ (3 h)$^{-1}$, shaded]; d) 500 hPa geopotential height (dam, solid) and absolute vorticity (10^{-5} s^{-1}, shaded); e) 300 hPa geopotential height (dam, solid) and wind speed (m s^{-1}, shaded); f) 200 hPa geopotential height (dam, solid) and wind speed (m s^{-1}, shaded).

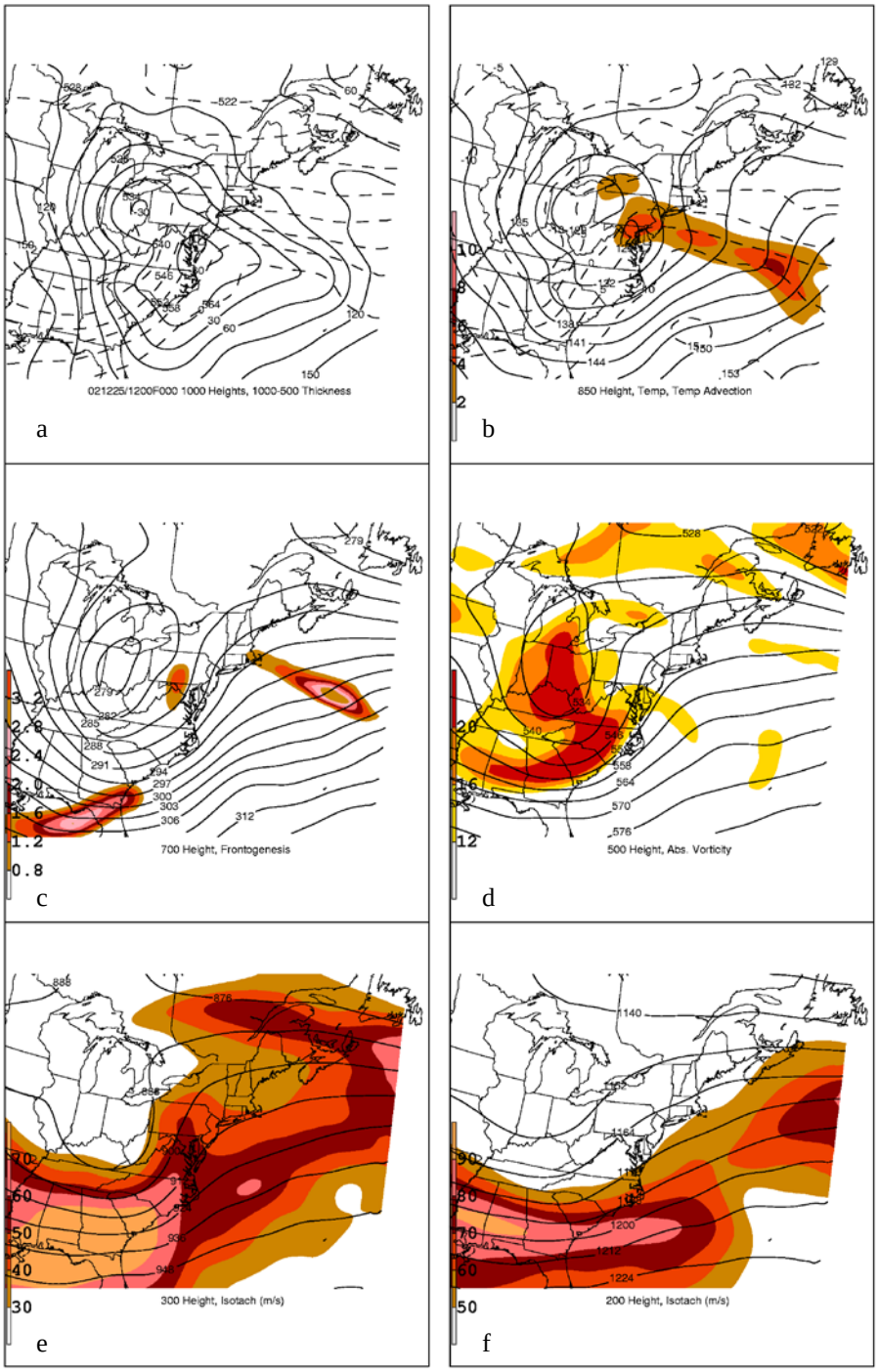

Fig. 4.17. As in Fig. 4.16, except for 1200 UTC 25 December 2002.

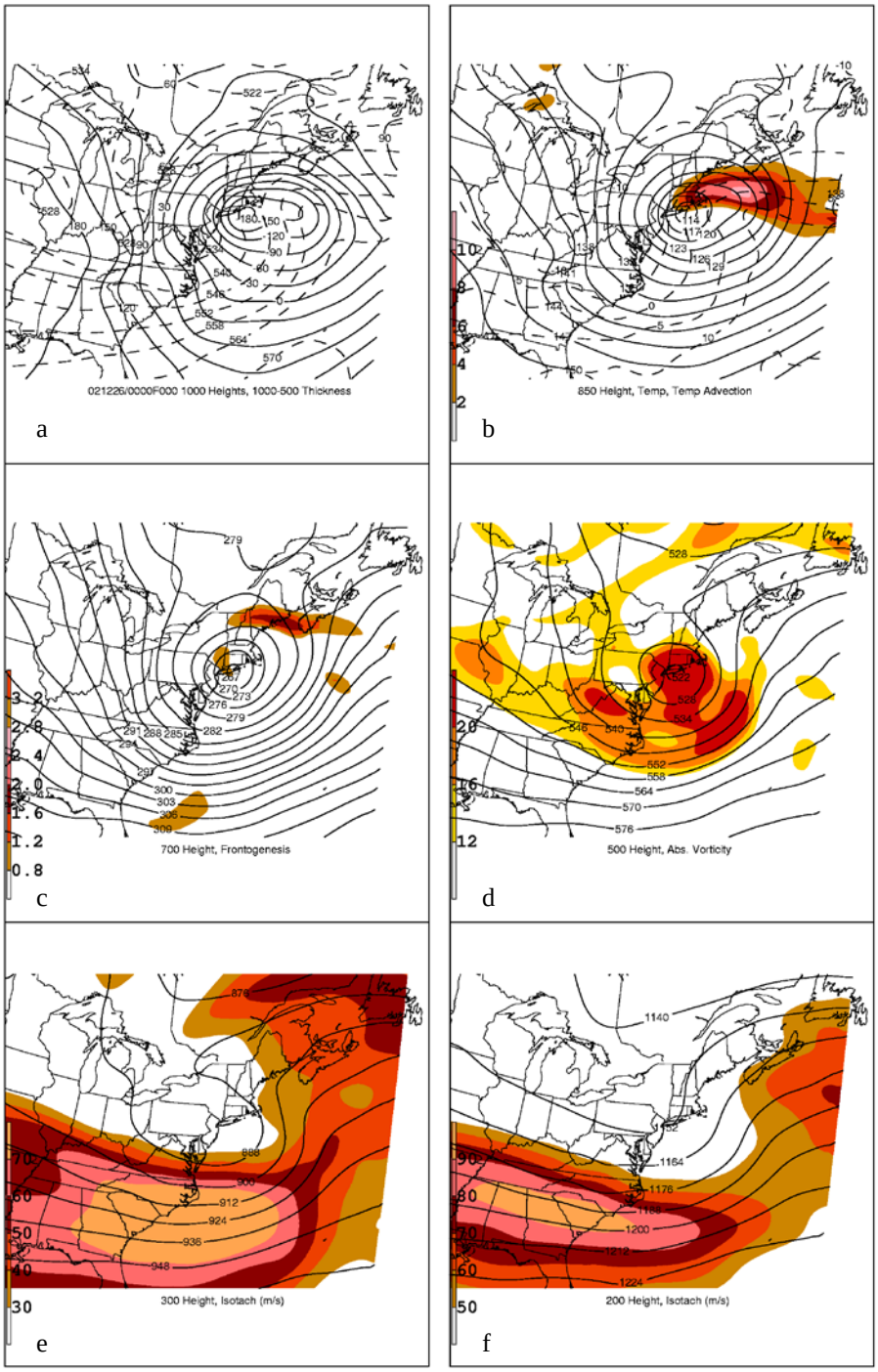

Fig. 4.18. As in Fig. 4.16, except for 0000 UTC 26 December 2002.

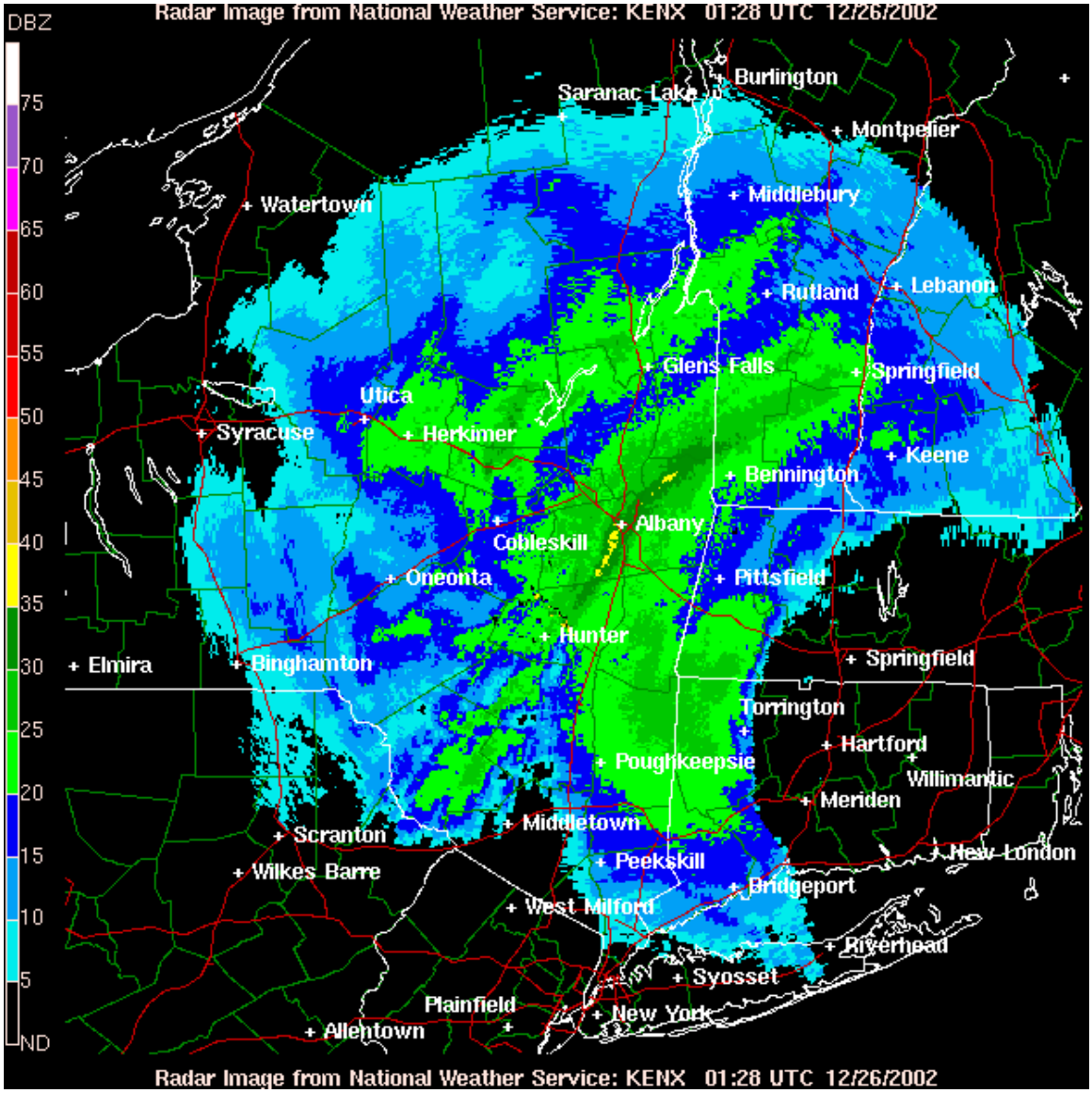

Fig. 4.19. Radar image from Albany, NY (KENX) Radar at 0128 UTC 26 December 2002.

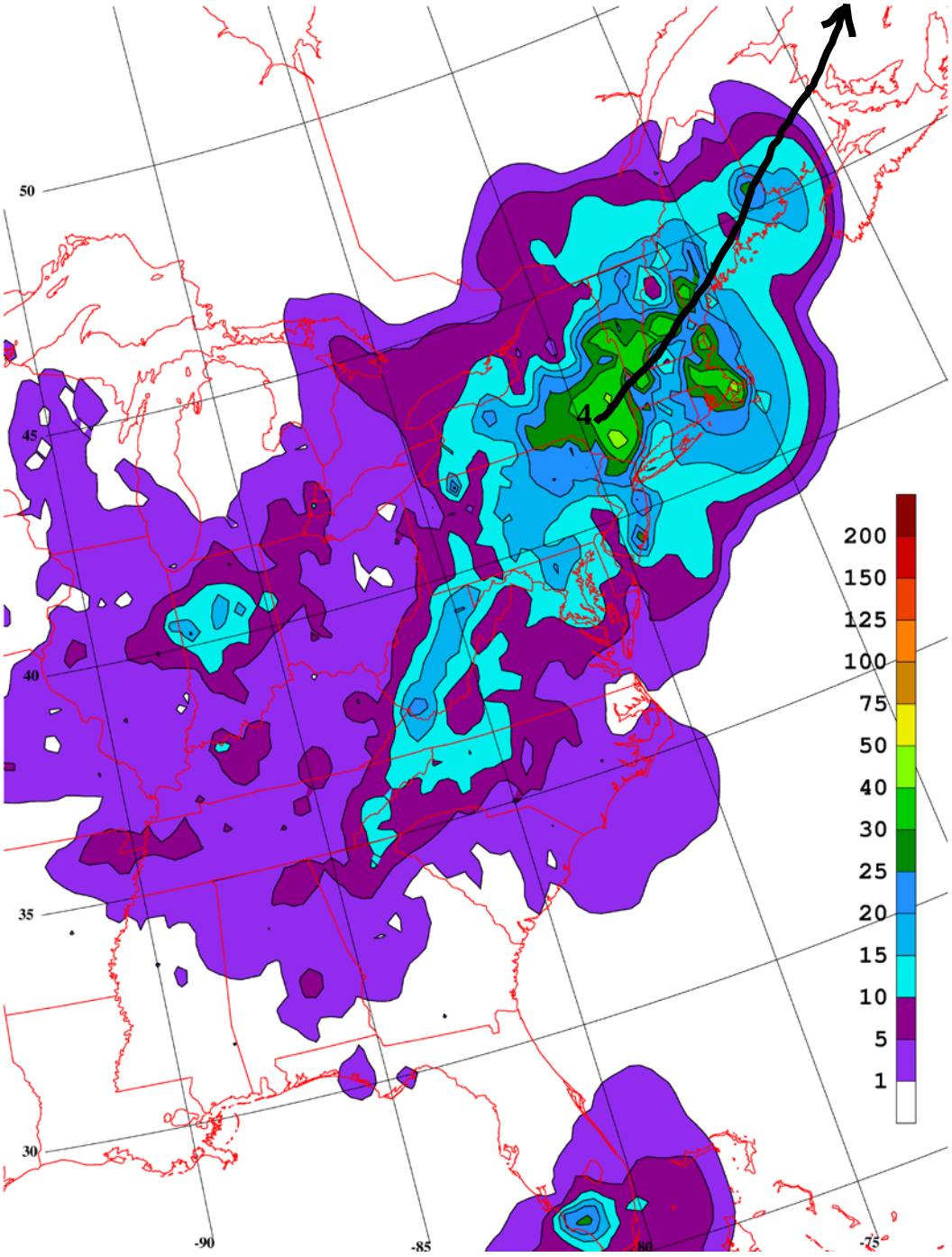

Fig. 4.20. As in Fig. 4.14, except for the period 1200 UTC 2 January 2003 through 1200 UTC 5 January 2003. Note that 1200 UTC 4 January is the first time the cutoff is observed.

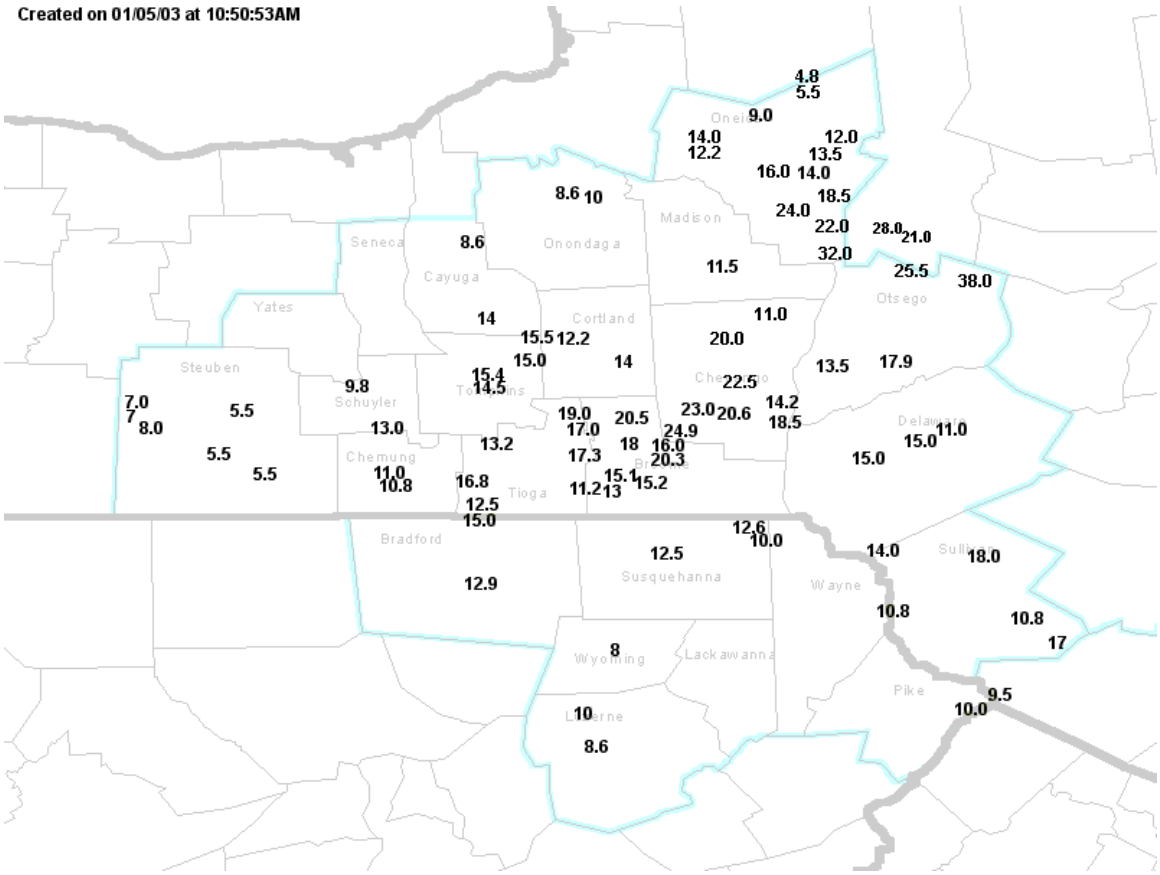

Fig. 4.21. As in Fig. 4.15 except for the period 3 January through 5 January 2003.

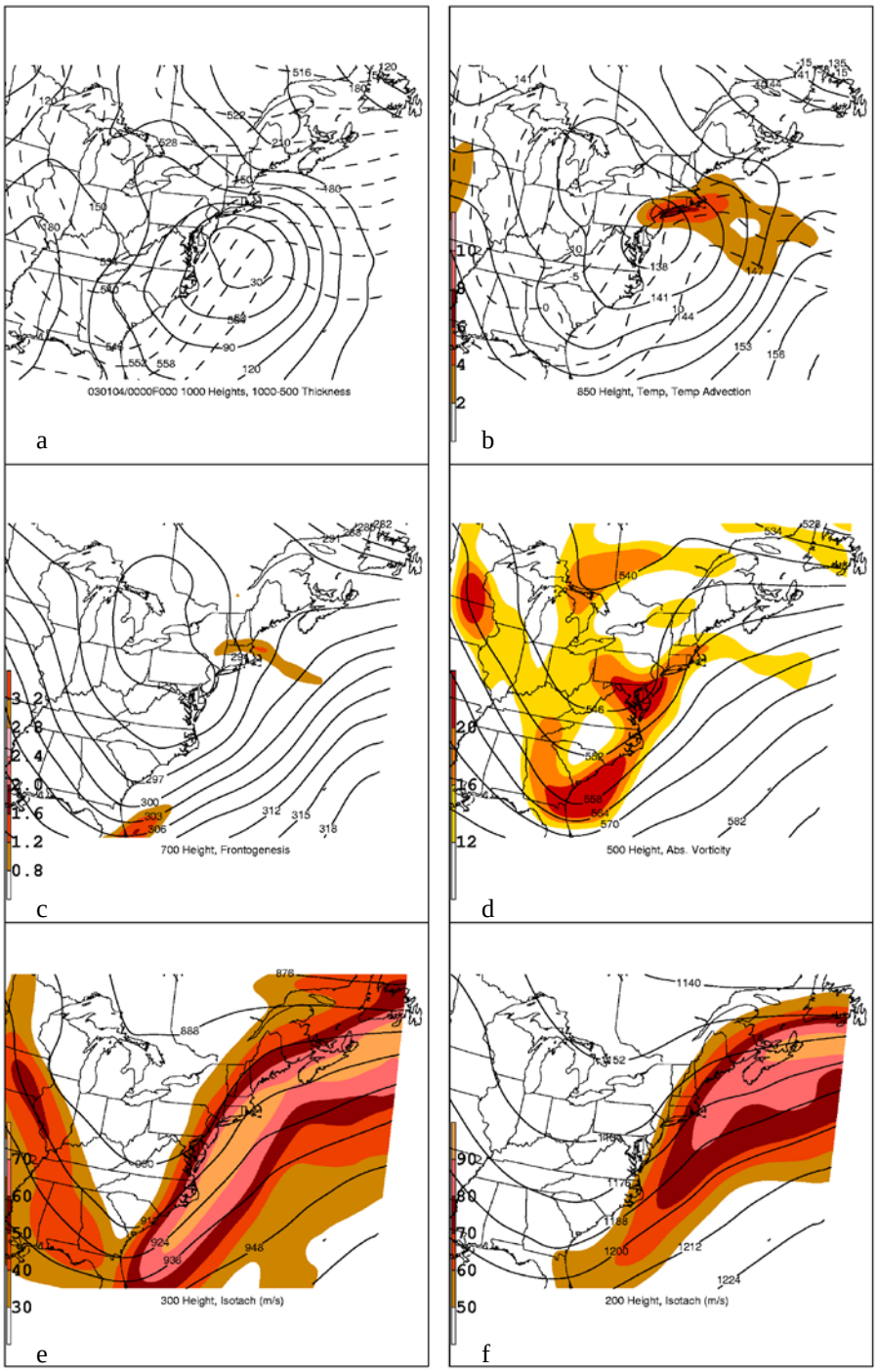

Fig. 4.22. As in Fig. 4.16, except for 0000 UTC 4 January 2003.

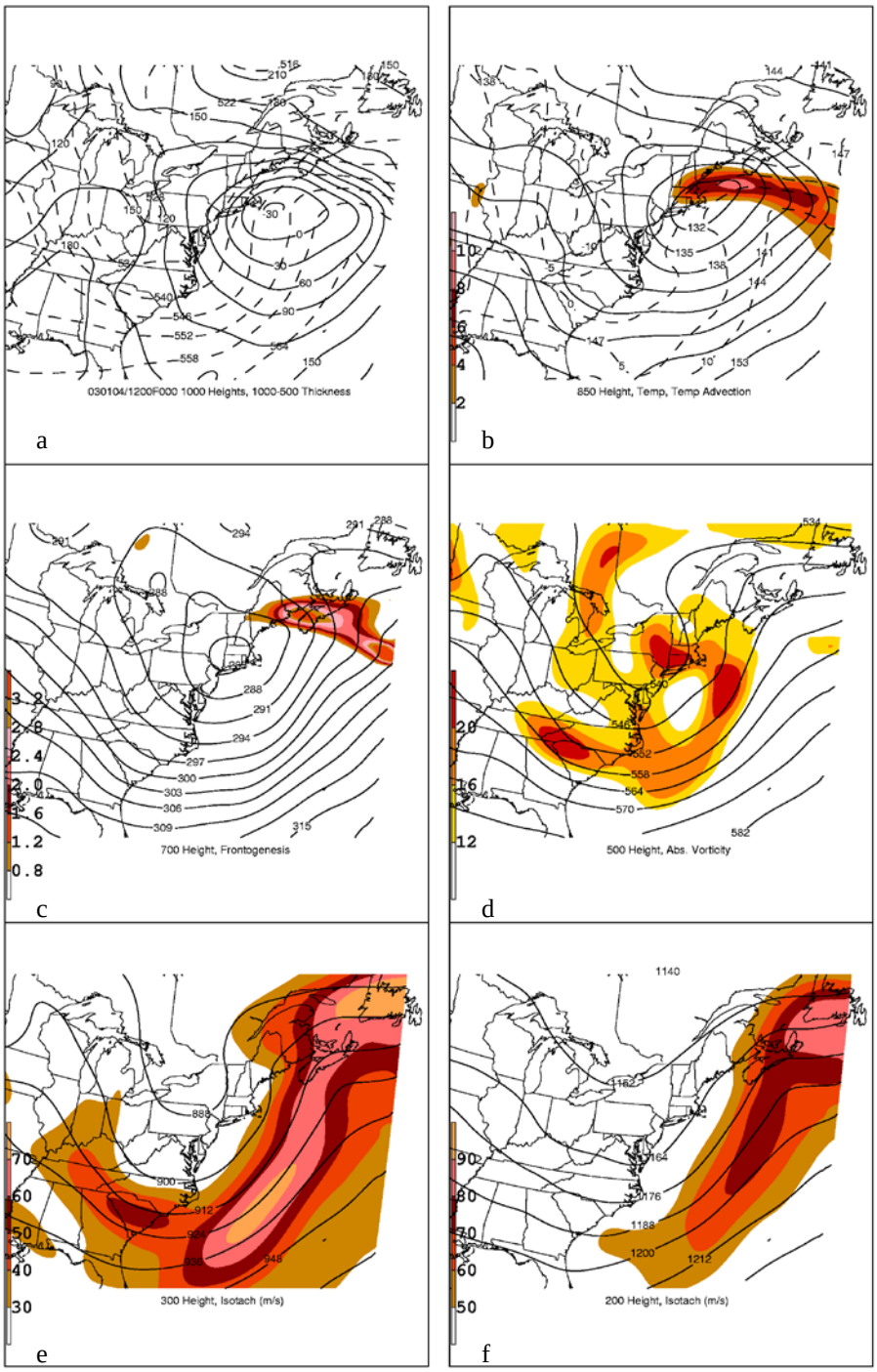

Fig. 4.23. As in Fig. 4.16, except for 1200 UTC 4 January 2003.

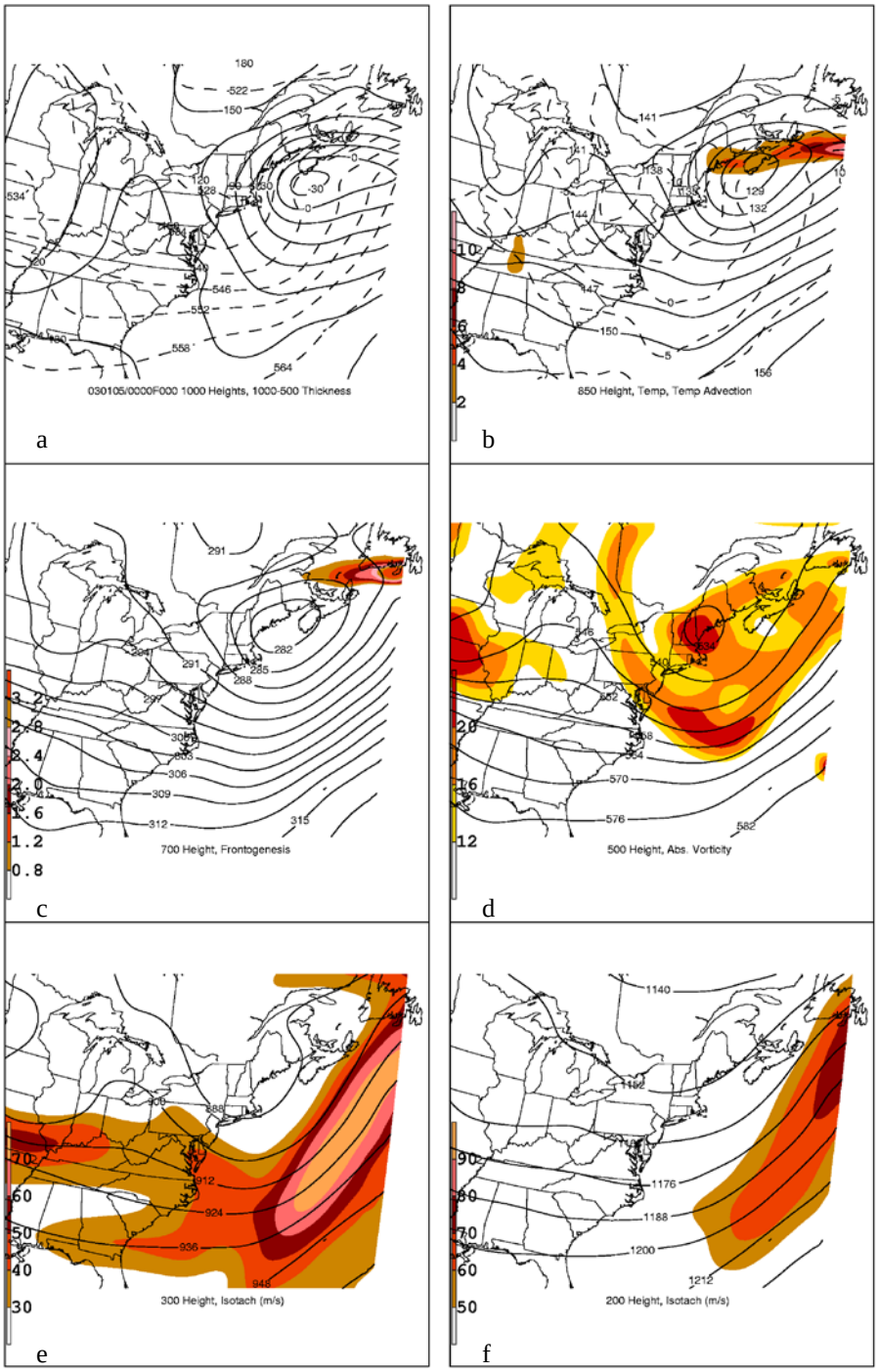

Fig. 4.24. As in Fig. 4.16, except for 0000 UTC 5 January 2003.

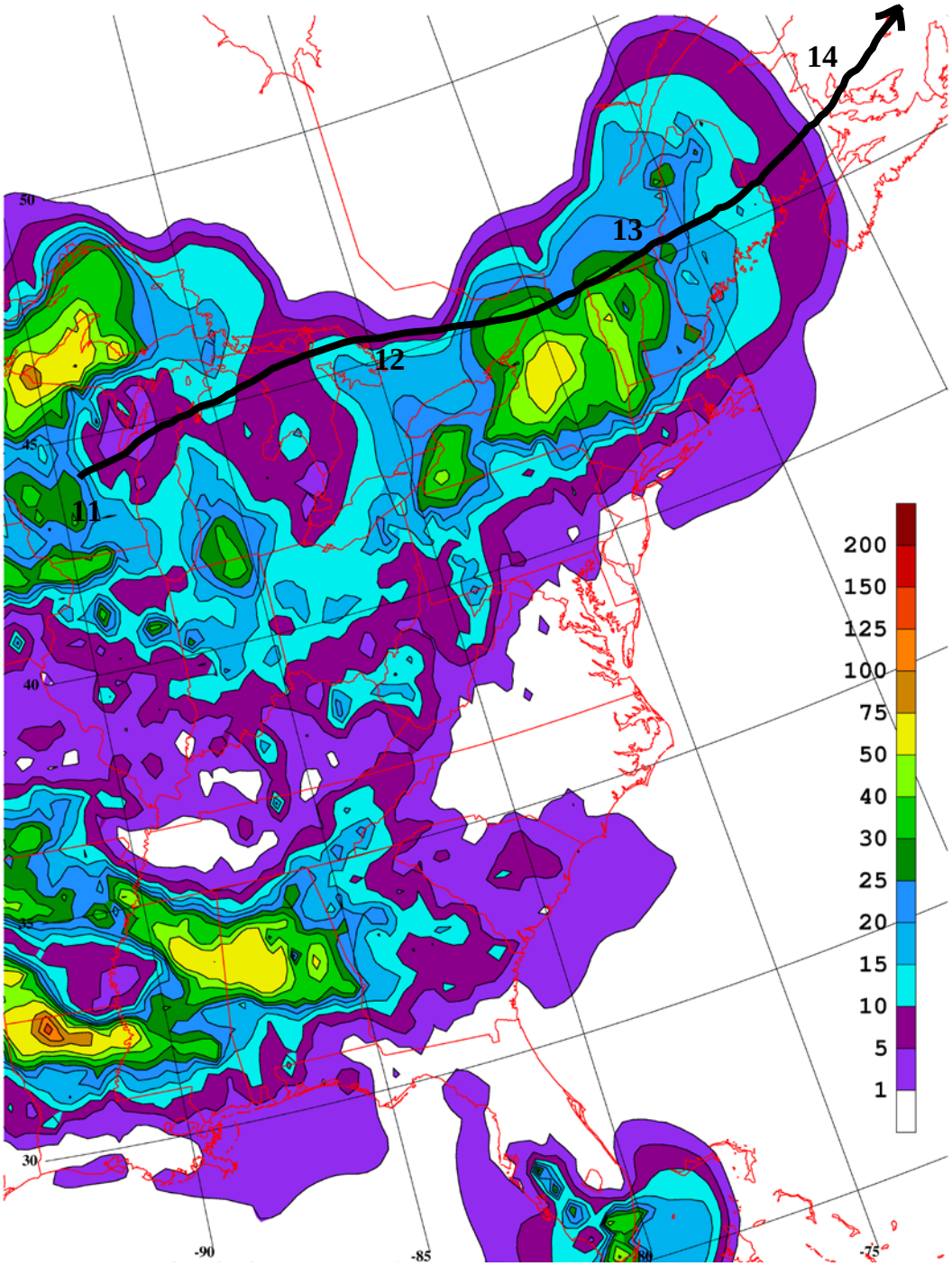

Fig. 4.25. As in Fig. 4.1 except for the period 1200 UTC 11 May 2003 through 1200 UTC 15 May 2003.

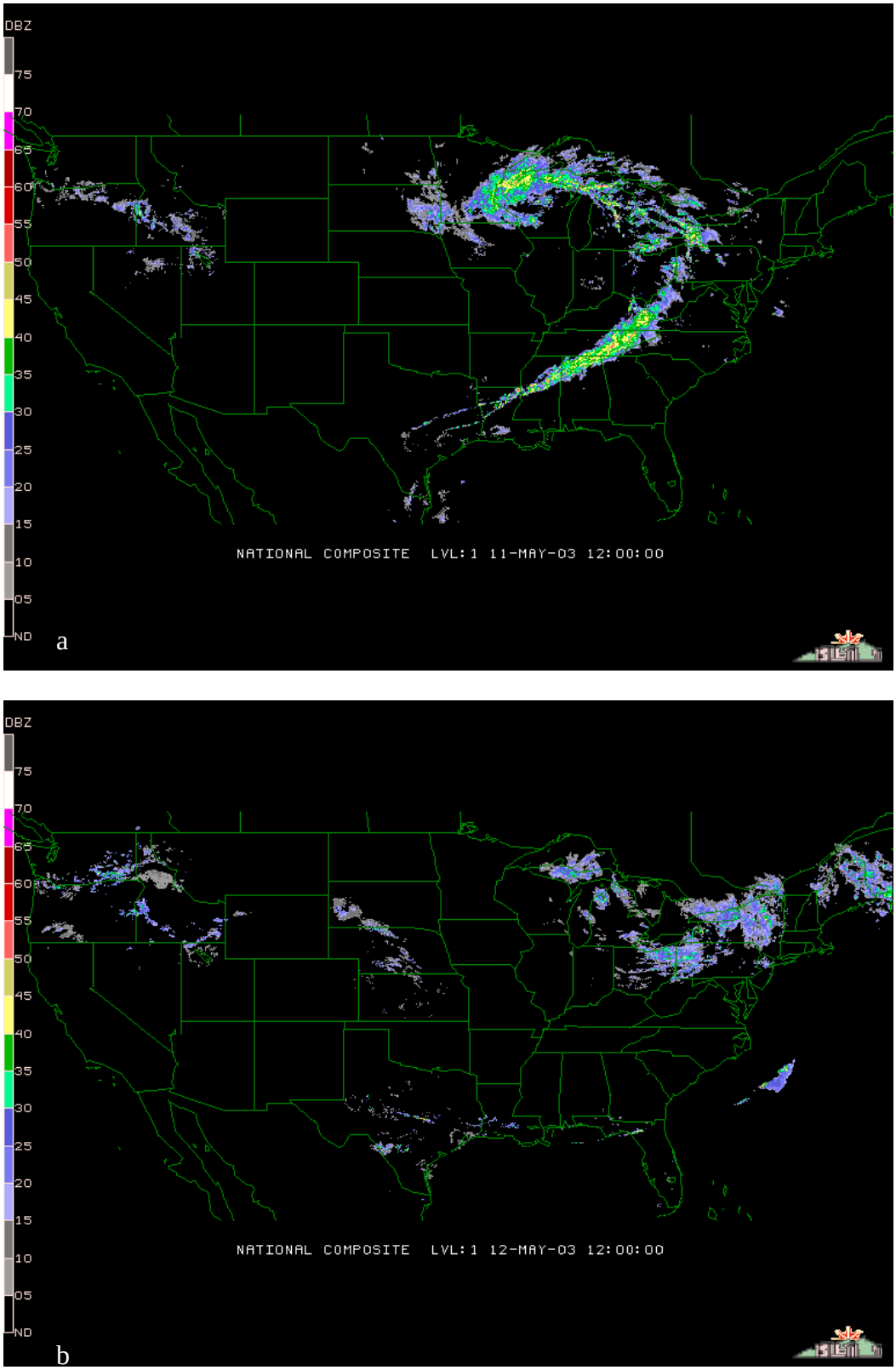

Fig. 4.26. Composite radar (0.5º elevation angle) at 1200 UTC on: a) 11 May 2003, b) 12 May 2003, c) 13 May 2003, d) 14 May 2003.

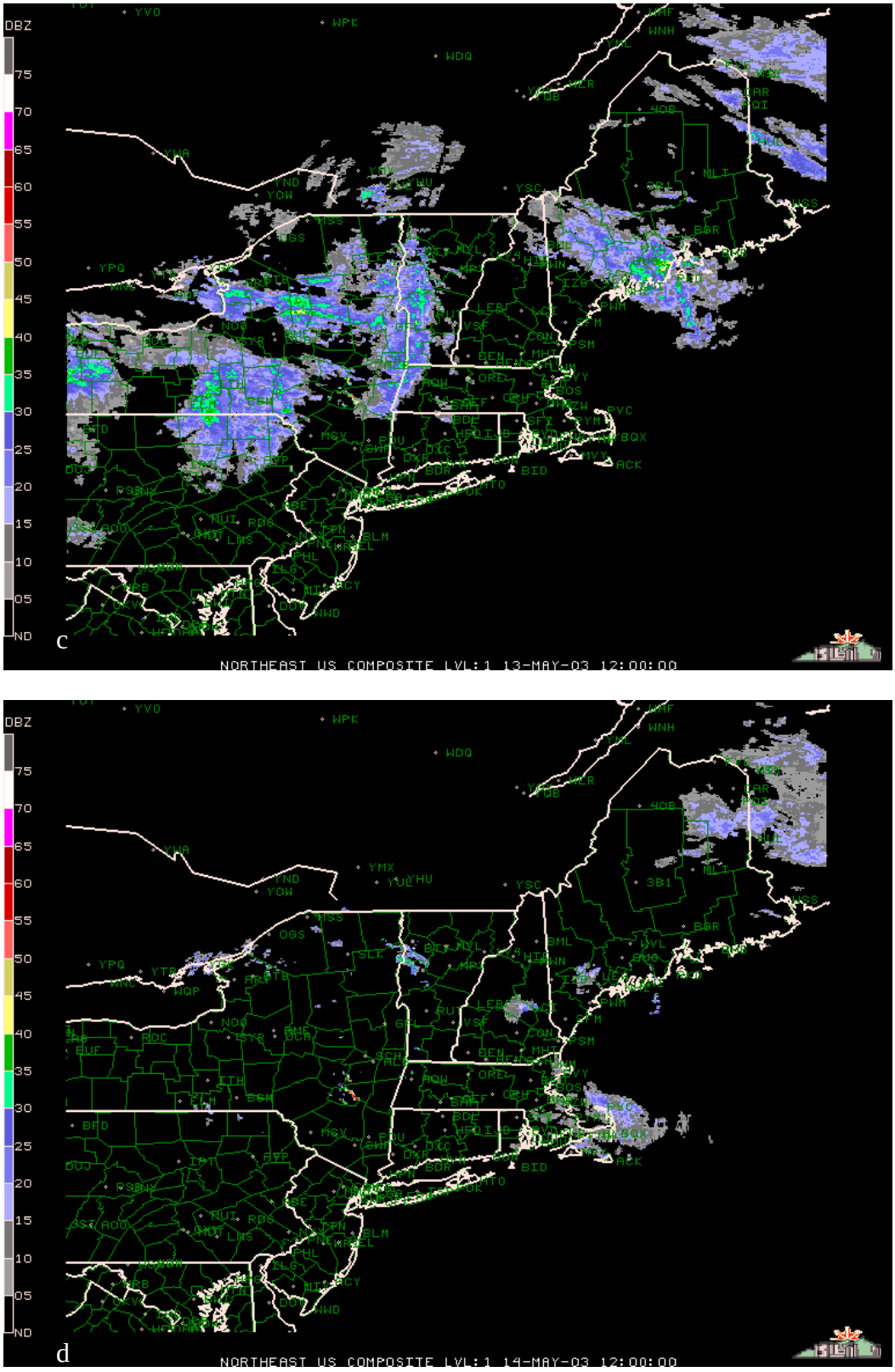

Fig. 4.26. Continued.

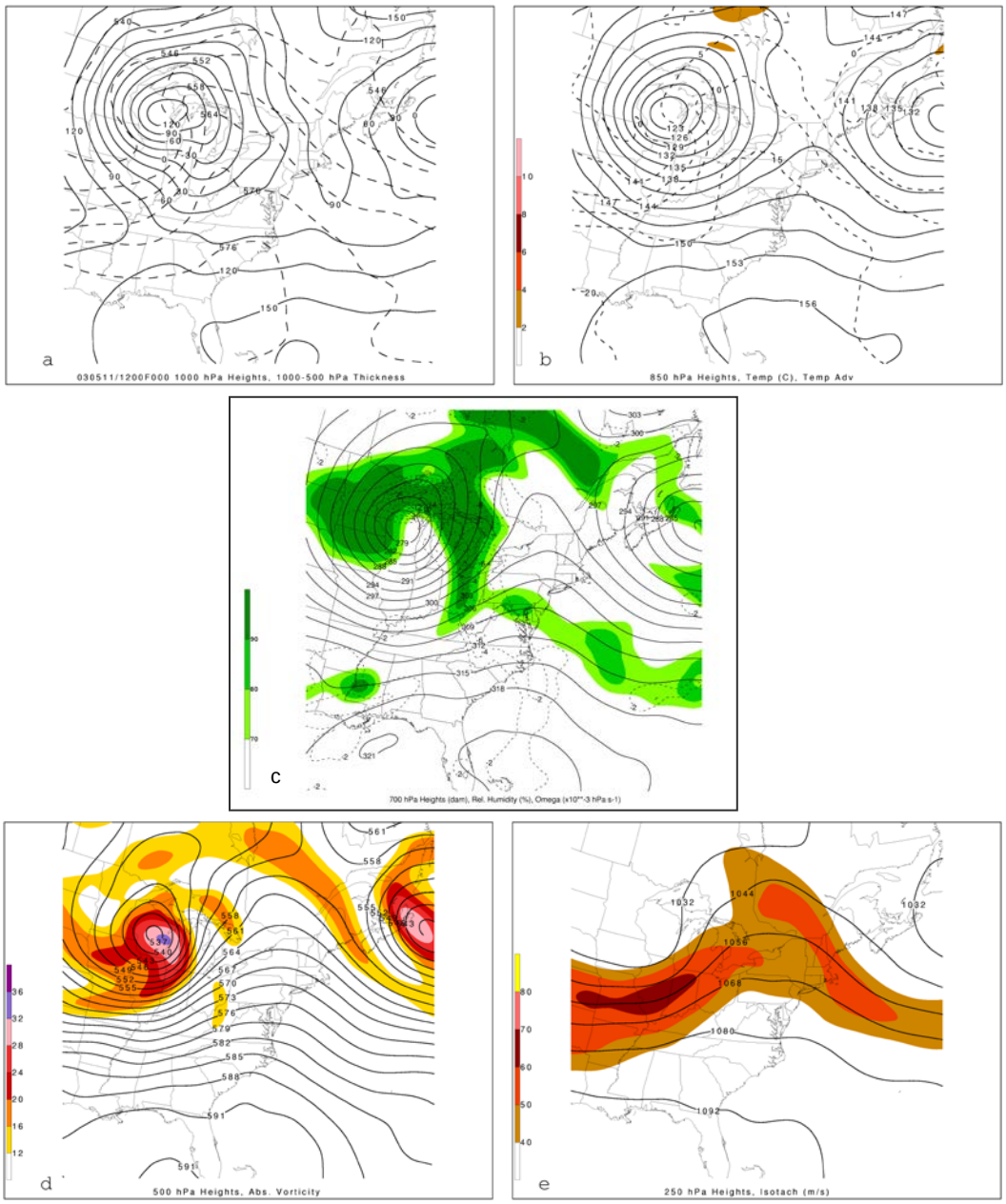

Fig 4.27. As in Fig. 4.4, except for 1200 UTC 11 May 2003.

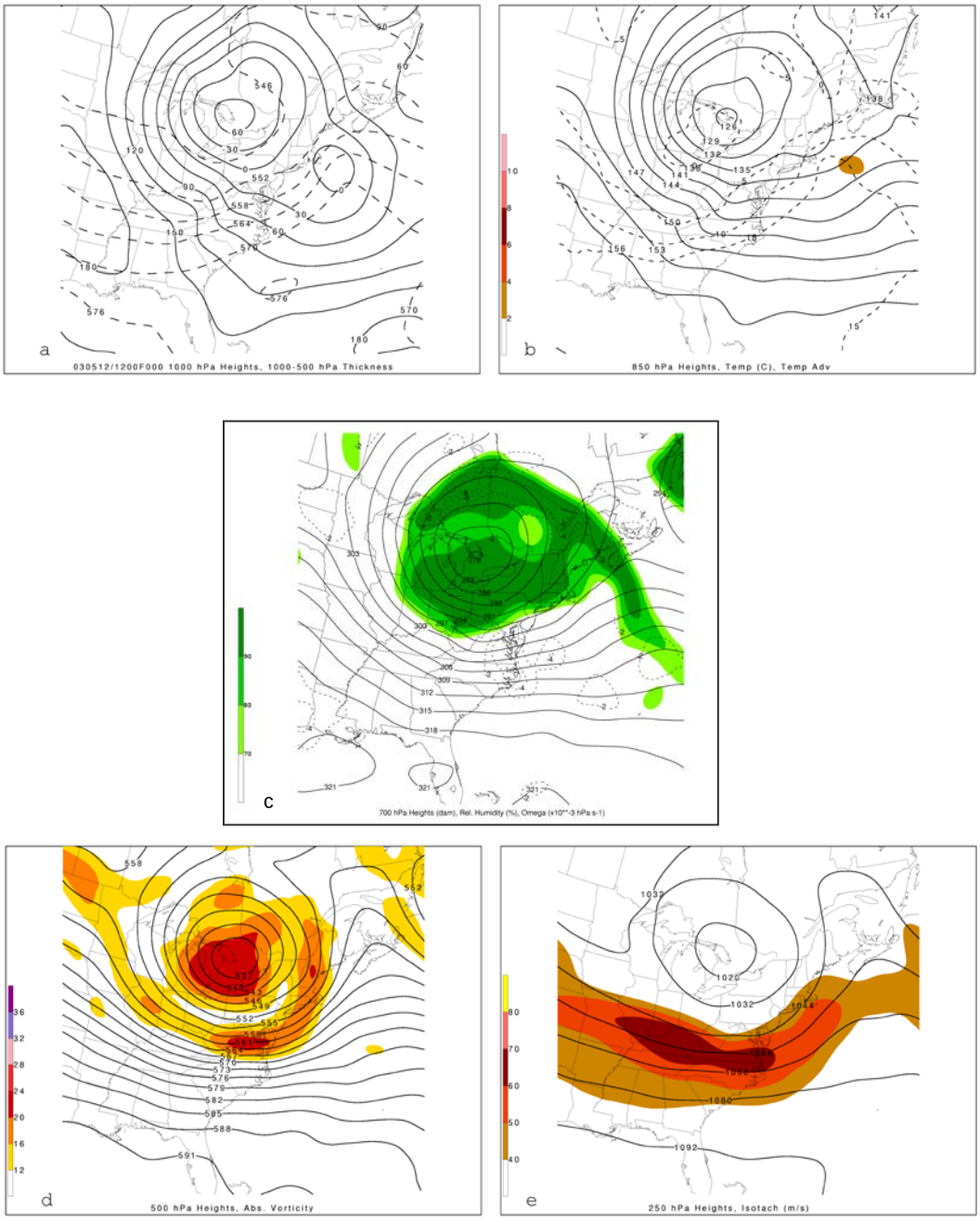

Fig 4.28. As in Fig. 4.4, except for 1200 UTC 12 May 2003.

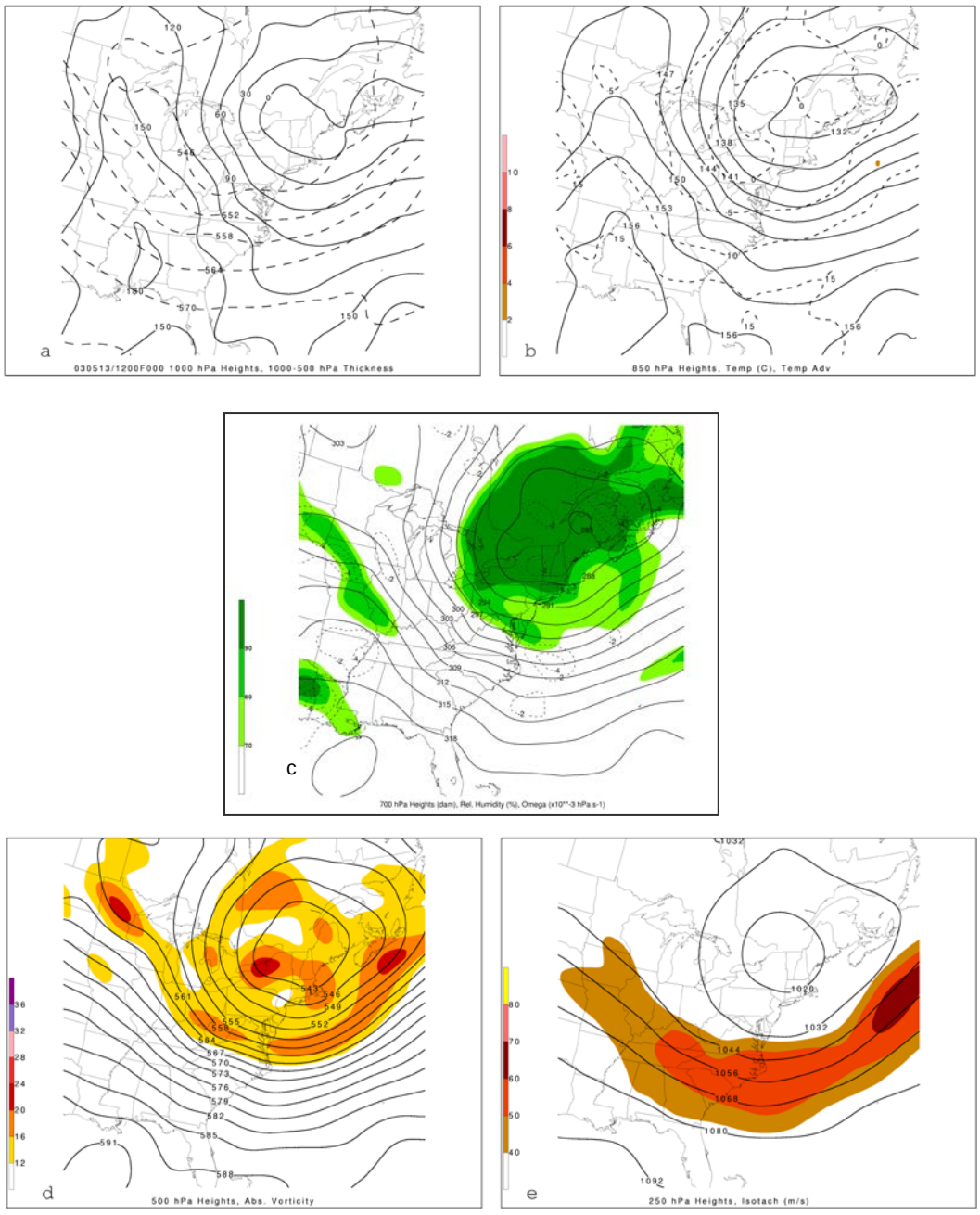

Fig 4.29. As in Fig. 4.4, except for 1200 UTC 13 May 2003.

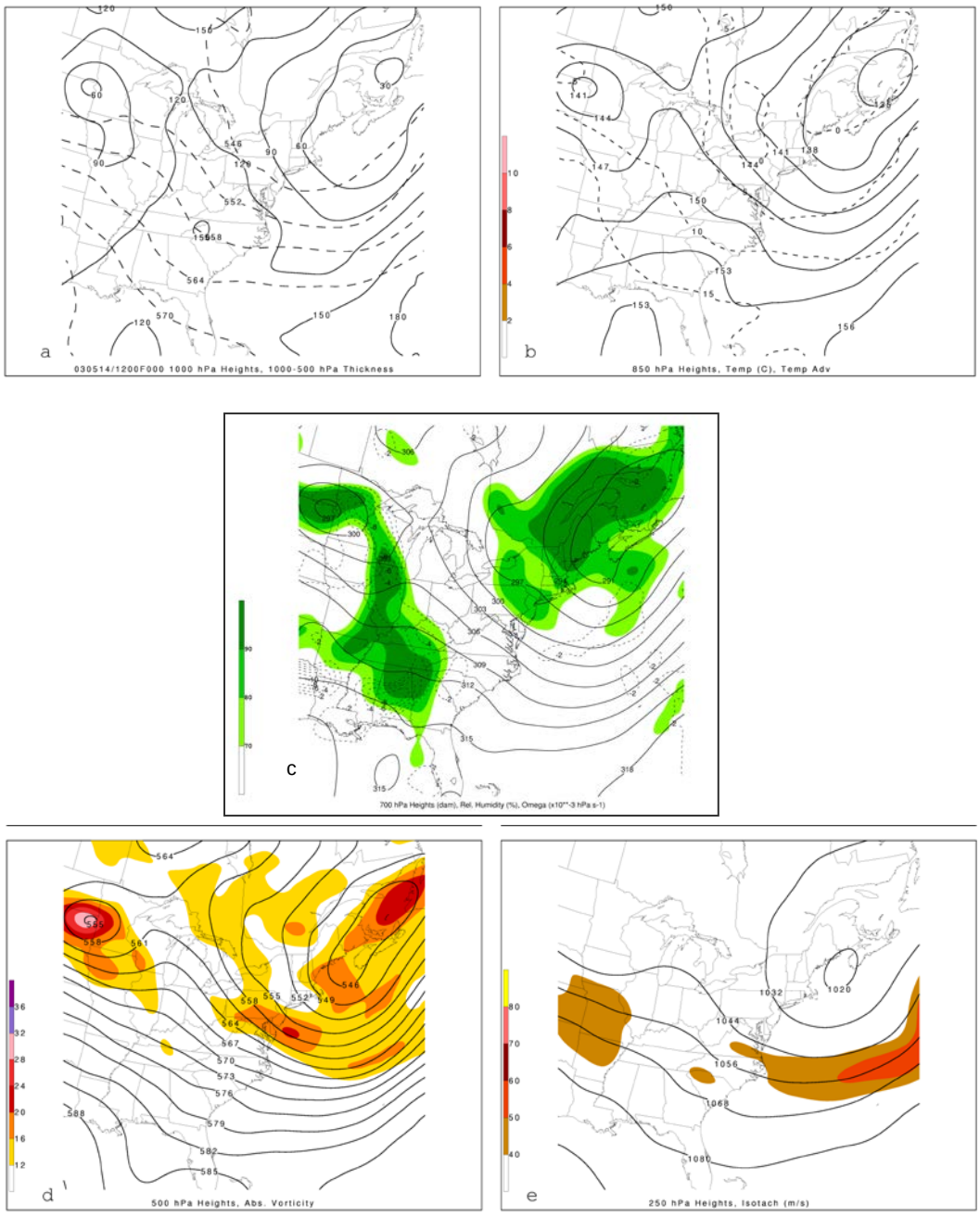

Fig 4.30. As in Fig. 4.4, except for 1200 UTC 14 May 2003.

5. Discussion

5.1 Precipitation Climatology

5.1.1 Average Daily Precipitation

The results from the average daily precipitation maps for the cool season months of October–May yield some insights into the precipitation variability of cutoff cyclones that affect the Northeast. Throughout the entire cool season (Figs. 3.2–3.9), the axis of maximum values of average daily precipitation (ADP) occurs along coastal areas of New England into New Jersey. At first glance, this distribution is to be expected since coastal areas climatologically receive more precipitation than inland areas. However, by April and especially May (Figs. 3.8–3.9), this axis shifts slightly inland. This shift might best be explained by the fact that convection tends to play a more dominant role in the mode of precipitation in April and May than in other cool season months. Since the nearby ocean waters are still quite cool in April and May, the convection tends to locate itself more inland, away from the immediate coast. Accordingly, the location of the coastal baroclinic zone might be stronger and located farther inland in late spring than in autumn, which may also tend to increase the APD values away from the coast. Also observed over the whole cool season is an overall decrease in the zonal gradient of ADP values. This decrease as well may be due to an increase in inland convection and/or perhaps a result of more variable cutoff tracks by spring due to the spindown of the Northern Hemispheric circulation.

Topographical effects are clearly evident in the APD maps throughout the cool season, but perhaps become less apparent by late spring. In addition, the shift in local maximum ADP values from just east of higher elevations to be nearly collocated with higher elevations may be the result of dominant upslope enhancement in winter (December–February) (e.g., Passarelli and Boehme 1983, Atallah and Aiyyer 2002) versus more of a convective mode in late spring (April and May).

5.1.2 Percent of Climatology

Cutoff lows are associated with between one-third to two-thirds of the average monthly precipitation across the Northeast during the cool season. A direct consequence of this fact is that a lack of cutoff activity in the area leads to a possibility of drought. Area-wide values decrease from October to January, then increase again to a maximum in April [coinciding with a maximum of cutoff frequency across the area (see Fig. 3.1)]. May values are slightly lower than April values across the Northeast. Higher values are consistently located in Maine, closer to the preferred cutoff tracks (see Fig. 1.9). Figure 3.1 shows that during October, November, and February a cutoff is observed about 30% of the time near the Northeast. However, note that values range from 50% to 70% in October and November (Figs. 3.10 and 3.11, respectively), yet are about 10% lower everywhere in February (Fig. 3.14). This distribution infers that cutoffs produce more precipitation on average in autumn than in late winter, relative to each month's average area-wide precipitation. Also evident during the cool season, contrary to the ADP maps, is a lack of an orographic signal, meaning that higher elevations usually receive more

precipitation than lower elevations in the same proportion from cutoffs as they do from all sources. In other words, if a higher elevation normally receives 100 mm of precipitation in a month compared to 75 mm for a nearby lower elevation, then the total monthly precipitation associated with cutoffs, relative to each location's climatological average, would be roughly the same (perhaps 50 mm for the higher elevation compared to 35 mm for the lower elevation). Overall, the percent of precipitation associated with cutoffs compared to the climatological normal appears to be related to cutoff occurrence; i.e., higher values occur closer to areas that experience more cutoffs.

5.1.3 Precipitation Distribution of Four Cutoff Tracks

Four preferred cool–season cutoff tracks that affect the Northeast (see Fig. 1.9) were used as a basis to categorize cutoffs over the period 1980–1998, based on a subjective reanalysis. Figures 3.18–3.25 show the average daily precipitation and storm-relative average daily precipitation for each of the four tracks. Cutoffs following the Mid-Atlantic track show a maximum in ADP values near the coast (see Fig. 3.18), along with an upslope enhancement to the east of the higher elevations, due to a mean easterly to northeasterly flow associated with cutoffs passing just to the south of New England. The storm-relative ADP plot reveals a maximum to the north of the cutoff's average ending 24 h location (see Fig. 3.19), ahead of and just to the left of its track. This location is likely a result of strong surface cyclone dynamics coupled with an influx of moisture from the Atlantic Ocean in a classic nor'easter type storm.

Southwest track cutoffs produce as much precipitation as Mid-Atlantic cutoffs and also have a coastal maximum in ADP values (see Fig. 3.20), but the distribution is more spread out than Mid-Atlantic cutoffs. The storm-relative ADP map (see Fig. 3.21) shows that the maximum in precipitation occurs well to the east of the average 24 h ending location. This separation is likely due to a deep and moist southerly or southwesterly flow around the cutoff into the Northeast, with areas near the cutoff unable to generate more precipitation. In addition, surface low pressure systems may develop on the periphery of the cutoff and move along the Northeast coast, enhancing precipitation. This scenario occurred during a cutoff event from 3–5 July 1996 (Najuch 2004), where a moist southeasterly flow over New England aided in precipitation enhancement.

Cutoffs following the Clipper track are comparatively much drier than cutoffs of the previous two tracks, but are still associated with distinct precipitation patterns. The ADP map (see Fig. 3.22) shows a clear lake-effect signal downwind of Lakes Erie and Ontario (aided by the elevated Tug Hill Plateau region), due to a mean westerly flow across the lakes as the cutoff passes to the north of these areas. The Berkshire and Green Mountains are also local maxima, but coastal New England receives the most precipitation, on average, from Clipper cutoffs. This increase in values may be attributed to an increase in the availability of moisture from the Atlantic Ocean perhaps with an associated surface cyclone development. The storm-relative map (see Fig. 3.23) shows a maximum in precipitation values along the cutoff's track and ahead of its average 24 h ending position. Clipper cutoffs typically produce light precipitation by cyclonic vorticity advection and warm air advection ahead of the system, with lesser amounts farther away from the cutoff.

Hudson Bay cutoffs primarily affect Maine, as evident in Fig. 3.24, with the absolute maxima located there. Other local maxima occur near Mount Washington and Mount Mansfield (and in the southwestern Tug Hill Plateau region) due to upslope enhancement, and also to the southeast of the east end of Lakes Erie and Ontario, due to lake enhancement. The storm-relative ADP map (see Fig. 3.25) reveals a similar pattern to Clipper cutoffs, with the maximum precipitation along the cutoff's track, but overall values are the least among the four tracks. Again, weak cyclonic vorticity and warm air advection are the primary causes for precipitation with Hudson Bay cutoffs.

5.2 Case Studies

5.2.1 23–31 May 2003

The first case study illustrates the importance of looking at the periphery of the cutoff, as this area tends to be where the bulk of precipitation will fall. During this cutoff's lifetime, it transitioned through three stages: a Southwest track, a stationary stage, and then its exiting phase out of the Northeast. Figures 4.3a–f show the progression of the precipitation associated with the cutoff as well as the five vorticity maxima that rotated around the cutoff. Comparing Fig. 4.10 with Figs. 4.1 and 4.2 reveals that the bulk of precipitation was well removed from the cutoff's track, and aligned closer to the tracks of the individual 500 hPa vorticity maxima rotating around the cutoff.

The precipitation immediately surrounding the cutoff during its initial stage was driven primarily by a weak upward increase in cyclonic vorticity advection and the associated divergence aloft, but both ceased during the cutoff's second stage. The contours of absolute vorticity became collocated with the geopotential height contours (thus eliminating any cyclonic vorticity advection), and the 250 hPa jet stream became elongated to the south of the cutoff (Figs. 4.5d,e–4.8d,e). Small-scale jet streaks were embedded within the 250 hPa jet stream, the former connected to vorticity maxima at 500 hPa and, sometimes, surface low pressure systems. Figure 4.5 shows this scenario explicitly with a 250 hPa jet streak (Fig. 4.5e) near a small vorticity maximum ("A") (Fig. 4.3b and Fig. 4.5d) above a surface low pressure system (Fig. 4.5a). Figure 4.7 shows the environment surrounding vorticity maximum "B" (Fig. 4.3d and 4.7d), with a 250 hPa jet streak (Fig. 4.7e) located near the surface low pressure system (Fig. 4.7a). Both "A" and "B" were associated with a small surface low pressure system, but "B" was stronger (i.e., higher values of absolute vorticity) and larger in area than vorticity maximum "A." As a result, vorticity maximum "B" was responsible for higher amounts of precipitation across southern New England during 26–27 May 2003 than "A." Vorticity maximum "C" followed closely behind "B," but with less available lower-tropospheric moisture. Consequently, considerably less rainfall was observed in association with vorticity maximum "C" (compare Fig. 4.1 to Fig. 4.2). Warm air advection at 850 hPa was fairly insignificant during the entire lifetime of this cutoff, but is an important player in two of the other three remaining cases.

Forecasting the precipitation patterns associated with a cutoff can be difficult. However, it is encouraging to note that the climatological results presented in Chapter 3

do show some usefulness. Comparing Fig. 4.1 with Fig. 3.20, it is noted how closely the areas of maximum precipitation align; namely, along coastal southern New England into New Jersey as well as east of Lake Ontario. Also, the ADP values are notably similar, for example, over Connecticut. Roughly 60 mm of precipitation accumulated over the four-day period (about 15 mm day^{-1}), which is nearly identical to the ADP value. Admittedly, most of the precipitation fell during a 24 h period, but the agreement in placement of the heaviest precipitation is a helpful first step towards improved overall forecastibility.

5.2.2 25–27 December 2002 and 3–5 January 2003

Both the 25–27 December 2002 (case A) and the 3–5 January 2003 (case B) are similar in their evolution, yet their impact on the Northeast was a bit different. The precipitation distributions (Figs. 4.14 and 4.20 for cases "A" and "B," respectively) show the area of maximum values both in east central New York. However, case A produced much more precipitation across the East Coast, with some portions receiving more than 50 mm of precipitation. Case B had most of the precipitation confined to the Northeast, and all values were under 50 mm. The main differences between these two systems, set apart by only about one week, include a stronger surface cyclone system and an earlier westward development in case A [compare Fig. 4.17d (case A) and Fig. 4.22d (case B)]. These differences allowed the system in case A to develop more by the time it impacted the Northeast, allowing more precipitation to fall. However, common to both cases is the relative inertness of the 500 hPa cutoff low, i.e., the surface features in these cases drive

the location of the upper level cutoff, rather than the cutoff controlling where the surface features propagate, such as in the 23–31 May 2003 case.

The key differences between both cases are best illustrated in a comparison at their relative closest position to the Northeast (Fig. 4.18 for case A and Fig. 4.23 for case B). In panel (a) of each figure, note the strength of the surface low pressure system, using the 1000 hPa geopotential height as a proxy for sea level pressure (–180 m versus –30 m). This deep cutoff characteristic extends upward in the troposphere to 500 hPa [panel (d)] where there are two closed contours in case A, but none in case B (using a 60 m contour interval). In addition, the distribution of absolute vorticity to the south side of the cutoff was similar in both cases (two distinct vorticity maxima), but it was much more compact in case A compared to case B. In both cases there was an interaction between the polar and subtropical jet streams [panels (e) and (f)], but the setup in case B was much farther offshore, whereas in case A the intersection of the equatorward entrance region of the polar jet and the poleward exit region of the subtropical jet was located near the Northeast. Although the 850 hPa warm air advection and 700 hPa frontogenesis patterns were in fact similar, it was the stronger surface low pressure system, juxtaposition of the polar and subtropical jet streams, and a more concentrated area of absolute vorticity that facilitated the ultimate greater precipitation distribution in case A, which was further aided by the longevity of a heavy band of precipitation.

5.2.3 11–15 May 2003

This last case is a hybrid of the previous three cases. It features an initially strong 500 hPa cutoff cyclone and surface cyclone (similar to the 25–27 December 2002 case and the 3–5 January 2003 case), but both decay over time. Similar to the 23–31 May 2003 case, the middle-tropospheric dynamics (e.g., 850 hPa warm-air advection and 700 hPa frontogenesis) are lacking. As a result, the precipitation distribution (Fig. 4.25) is different from those in the previous three cases. The local maximum in the upper peninsula of Michigan is attributed to the strong surface cyclone located just to the south, and coincides with 1000–500 hPa warm air advection [note the 1000 hPa, 850 hPa, 700 hPa, and 500 hPa geopotential height contours (Figs. 4.27a–d, respectively) are nearly normal to the 1000–500 hPa thickness contours in the upper peninsula of Michigan in Fig. 4.27a], 500 hPa cyclonic vorticity advection (Fig. 4.27d), and a diffluent jet exit region (Fig. 4.27e).

As the system moves eastward, the cold front triggers two areas of maximum precipitation downwind of Lakes Erie and Ontario, perhaps a result of lake enhancement with strong westerly flow. Also a possible cause of this increase in precipitation is the growth of the area of 500 hPa absolute vorticity along the front (compare Fig. 4.27d with 4.28d to the west and east of New York, respectively). Along the Green Mountains in Vermont, another local maximum of precipitation is noted. This maximum is suggestive of upslope enhancement, perhaps aided by the 850 hPa wind aligning more normal to the mountains, as noted by Smith (2003), by 1200 UTC 13 May 2003 (see Fig. 4.26c). As the cutoff continues to decay rapidly, signified by its loss of concentrated absolute vorticity, nearly all precipitation decays over the Northeast (Figs. 4.26c,d). Since this cutoff was considerably more mobile than the 23–31 May 2003 cutoff, there was no time

for other vorticity maxima to rotate around the cutoff. Therefore, all precipitation was dependent upon the cutoff itself; i.e., as the cutoff decayed, so too did the precipitation.

5.3 Cutoff Schematic

Figure 5.1 shows an idealized cutoff schematic that summarizes the general environment surrounding a cutoff as well as some other features that are variable. Common features to all cutoffs are noted in solid contours while variable features, which may or may not be present depending on the "flavor" of the cutoff, are dashed. The center of the cutoff, denoted by the "X," is shown with two closed 500 hPa geopotential height contours. The jet stream is located to the south and perhaps to the north and east of the cutoff, possibly aiding development of a surface cyclone, denoted by the "L." To the south of the cutoff is a "vorticity highway," within the 500 hPa flow, where vorticity maxima "A" and "B" may travel along with the cutoff (if it travels with the mean flow) or rotate around the cutoff (if it is isolated from the mean flow and is slow moving). Areas of precipitation are noted ahead of and within the vorticity maxima. Precipitation is also noted near and to the north of the cutoff itself, which may be heavy depending on the strength of the surface cyclone.

5.4 Forecasting Considerations

Previous work done relating to the climatological distribution of precipitation from upper level cutoff cyclones was limited to Jorgenson (1967) and Klein et al. (1968).

They found that the heaviest precipitation tends to fall to the southeast of the upper-level cutoff cyclone. While this statement is true for the first half of the 23–31 May 2003 case (see Fig. 4.2) and the second half of the 11–15 May 2003 case (see Fig. 4.25), it is not true for the 25–27 December 2002 case (see Fig. 4.14) and the 3–5 January 2003 case (see Fig. 4.20). This variability again illustrates that cutoffs do in fact have many "flavors," and that forecasting the associated precipitation needs to be performed on a case-by-case basis. In general, initially strong surface cyclones with later-developing upper-level cyclones tend to focus the heaviest precipitation just to the northwest of the upper-level cyclone. In the case of initially strong upper-level cyclones and later-developing surface cyclones, the precipitation distribution becomes more varied and tends to follow the rotating vorticity maxima (e.g., "A" and "B" in Fig. 5.1) around the periphery of the cutoff cyclone and also the area of absolute vorticity near the cutoff center.

In order to best improve the forecastibility of cutoffs, it is prudent to facilitate a "top down" approach in the following manner:

1) Be cognizant of the monthly variations of cutoff precipitation patterns.
2) If possible, categorize the cutoff into one of the four favored tracks and create a conjoined precipitation picture.
3) Note which tropospheric features initially form and dominate—the upper-level cyclone or the surface cyclone system. In Fig. 5.1, expect heavy precipitation in the indicated area if the 500 hPa cutoff develops after the surface low pressure system. Otherwise, generally light precipitation will occur near the cutoff while heavier precipitation may occur with vorticity maxima "A" and "B."

4) Use model guidance to help forecast the track and evolution of the cutoff and associated features. In the case of a blocking pattern, note that numerical models tend to favor a mobile rather than stagnant atmosphere.
5) Important surface and middle-tropospheric features (such as warm air advection, frontogenesis, and deformation zones) and their interaction with orography should be noted as possible areas of heavier precipitation.
6) In the near term, rely on radar and satellite data as well as ground observations to track mesoscale features/disturbances.

It is the hope of the author that these basic steps, along with a broad and thorough meteorological sense, will at least improve forecaster situation awareness and perhaps the forecast of a cutoff's precipitation itself.

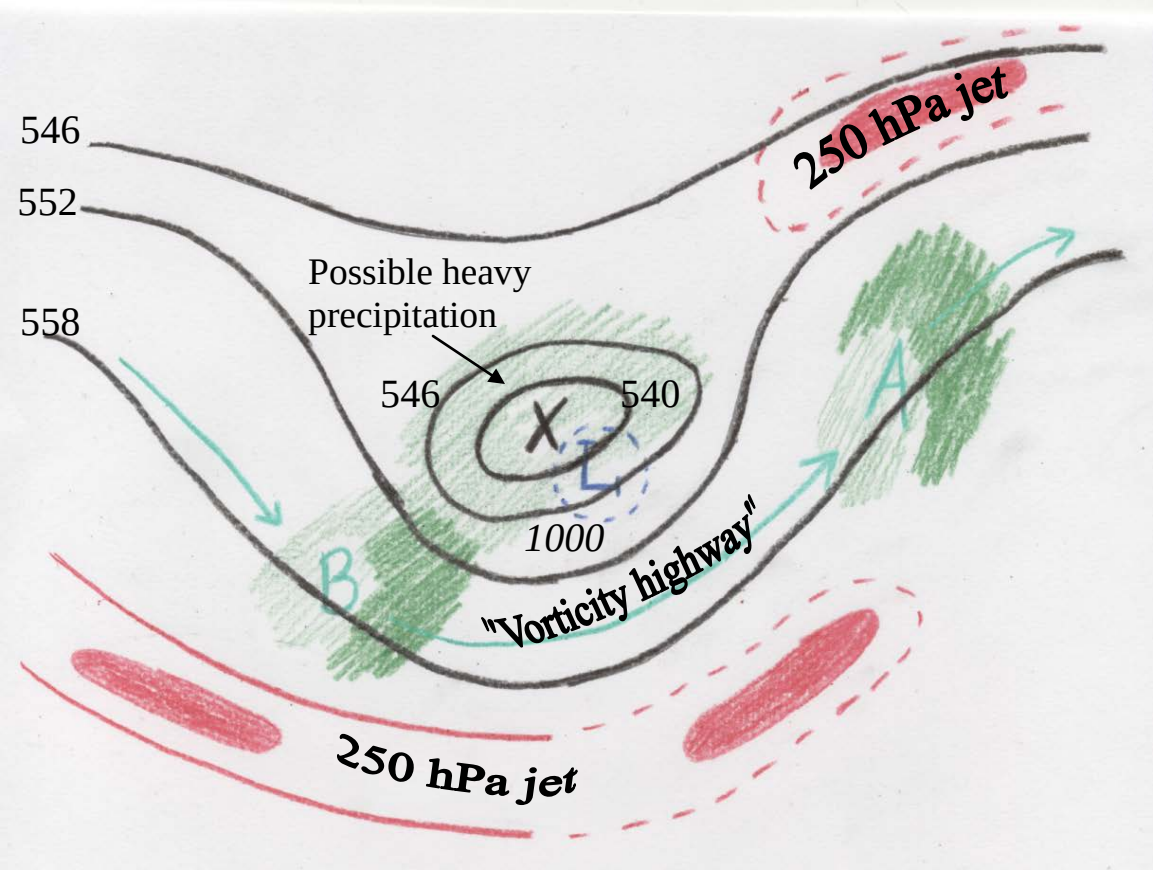

Fig. 5.1. Schematic of an idealized cutoff cyclone, denoted by the "X." Black contours indicate 500 hPa geopotential heights (dam), with associated vorticity maxima "A" and "B" embedded within the "vorticity highway" (light blue arrows). The upper-level jet stream (e.g., 250 hPa) is outlined in red, with jet streaks shaded, and extensions dashed. A surface low pressure system is denoted by the "L" with a surrounding closed isobar (1000 hPa, dashed blue line). Areas of light (heavy) precipitation are illustrated in light (dark) green, with a possible heavier area as marked.

6. Conclusions and Future Work

6.1 Conclusions

A 51-year (1948–1998) Northeast climatology of the precipitation distribution in association with 500 hPa cutoff lows during the cool season (October–May) is shown. Using the NCEP/NCAR reanalysis and the subset of objectively defined closed lows by Smith (2003), who defined a cutoff to be a geopotential height minimum surrounded by at least a 30 m height rise in all directions, in conjunction with the UPD, monthly maps of average daily precipitation (ADP) in association with cutoff lows were produced. October and November show the highest values of ADP (up to 9 mm day^{-1}) along the Northeast coast. The ADP amounts decrease area-wide through winter, then increase again by April and May over all areas except the immediate coast, where values slightly decrease. Higher values generally occur on or just east of higher elevations and to the northeast, whereas lower values occur in lower elevations and to the southwest. Adjacent warm ocean temperatures (acting as a continuous moisture reservoir) may allow for the high ADP values in autumn, whereas convection is a likely cause for higher ADP values in April and May. This pattern generally mimics the percentage of occurrence of cutoff lows in the vicinity of the Northeast, which shows a local maximum of occurrence in late October and early November and an absolute maximum of occurrence in early April.

Monthly maps showing the percentage of precipitation in association with cutoff lows with respect to the monthly climatological average also were created from this dataset. Over the cool season, one-third to two-thirds of the monthly precipitation occurs

in association with cutoff lows across the Northeast. Although January has the lowest area-wide cutoff precipitation percentage amounts (30%–50%) and April has the highest (50%–70%), the distribution consistently increases from southwest to northeast across the Northeast throughout the cool season. Cutoff low frequency is a linked directly to how much precipitation will occur over a given month; e.g., Maine is affected by cutoffs the most and consequently has the highest values.

Based on Smith's (2003) five cool-season mean cutoff cyclone tracks impacting eastern North America, subjective tracks of cutoffs over the 19-year period 1980–1998 were categorized into Mid-Atlantic, Southwest, Clipper, and Hudson Bay type cutoffs. Average daily precipitation maps show the orographic and geographic signal between different tracks, and storm-relative ADP maps show the distribution of precipitation relative to each track's average 24 h ending position. Mid-Atlantic cutoffs typically focus the precipitation along eastern Massachusetts, aided by a moist easterly flow off the Atlantic Ocean. Relative to the track of the cutoff, the heaviest precipitation falls along the track and to the north of the average 24 h ending position. Southwest cutoffs typically produce as much precipitation as Mid-Atlantic cutoffs and also focus the precipitation over coastal New England, but cover a greater area. The area of maximum precipitation falls well to the east of the average 24 h ending position, likely due to a broad and moist southerly flow into New England, perhaps enhanced by surface cyclogenesis.

Clipper cutoffs produce much less precipitation across the Northeast, but show a clear lake-effect signal. ADP values increase over New England, likely due to an ability to utilize the moist Atlantic once cutoffs reach the coast. Relative to the track, the

heaviest precipitation typically falls along the track and just ahead of the average 24 h ending position. Hudson Bay cutoffs are the driest of the four types, and primarily affect Maine, but a weaker lake-effect signal still exists. Similar to Clipper cutoffs, the precipitation is focused along the track and near the average 24 h ending position. All four tracks show locally higher (lower) ADP values nearly collocated with higher (lower) elevations. However, locally higher values are displaced farther from the highest elevations, as a consequence of upslope enhancement.

Four case studies provided four distinct perspectives of cutoff behavior. The 23–31 May 2003 cutoff followed a Southwest track, stalled, and then exited the Northeast. Fortuitously, ADP values over southern New England during the first four days of the event nearly matched those from the Southwest track ADP map, illustrating a first-order quantitative forecasting aid. Over the period, five vorticity maxima rotated around the cutoff and were the primary foci for the bulk of the precipitation, rather than the cutoff itself. Small surface low pressure systems, associated with two of the vorticity maxima and aided by upper-level jet streaks, locally enhanced the precipitation.

The 25–27 December 2002 and 3–5 January 2003 cases showed an initially developing surface cyclone followed by a 500 hPa cutoff. As a result, the strength of the surface cyclone determined where the heaviest precipitation would fall, and the 500 hPa cutoff served to focus the precipitation in a band (as in the 25–27 December 2002 case) or along its track (as in the 3–5 January 2003 case). The 10–15 May 2003 case featured a weakening surface and 500 hPa cutoff cyclone. As a result, the precipitation at first was focused near the surface cyclone, aided by strong cyclonic vorticity advection and associated upper-level divergence in the poleward exit region of a 250 hPa jet streak.

However, a local maximum of precipitation later formed as a result of an elongated vorticity maximum ahead of the decaying cutoff.

6.2 Future Work

This research [and Najuch's (2004) parallel research] is the first in some time to investigate the multiscale effect that 500 hPa cutoffs have on precipitation (Najuch 2004), aside from related case study investigations (e.g., Novak et al. 2002, Smith 2003). The work presented clearly points the way for continued progress in this area, especially in improving the forecastibility of cutoffs. Some issues to be addressed in the future include:

1) Extend the track climatology back to 1948 and up to the present (and the overall climatology to the present) to include more members in the composites and perhaps obtain a clearer precipitation distribution. Also, a finer resolution dataset could be used to better pinpoint cutoff location relative to the precipitation distribution (i.e., closer to the 0.25^{o} x 0.25^{o} UPD resolution).
2) Composite some synoptic features (e.g., upper-level jet stream configuration, mid-level ridges and troughs, etc.) among the four tracks. Pattern recognition can be a valuable tool in the medium- and perhaps long-range forecasting of cutoffs.
3) Analyze and composite precipitation patterns associated with cutoffs of different orientations and aspect ratios (i.e., circular/elliptical) and cutoffs that are deepening or filling.

4) Investigate additional case studies, including the April 2004 cutoff that produced over 100 mm of precipitation at Boston, Massachusetts, in 24 h.

Case Studies of Cool Season 500 hPa Cutoff Cyclone Precipitation Distribution

Abstract of

a thesis presented to the Faculty

of the University at Albany, State University of New York

in partial fulfillment of the requirements

for the degree of

Master of Science

College of Arts & Sciences

Department of Earth and Atmospheric Sciences

Anthony R. Fracasso
2004

ABSTRACT

The precipitation due to cutoff cyclones poses a challenge to forecasters, especially in the northeastern United States. The purpose of this research is to diagnose and understand the distribution of precipitation associated with the passage of 500 hPa cutoff cyclones in the Northeast by means of composite and case studies, and to determine whether or not there are characteristic precipitation signals associated with particular cutoff cyclone tracks. This research was conducted under the National Weather Service (NWS) Collaborative Science, Technology, and Applied Research (CSTAR) program, whose goal is to improve forecasts of heavy precipitation events in the Northeast. Precipitation composites were constructed from the gridded reanalysis datasets available from the National Centers for Environmental Prediction/National Center for Atmospheric Research (NCEP/NCAR) along with the NCEP Unified Precipitation Dataset (UPD), a once-daily (1200–1200 UTC) gridded precipitation dataset available on a 0.25º grid.

A monthly climatology of cool-season (October–May) 500 hPa cutoff cyclones has been produced for the 51-year period 1948–1998. These maps show average daily precipitation for all cases when a cutoff cyclone was present in the vicinity of the Northeast. A maximum is shown along coastal areas and near higher elevations, while a minimum is shown to the south and west and in lower elevations away from the coast. In addition, monthly summed average daily precipitation amounts were then compared to climatology, showing a significant seasonal variation of the climatological precipitation throughout the Northeast in association with cutoff lows. Values decrease from October

to reach a minimum in January, when roughly one third of the climatological precipitation is associated with cutoffs. Values reach a maximum in April, when nearly two thirds of the climatological precipitation occurs in association with cutoffs.

A 19-year (1980–1998) subset was chosen to subjectively categorize cutoffs that followed one of four favored tracks near the Northeast (Mid-Atlantic, Southwest, Clipper, and Hudson Bay). Average daily precipitation maps for all cutoffs within a track for the entire cool season (except May) were produced. These maps show a coastal maximum as well for all tracks, but this maximum is displaced towards the northeast for Clipper and Hudson Bay cutoffs, which typically affect northern New England. Also, storm-relative average daily precipitation maps were constructed for each track using storms that were within or close to US land. A maximum typically occurs near or just ahead of the average 24 h ending location of a cutoff, except for Southwest track cutoffs, whose maximum is located far to the east of the cutoff center.

One case study, occurring during the period 23–31 May 2003, was initially representative of a Southwest type cutoff. The cutoff tracked across the Great Lakes and then looped around and passed through New York State and Northern New England. Some locations received well under 25 mm, while other areas received closer to 100 mm over the period. Precipitation was most closely linked to vorticity maxima rotating around the cutoff, aided by upper-level jet streaks and associated surface low pressure systems. Three other case studies show some differing “flavors” of cutoff behavior. The first two (25–27 December 2002 and 3–5 January 2003) feature a rapidly developing surface cyclone and a later developing and comparatively weaker 500 hPa cutoff low. The last case study (10–15 May 2003) shows a decaying surface and upper-level cyclone,

with varying precipitation distributions during its journey over the Northeast. In these cases, the precipitation is tied to the initially formed surface cyclone but amplified due to the presence of a 500 hPa cutoff. After the surface cyclone decays, as in the last case study, precipitation is once again dictated by vorticity maxima ahead of the cutoff.

Case Studies of Cool Season 500 hPa Cutoff Cyclone Precipitation Distribution

A thesis presented to the Faculty of the University at Albany, State University of New York in partial fulfillment of the requirements for the degree of

Masters of Science

College of Arts & Sciences

Department of Earth and Atmospheric Sciences

Anthony R. Fracasso
2004

ACKNOWLEDGEMENTS

I cannot begin to explain how the past two years have affected me in such a wonderful way. Not only have I gained a tremendous perspective on my inner self, as well as a sense of accomplishment, but I have also gained a huge appreciation for those who have helped me in so many avenues along the way. The following is an attempt to identify some people who either came into my life or continued to be my support over the past two years—all of whom deserve some recognition.

First and foremost my two advisors, Lance Bosart and Dan Keyser, deserve the most recognition. Their reputation in the field of meteorology is at the top, but their demeanor is by far down-to-earth. This combination allows for a tremendous intellectual exchange between us emerging graduate students and themselves, the wise "elders" (though they are quite young at heart). I have gained a wealth of knowledge from my many interactions with them, and also improved my ability to transfer some of the usefulness of my research to those who may find it helpful. Overall, I am certain that Lance and Dan have had a significant positive influence on my future.

This research would not have been possible without the financial support provided by NOAA as part of the Collaborative Science and Technology Applied Research (CSTAR) program (Grant # NAO7WAO548). CSTAR allows for an exchange opportunity between student research and applied forecast operations at the National Weather Service that is unlike many other programs. In this capacity, both parties benefit greatly with continued interaction, and this has helped me to appreciate the specific role my research will play with the forecasters.

Specifically within the NWS, I would like to thank my focal point, Mike Evans (NWS BGM). Through many meetings we had countless ideas for research opportunities within my topic, though many remain future options. Gigabytes of data were also obtained through the help of Mike, many of which provided some insight into the case studies. It was a pleasure to work with such an individual.

The results from this research would not have been possible without the aid of many people within the department. First and foremost, Anantha Aiyyer provided the necessary computing expertise that is unparalleled. His ability to help so many graduate students with our continual problems while maintaining his sanity and cheery disposition is remarkable. I'd also like to thank my CSTAR student colleagues Heather Archambault, Dave Deluca, and especially Jessica Najuch. Jessie and I have maintained a close relationship not only with our complimentary research topics, but also personally. I am eternally grateful to her for lending an ear to me when I needed it the most. To past CSTAR students Brandon Smith and Matty Novak, from whom I have learned so much and with whom I have fostered a wonderful friendship, I offer my thanks. The added stresses of ATM 107 that Matty and I shared allowed opportunities I wouldn't have had otherwise. The CSTAR support staff, including Celeste, Diana, Sally, and Lynn, I thank for all their help. Other graduate students who deserve some thanks for their unique role in my life include Susanna Hopsch, Alicia Wasula, Kristen Corbosiero, Scott Runyon, Dan Lipper, and Joe Kravitz (for the occasional comic relief needed when I least expected it). Also to two of my students, Dave Ross and Anyee Fields, many thanks for kicking back and relaxing with your TA. Kevin Tyle and Dave Knight deserve so much credit for keeping the department running with the seemingly infinite supply of data.

Others who deserve some recognition include Garett Argianas and Heidi Smith, for their advice and help and for just being able to talk about anything and everything. To my Cornell friends Elizabeth Gingold, Jess Sheldon, and Rose Kwok, I thank for our many conversations and also for just being a friend. To Tim White, you've allowed my to be myself and to not be afraid of what lies ahead, and I am eternally grateful. Those who deserve the most appreciation are my family. My parents have provided me with opportunities than few people have a chance to experience. Without their sacrifices I wouldn't be where I am today, and when I explain how eternally grateful I am, they will still respond with "because you're our son," which means the world to me. My two sisters and brother-in-law were also much needed support over the past two years. Though we may be separated by distance, we will always be family, which has become so important to me. Thank you to all who have helped in some way make this research and more possible.

CONTENTS

LIST OF FIGURES

Case Studies of Cool Season 500 hPa Cutoff Cyclone Precipitation Distribution

A thesis presented to the Faculty of the

University at Albany, State University of New York

in partial fulfillment of the requirements

for the degree of

Master of Science

College of Arts & Sciences

Department of Earth and Atmospheric Sciences

Anthony R. Fracasso
2004

University at Albany, State of New York
College of Arts and Sciences
Department of Earth and Atmospheric Sciences

The thesis for the master's degree submitted by
Anthony R. Fracasso
under the title

Case Studies of Cool Season 500 hPa
Cutoff Cyclone Precipitation Distribution

Has been read by the undersigned. It is hereby recommended
for acceptance by the Faculty with credit to the amount of
_____ semester hours.

(Signed)_____(Date)_____

(Signed)_____(Date)_____

Recommended for approval on behalf of the Department

(Signed)_____(Date)_____

Recommendation accepted by the Dean of Graduate Studies
for the Graduate Academic Council

(Signed)_____(Date)_____

REFERENCES

Alpert, P., B. U. Neeman and Y. Shay-El, 1990: Intermonthly variability of cyclone tracks in the Mediterranean. *J. Climate*, **3**, 1474–1478.

Anthes, R. A., 1983: Regional models of the atmosphere in middle latitudes. *Mon. Wea. Rev.*, **3**, 1306–1335.

Atallah, E. H. and A. R. Aiyyer, 2002: Precipitation associated with 500 hPa closed Cyclones. *4th Northeast Operational Regional Workshop, 5–6 November 2002, Albany, NY.*

Bell, G. D. and L. F. Bosart, 1989: A 15-year climatology of 500 hPa closed cyclone and anticyclone centers. *Mon. Wea. Rev.*, **117**, 2142–2163.

——— and ———, 1993: A case study diagnosis of the formation of an upper-level cutoff cyclonic circulation over the eastern United States**.** *Mon. Wea. Rev.*, **121**, 1635–1655.

——— and ———, 1994: Mid-tropospheric closed cyclone formation over the southwestern United States, the eastern United States, and the Alps. *Mon. Wea. Rev.*,**122,** 791–813.

——— and D. Keyser, 1993: Shear and curvature vorticity and potential-vorticity interchanges: Interpretation and application to a cutoff cyclone event. *Mon. Wea. Rev.*, **121,** 76–102.

Bergeron, T., 1949: The problem of artificial control of rainfall on the globe II: The coastal orographic maxima of precipitation in autumn and winter. *Tellus,* **1**, 15–32.

Blender, R., M. Schubert, 2000: Cyclone tracking in different spatial and temporal resolutions. *Mon. Wea. Rev.*, **128,** 377–384.

Bowie, E. H., and R. H. Weightman, 1914: Types of storms of the United States and their average movement. *Mon. Wea. Rev.*, **42** (Suppl.), 1–37.

Colucci, S. J., 1985: Explosive cyclogenesis and large-scale circulation changes: implications for atmospheric blocking. *J. Atmos. Sci.*, **42,** 2701–2717.

———, 1987: Comparative diagnosis of blocking vs. non-blocking planetary-scale circulation changes during synoptic-scale cyclogenesis. *J. Atmos. Sci.* **44,** 124–139.Junker, N. W. and E. Hoke, 1990: An examination of Nested Grid Model precipitation forecasts in the presence of moderate-to-strong low-level southerly inflow. *Wea. Forecasting*, **5**, pp. 333–345.

Crocker, A. M., W. L. Godson, and C.M. Penner 1947: Frontal contour charts. *J. Meteorol.,* **4,** 95–99.

Davies, H. C., C. Schär and H. Wernli, 1991: The palette of fronts and cyclones within a baroclinic wave development. *J. Atmos. Sci.***, 48,** 1666-1689.

desJardins, M. L., K. F. Brill, and S. S. Schotz, 1991: Use of GEMPAK on UNIX workstations. *Proc. Seventh Int. Conf. On Interactive Information and Processing Systems for Meteorology, Oceanography, and Hydrology*, New Orleans, LA, Amer. Meteor. Soc., 449–453.

Dole, R. M., 1986: Persistent anomalies of the extratropical Northern Hemisphere wintertime circulation: Structure. *Mon. Wea. Rev.*,**114,** 178–207.

Doyle J. D., and M. A. Shapiro, 1999: Flow response to large scale topography: The Greenland tip jet. *Tellus*, **51A**, 728–748.

Eliassen, A., and E. Kleinschmidt, 1957: Dynamic Meteorology *Handbuch der Physik* Vol. 48, Springer-Verlag, 154 pp.

Geng, Q. and M. Sugi, 2001: Variability of the North Atlantic cyclone activity in winter analyzed from the NCEP/NCAR Reanalysis data. *J. Climate.* **14,** 3863–3873.

Hawes, J. T. and S. J. Colucci 1986: An examination of 500 mb cyclones and anticyclones in National Meteorological Center prediction models. *Mon. Wea. Rev.* **114,** 2163–2175.

Higgins, R. W., J. E. Janowiack, and Y. –P. Yao, 1996: A gridded hourly precipitation data base for the United States (1963–1993). NCEP/Climate Prediction Center Atlas 1, National Centers for Environmental Prediction, 46pp.

Hodges, K. I., 1994: A general method for tracking analysis and its application to meteorological data. *Mon. Wea. Rev.,* **122,** 2573-2586.

Hoskins, B. J., M. E. McIntyre and W.A. Robertson, 1985: On the use and significance of isentropic potential vorticity maps. *Quart. J. Roy. Meteorol. Soc.*, **111,** 877-946.

Hsieh, Y. P., 1949: An investigation of a selected cold vortex over North America. *J. Meteorol.* **6,** 401–410.

Jorgensen, D. L., 1963: A computer derived synoptic climatology of precipitation from winter storms. *J. Appl. Meteor.*, **2,** 226–234.

———, W. H. Klein and A. F. Korte 1967: synoptic plimatology of precipitation from 700 mb lows for the intermountain West. *J. Appl. Meteor.,* **6,** 782–790.

Kalnay, E., M. Kanamitsu, R. Kistler, W. Collins, D. Deaven, L. Gandin, M. Iredell, S. Saha, G. White, J. Woollen, Y. Zhu, A. Leetmaa, B. Reynolds, M. Chelliah, W. Ebisuzaki, W. Higgins, J. Janowiak, K. C. Mo, C. Ropelewski, J. Wang, R. Jenne, and D. Joseph, 1996: The NCEP/NCAR 40-year reanalysis project. *Bull. Amer. Meteor. Soc*., **77**, 437–471.

Kerr, I. S., 1953: Some features of upper level depressions. *Tech. Note. Meteorol. New Zealand*, No. 106.

Keyser, D. and M. A. Shapiro, 1986: A review of the structure and dynamics of upper-level frontal zones. *Mon. Wea. Rev.*, **114,** 452–499.

Kistler, R., E. Kalnay, W. Collins, S. Saha, G. White, J. Woolen, M. Chelliah, W. Ebisuzaki, M. Kanamitsu, V. Kousky, H. Van den Dool, R. Jenne, and M. Fiorino, 2001: The NCEP–NCAR 50-year reanalysis: Monthly means CD-ROM and documentation. *Bull. Amer. Meteor. Soc*., **82**, 247–267.

Klein, W. H., 1957: Principal tracks and mean frequencies of cyclones and anticyclones in the Northern Hemisphere. *Res. Paper No. 40*, US Dept. of Commerce, Wea. Bur., Washington, DC, 60 pp.

———, D. L. Jorgensen, and A. F. Korte, 1968: Relation between upper-air lows and and winter precipitation in the western plateau states. *Mon. Wea. Rev*., **96,** 162─168.

König, W., R. Sausen and F. Sielmann, 1993: Objective identification of cyclones in GCM simulations. *J. Climate,* **6,** 2217–2231.

Konrad C. E. and S. J. Colucci, 1988: Synoptic climatology of 500 mb circulation changes during explosive cyclogenesis. *Mon. Wea. Rev.,* **116,** 1431─1443.

Najuch, J. 2004: Case Studies of Warm Season Cutoff Cyclone Precipitation Distribution. Masters of Science Thesis, Department of Earth and Atmospheric Sciences, University at Albany/SUNY, Albany, NY, 117 pp.

Novak D. R., L. F. Bosart, D. Keyser, and J. S. Waldstreicher, 2004: An observational study of cold season–banded precipitation in Northeast U.S. cyclones, *Wea. Forecasting, in preparation.*

Novak, M. J., L. F. Bosart, D. Keyser, K. D. LaPenta and T. A. Wasula, 2002: Climatology of warm-season cutoff cyclones and case study diagnosis of 14–17 July 2000. *19th Conf. On Weather Analysis and Forecasting, 12–16 Aug 2002, San Antonio, TX.*

Palmén, E., 1949: Origin and structure of high-level cyclones south of the maximum westerlies. *Tellus,* **1,** 22–39.

——— and K. M. Nagler, 1949: The formation and structure of large-scale disturbances in the westerlies.: *J. Meteorol.*: **6,** 227–242.

——— and Newton, 1969: *Atmospheric Circulation:* The Academic Press, New York, New York. 603 pp.

Parker, S. S., J. T. Hawes, S. J. Colucci, and B. P. Hayden, 1989: Climatology of 500 mb cyclones and anticyclones, 1950–85. *Mon. Wea. Rev.*, **117**, 558–571.

Passarelli, R. E., and H. Boehme, 1983: The orographic modulation of pre-warm-front precipitation in southern New England. *Mon. Wea. Rev.*, **111**, 1062–1070.

Peltonen, T., 1963: A case study of an intense upper cyclone over eastern and northern Europe in November 1959. *Geophysica (Helsinki),* **8,** 225─251.

Reitan, C. H., 1974: Frequencies of cyclones and cyclogenesis for North America, 1951─1970. *Mon. Wea. Rev.,* **102,** 861─868.

Rex, D.F., 1950: Blocking action in the middle troposphere and its effect on regional climate, I. An Aerology Study of Blocking Action. *Tellus,* **3,** 196─211.

Roebber, P. J. and L. F. Bosart, 1998: The sensitivity of precipitation to circulation details. Part I: An analysis of regional analogs. *Mon. Wea. Rev.*, **126**, 437–455.

Rogers, E., and L. F. Bosart 1986: An investigation of explosively deepening oceanic cyclones. *Mon. Wea. Rev.,* **66,** 702─718.

Rossby, C. G., 1940: Planetary flow patterns in the atmosphere. *Quart. J. Roy. Meteorol Soc.*, **66,** Suppl. 68─87.

Sanders, F. and J. R. Gyakum, 1980: Synoptic-dynamic climatology of the bomb. *Mon. Wea. Rev.*: **108**, 1589–1606.

Sinclair, M. R., 1997: Objective identification of cyclones and their circulation, intensity, and climatology. *Wea. Forecasting,* **12**, 595–612.

Smith, B. A., 2003: Cutoff Cyclones: A Global and Regional Climatology and Two Case Studies. Masters of Science Thesis, Department of Earth and Atmospheric Sciences, University at Albany/SUNY, Albany, NY, 165 pp.

Taljaard, J. J., 1985: Cut-off lows in the South African region. *South African Weather Bureau Tech Paper No. 14*, 153 pp.

——— and P. C. L. Steyn, 1991: Relationships between circulation and rainfall in the South African region. *South African Weather Bureau Tech. Paper No. 24***,** 62 pp.

Tennant, W. J., and J. Van Heerden, 1994: The influence of orography and local sea-surface temperature anomalies on the development of the 1987 Natal floods: A general circulation model study. *S. African J. Sci.,* **90,** 45–49.

Thorncroft, C. D., B. J. Hoskins, and M.E. McIntyre, 1993: Two paradigms of baroclinic wave life cycles. *Quart. J. Roy. Meteorol. Soc.*, **119,** 17–56.

Thorpe, A. J, 1986: Synoptic scale disturbances with circular symmetry. *Mon. Wea. Rev.*, **114,** 1384–1389.

Tyson, P. D., 1986: *Climate change and variability in Southern Africa.* Oxford University Press, 220 pp.

Ueno, K., 1993: Interannual variability of surface cyclone tracks, atmospheric circulation patterns, and precipitation patterns in winter. *J. Meteorol. Soc. Japan*, **45**, 439–462.

van Loon, H., 1956: Blocking action in the Southern Hemisphere. *Notos*, **6**, 171–175.